WRPS-66058
Revision 0

Acetonitrile Destruction in ETF Feed Solutions by UV/OX and Persulfate

Prepared for the U.S. Department of Energy
Assistant Secretary for Environmental Management

Contractor for the U.S. Department of Energy
Office of River Protection under Contract DE-AC27-08RV14800

P.O. Box 850
Richland, Washington 99352

WRPS-66058
Revision 0

Acetonitrile Destruction in ETF Feed Solutions by UV/OX and Persulfate

I. L. Pegg
The Catholic University of America

M. Brandys
The Catholic University of America

N. Mecholsky
The Catholic University of America

R. S. Skeen
Washington River Protection Solutions

Date Published
February 2021

Department of Energy

Prepared for the U.S. Department of Energy
Assistant Secretary for Environmental Management

Contractor for the U.S. Department of Energy
Office of River Protection under Contract DE-AC27-08RV14800

P.O. Box 850
Richland, Washington 99352

Release Approval Date

VSL-20R4850-1

Final Report

Acetonitrile Destruction in ETF Feed Solutions by UV/OX and Persulfate

prepared by

Marek Brandys, Nicholas Mecholsky, and Ian L. Pegg

Vitreous State Laboratory
The Catholic University of America
Washington, DC 20064

for

Atkins Energy Federal EPC, Inc.
Columbia, MD 21046

and

Washington River Protection *Solutions*, LLC
Richland, WA

November 27, 2020

Rev. 0, 2/11/21

Completeness of Testing:

This report describes the results of work and testing specified by the referenced WRPS approved Test Plan(s). The work and any associated testing followed established quality assurance requirements and were conducted as authorized. The descriptions provided in this test report are an accurate account of both the conduct of the work and the data collected. Results required by the Test Plan are reported. Also reported are any unusual or anomalous occurrences that are different from the starting hypotheses. The test results and this report have been reviewed and verified.

I.L. Pegg: _____ **Date:** 2/15/21
VSL Program Director/Principal Investigator

I. Joseph: Innocent Joseph **Date:** 2/15/2021
Atkins Sub-Contract Manager

TABLE OF CONTENTS

List of Tables

List of Figures

List of Abbreviations

ASME	American Society of Mechanical Engineers
CUA	Catholic University of America
DF	Decontamination Factor
DFLAW	Direct Feed Low Activity Waste
DOE	Department of Energy
EMF	Effluent Management Facility
ERDF	Environmental Restoration Disposal Facility
ETF	Effluent Treatment Facility
GC-MS	Gas Chromatography - Mass Spectroscopy
IC	Ion Chromatography
IDF	Integrated Disposal Facility
LAW	Low Activity Waste
MEK	Methyl Ethyl Ketone
NIST	National Institute of Standards and Technology
NQA	Nuclear Quality Assurance
QA	Quality Assurance
QAPP	Quality Assurance Project Plan
QARD	Quality Assurance Requirements and Description
SBS	Submerged Bed Scrubber
SOW	Statement of Work
UV	Ultra-Violet
UV/OX	Ultra-Violet/Oxidation
VSL	Vitreous State Laboratory
WESP	Wet Electrostatic Precipitator
WTP	Hanford Tank Waste Treatment and Immobilization Plant
WRPS	Washington River Protection *Solutions*, LLC

Registered Trademarks

Pen-Ray® is registered trademark of UVP, LLC., Upland, California

Hanovia® is registered trademark of Hanovia Specialty Lightning, LLC., Fairfield, New Jersey

LabVIEW® is registered trademark of the National Instruments Corporation, Austin, Texas

Tekmar® is registered trademark of Teledyne Instruments, Inc., Thousand Oaks, California

Agilent Technologies® and ChemStation® are registered trademarks of Agilent Technologies, Inc., Santa Clara, California

IonPac® and Chromeleon® are registered trademarks of Dionex Corporation, Sunnyvale, California

Geochemist's Workbench® is registered trademark of Aqueous Solution, LLC., Urbana Illinois

Mathematica® is registered trademark of Wolfram Group, LLC., Champaign, Illinois

Rayox Clagon® is registered trademark of Clagon Carbon US Technologies, LLC., Coraopolis, Pennsylvania

SECTION 1.0
INTRODUCTION

1.1 Background

The Hanford Site Effluent Treatment Facility (ETF) currently treats aqueous waste streams that include condensates from the 242-A evaporator, leachate from the Environmental Restoration Disposal Facility (ERDF), as well as laboratory wastes and, in the future, will treat liquid effluents from the Hanford Waste Treatment and Immobilization Plant (WTP) and Integrated Disposal Facility (IDF) leachate. Liquid effluents from the WTP will have significant concentrations of acetonitrile. Acetonitrile is formed by reaction of nitrates and sugar in the WTP low activity waste (LAW) melters and is prevalent in the submerged bed scrubber (SBS) and wet electrostatic precipitator (WESP) liquid effluents from WTP off-gas treatment [1, 2]. When these liquids are concentrated in the WTP Effluent Management Facility (EMF) evaporator in the direct feed low activity waste (DFLAW) flow-sheet, testing has shown that the majority of the acetonitrile partitions to the evaporator condensate [3, 4]. Since the evaporator condensate is directed to the ETF, this creates a potential issue with the ETF waste acceptance criteria and, specifically, the ETF Delisting Modification treatability envelope limits. Consequently, there is a need to assess possible mitigation approaches, one of which involves identification and assessment of potential treatment processes to destroy the acetonitrile, which is the subject of the present report.

Washington River Protection *Solutions*, LLC (WRPS) previously contracted with Atkins and the Vitreous State Laboratory (VSL) of The Catholic University of America (CUA) to perform development and testing work to evaluate potential methods for destruction of acetonitrile in WTP secondary liquid effluents [5]. Based on the results of that work [6], WRPS has requested that follow-on testing be conducted to further evaluate acetonitrile destruction using ultraviolet oxidation (UV/OX) with either hydrogen peroxide or persulfate [7], the results of which are presented in this report.

1.2 Test Objectives and Scope of Work

This work was conducted according to a Test Plan [8] that is responsive to the WRPS statement of work (SOW) [7].

In FY19 VSL completed tests with a variety of UV activated oxidants and found that the persulfate ion ($S_2O_8^{-2}$) provided rapid and complete destruction of acetonitrile under certain conditions [6, 9]. In contrast, the oxidant currently employed at ETF, hydrogen peroxide, had little effect on acetonitrile concentrations. Persulfate was also able to oxidize the other organic compounds that are predicted to be present within the ETF feed. However, the data also indicated that some aqueous species may interfere with the destruction reaction and that additional testing was necessary to determine the impacts of key process variables. Accordingly,

one objective of the FY20 work described herein was to further investigate these effects and assess potential methods to mitigate their impacts. A further objective of this work was to perform testing at a larger-scale and higher UV power in a configuration that represents the new Calgon UV oxidation reactor system which is to be installed in the main treatment train of the ETF.

In addition, WRPS is pursuing a steam stripping approach to remove acetonitrile from the main treatment train of the ETF. In that approach, the stripped acetonitrile would be concentrated in a stream that is essentially pure water with high concentrations of acetonitrile. There is therefore a need to further evaluate the potential for UV/OX processes to destroy acetonitrile in that stream.

In summary, therefore, this work addressed: (i) The destruction of acetonitrile at relatively low concentrations (tens of ppm) in representative ETF feed simulants and (ii) The destruction of acetonitrile at much higher concentrations (up to tens of grams per liter) in pure water representing the steam stripping stream.

The testing with the ETF feed simulants addressed the impacts of persulfate concentration, acetonitrile concentration, the presence of other organics expected to be present in the ETF feed, and the presence of potential radical scavengers on the rate and extent of acetonitrile destruction using UV/OX with persulfate. Radical scavengers that were considered include ammonium, chloride, nitrate, and bicarbonate. Testing was also performed with the existing ETF treatment method of UV/OX with hydrogen peroxide as a baseline to compare with the persulfate results.

The testing with the simulated steam stripping liquid addressed the impacts of persulfate concentration and acetonitrile concentration.

The testing was conducted at two scales. One set of tests was conducted in the same micro-scale (16 mL) reactor system used in the previous work [9]. A second set of tests was conducted on a new larger (~14 L) reactor system that was designed and constructed for this testing. The new reactor system represents a full-scale transverse section through one of the new Calgon UV/OX reactor tubes to be installed in the ETF. This test system was designed such that the UV lamp power could be varied and could achieve the same UV intensity as the full-scale system.

1.3 Methods Selected for Evaluation

Acetonitrile is very stable and, compared to other organics, is relatively difficult to destroy. Some of the most promising methods for destruction of acetonitrile involve photolysis using ultra-violet (UV) light [10-19]. Many such UV processes combine the use of UV light and chemical oxidants such as hydrogen peroxide to destroy organic contaminants. The UV light interacts with the hydrogen peroxide to generate hydroxyl radicals ($OH^{\bullet}$), which are highly reactive. The hydroxyl radicals then attack the organic molecules resulting in their destruction. The reaction can be assisted by the direct photolysis of the organic molecule by the UV light,

which can break or activate certain bonds making the molecule more susceptible to oxidation. Other processes include UV light alone, UV light with ozone, UV light with ferric ion, UV light with Fenton's reagent (H_2O_2/Fe^{2+}), UV light with persulfate, UV light with chlorine, UV light with ferrioxalate, and UV light with TiO_2 and with other photocatalysts [10, 12, 13]. While most of these are based on generation of hydroxyl radicals, others generate sulfate or chlorine ($SO_4^{-\bullet}$ or $^{\bullet}Cl$) radicals [14, 16, 18, 19].

In the previous work [9], several such combinations of UV light and chemical additives were tested, including:

- UV light + hydrogen peroxide
- UV light + Fenton's reagent
- UV light + ferrioxalate
- UV light + persulfate
- UV light + hypochlorite.

Based on the results of that work [9], UV light + persulfate and UV light + hydrogen peroxide were subjected to more detailed testing in the present work.

1.4 Quality Assurance

This work was performed under a quality assurance (QA) program compliant with the applicable criteria of 10 CFR 830.120; the American Society of Mechanical Engineers (ASME) Nuclear Quality Assurance (NQA)-1, 2008 including NQA-1a 2009 Addenda, and Department of Energy (DOE) Order 414.1D, Quality Assurance. These QA requirements are implemented through a Quality Assurance Project Plan (QAPP) for WRPS work [20] that is conducted at the VSL. Test and procedure requirements by which the testing activities are planned and controlled are also defined in this plan. The program is supported by VSL standard operating procedures that were used for this work [21]. This is LAW work and is therefore not subject to the requirements of DOE/RW-0333P, Office of Civilian Waste Management Quality Assurance Requirements and Description (QARD).

SECTION 2.0
TEST SYSTEMS

2.1 Micro-Scale Reactor Test Setup

Some of the tests were conducted in a micro-scale laboratory reactor, as shown in Figures 2.1 and 2.2. The reactor body is made from borosilicate glass and has a quartz jacketed insert to accommodate the UV light source. The testing used a 5.5 W mercury lamp (Pen Ray Model 90-0012-10, 11SC-1) as the UV light source with primary emission at 254 nm. The reactor includes provisions for sampling and reagent addition during testing as well as for temperature control. The liquid volume in the reactor is about 16 mL. All tests were conducted at 25 ºC. All tests that were conducted on the micro-reactor are identified with the prefix "MR-".

2.2 Large-Scale Reactor Test Setup

Each of the three planned Calgon reactor units for the ETF consists of eight reaction tubes in series. Each of the eight tubes are approximately 1.1 m long with a central UV lamp along its length, forming a toroidal cavity through which the process fluid flows. The basis of design for the new large-scale test reactor was a full-scale transverse cross-section through one of the full-scale reactors but smaller in length (0.17 m). Since the test system is designed as a batch reactor, other design features included stirring to simulate fluid flow, active temperature control to manage the heat from the lamp, and variable lamp power up to the same UV intensity as the full-scale system. To span the required range of UV power, the system was designed to accept two sizes of UV lamps (450 W and 4800 W). Since these lamps had slightly different dimensions, two test system configurations were used. Cross-sectional diagrams of these two configurations are show in Figures 2.3 and 2.5 for the 450 W lamp and the 4800 W lamp, respectively; photographs of these systems are shown in Figures 2.4 and 2.6, respectively.

The large-scale reactor has a total volume of 14.68 L; all tests were conducted with a fluid volume of 14.0 L. The system uses two different Hanovia medium pressure mercury light sources of 450 W and 4800 W. The vendor specifications for these two lamps are listed in Table 2.1. The reactor is a cylindrical jacketed stainless reaction vessel with the lamp cavity located along its axis. The lamp cavity is formed from two concentric quartz tubes which have fittings to allow cooling water to flow between them. Other fittings allow nitrogen to be flowed through the inner tube, which contains the lamp, which prevents ozone generation and provides some cooling. The reactor is fitted with a mechanical stirrer and a variety of ports for liquid introduction and sampling. The fluid cavity is sealed and can be pressurized, as was the case for tests conducted with an overpressure of carbon dioxide. The reactor is equipped with pH, temperature, and pressure sensors for monitoring these parameters throughout testing. These data were recorded using a custom LabVIEW control and data acquisition system. The temperature of the reactor contents is maintained by circulating water through both the exterior reactor jacket

and between walls of the quartz cavity surrounding the UV lamp. This type of arrangement is necessary due to very high operating temperature of medium pressure mercury lamp, which reaches a surface temperature of ~900°C.

For each test, the waste simulant solution containing all of the components except any organics was first pumped by means of a peristaltic pump into the reactor. The pH was then adjusted, as needed, *in situ*. The liquid in the reactor is continuously stirred during testing. The UV lamp is initially blinded with a tubular metal shutter for the duration of lamp heat-up period (~12 minutes), during which time, any and all organic reagents are added as liquid concentrates from a syringe through a valved luer port. The initial (i.e., time zero) sample is then drawn using the same luer port, the shutter is raised, and the reaction time count begins. Sampling during testing was done with a syringe connected to the aforementioned luer port.

All tests were conducted starting with the fluid at room temperature and there was typically a gradual temperature rise (~5 - 10°C) over the course of the test, as described in Section 3.

All of the tests conducted on the large reactor are identified by the prefix "LR-".

2.3 Sample Analysis

The liquid samples from all of the tests were analyzed for acetonitrile and other target organics by capillary gas chromatography - mass spectroscopy (GC-MS) by injection into a Purge and Trap sample concentrator.

In the Purge and Trap method, a liquid sample is first injected into a sparge vessel. During the purge stage, organics are removed from the sample by a purge gas (usually high purity helium) passing through a frit before flowing through the sample. The frit disperses the gas into finely divided bubbles allowing a large surface area of the sample to be contacted. This process allows the inert gas stream to strip the analytes from the sample matrix and concentrate them on a solid adsorbent trap. The desorb mode follows, during which the purged analytes, now trapped onto a solid sorbent, are released when the trap is heated and back-flushed with desorption gas to release and transfer the analytes of interest into the GC. The GC carrier gas is used as the desorb gas and involves switching a six-port valve to place the trap in-line with the GC column.

A Tekmar Dohrmann 3100 Purge and Trap Sample Concentrator was used for liquid samples in this work together with an Agilent Technologies Model 6890 GC with 5973N Mass Selective Detector and a G1560A Split/Splitless inlet. Compounds of interest were identified using the National Institute of Standards and Technology (NIST) spectral library built into the ChemStation GC-MS analysis software and were quantified using the integrated area under the relevant peak of the chromatograph.

The sample size collected from the reactor during testing ranged from 0.20 ml for the micro-reactor to 5.0 ml for the large reactor. The samples were stored in the sealed amber vial until they were analyzed – usually within a few hours.

Acetate was measured in selected samples by ion chromatography (IC) using a Dionex DX-120 ion chromatograph. The DX-120 consists of a CDM-3 conductivity detector and an anion self-regenerating suppressor and was equipped with IonPac AS-14/AG-14 column/column guard for anion separation. Column elution was performed with a solution of Na_2CO_3/$NaHCO_3$. The instrument was controlled using the Chromeleon (version 6.50) data system software. Calibration standards were prepared with NIST traceable standards.

SECTION 3.0
WASTE SIMULANTS AND TEST MATRIX

Three waste simulants were used in this work. Two of these are the same ETF simulants that were used in the previous work [9], referred to as the "simple simulant" and the "complex simulant." The third simulant, the "steam stripping simulant," represents the projected composition of the waste effluent from the steam stripping process for acetonitrile removal that is being developed by WRPS. Each of these are described below.

3.1 Simple Simulant

The simple simulant consisted of a solution of sodium sulfate (5000 mg/L) in water, to which various other components (ammonium, chloride, nitrate, or bicarbonate), were added according to the specific test purpose. The pH was then adjusted to 6.0±0.1 with sulfuric acid or sodium hydroxide. Acetonitrile was then added at nominally 80 mg/L, as used previously [9]; this is somewhat higher than the projected concentration in the WTP feed to the ETF of about 46.4 mg/L [22, 23].

The simple simulant was used exclusively in the micro-scale reactor tests (MR-).

3.2 Complex Simulant

The complex simulant was based on information provided by WRPS on the composition of the ETF evaporator concentrate from projected WTP EMF feeds [22]; the composition is shown in Table 3.1. The second column in Table 3.1 shows the source data, the third column shows the composition after charge balancing with bicarbonate, and the fourth column shows the composition after adjustment to pH 6 with sulfuric acid, which is the current practice at ETF [2, 23]. The fifth column shows the target simulant selected for the previous work [9] and the present work, which is the charge-balanced composition in column three after deletion of all constituents with concentrations below 1 mg/L.

Since the tests were conducted under acidic conditions (pH 6), the majority of the bicarbonate shown in Table 3.1 would be expected to decompose to produce carbon dioxide. Calculations show that at pH 6, the equilibrium bicarbonate concentration would be only 5.7 x 10^{-6} M (4.8 x 10^{-4} g/L as $NaHCO_3$). Consequently, the amount of bicarbonate added in the simulant recipe was decreased to this value from the target value. The pH of the as-prepared simulant was 10.2. The adjustment of the pH to 6 with sulfuric acid resulted in an increase of the sulfate concentration by ~0.23 g/L (~7.5%). The recipe for the complex simulant is shown in Table 3.2.

It was convenient to prepare a 28x concentrate of the simulant such that 0.5 liters of concentrate could be mixed with 13.5 kg of water to make up a 14-liter large reactor load; the composition of that concentrate is also listed in Table 3.2.

This complex simulant was used exclusively in the large reactor tests (LR-).

3.2.1 Additional Organics

Some of the tests with the complex simulant included spiking with a set of other organics, in addition to acetonitrile, that WRPS has identified [24]. The list of these organics and their concentrations, provided in Table 3.3, are based on projections of the composition of the waste feed to the ETF. The organic mix used for testing was prepared by dissolving all of the components in acetonitrile, when it was present in the test, or acetone otherwise, in the appropriate ratio, as shown in Table 3.3. For tests including acetonitrile, the amount of this organic mixture that was used in each test was that required to achieve the same concentration of acetonitrile as in tests involving acetonitrile only, as shown in Table 3.3.

Two tests involved the addition of acetamide or acetate; they were added as a solution of acetamide or as acetic acid dissolved in ~5 ml of simulant.

3.2.2 Added Bicarbonate

As shown in Table 3.1, the projected feeds to ETF have a very high concentration of bicarbonate. When sulfuric acid is added in the ETF surge tank to adjust the pH to the desired value (6), the vast majority of the bicarbonate will be converted to gaseous carbon dioxide, which could be lost from the solution [6, 23]. However, the ETF UV/OX units operate above atmospheric pressure (about 10.5 psi with a 6 psi pressure drop between the inlet and outlet [8]), which would tend to retain some of these species in solution. There is some concern that dissolved carbon dioxide species may interfere with the UV/OX process and reduce the destruction efficiency [23]. Consequently, there is a need to perform testing over a representative range of the concentrations of these species. Information provided by WRPS indicates that the range of interest is from about 360 to 2890 ppm as carbonate. This requires the provision to maintain an over-pressure of carbon dioxide in the headspace of the reactor, which is included in the design of the large reactor test system.

Two tests were conducted with an overpressure of carbon dioxide. In the “medium bicarbonate” test (LR-5), carbon dioxide was added to the air in the headspace to increase the pressure by 6 psi above atmospheric. In the “high bicarbonate” test (LR-6), the headspace was flushed with carbon dioxide and the pressure was increased to 16.9 psi above atmospheric. The respective carbon dioxide fugacities are 0.41 atm and 2.15 atm. These values were selected based on previous model calculations with the ETF simulant composition using a geochemical speciation code (Geochemist’s Workbench, Release 8.0) [8]. The same modeling approach was used to calculate the concentrations of various species in solution for the actual carbon dioxide fugacities achieved in the two tests, with the results shown in Table 3.4. For comparison, the

values of about 360 to 2890 ppm as carbonate provided by WRPS correspond to about 0.006 to 0.048 molal as total carbon versus 0.012 and 0.063 molal for the two tests.

3.3 Steam Stripping Simulant

The third simulant, the "steam stripping simulant," represents the projected composition of the waste effluent from the steam stripping process for acetonitrile removal that is being developed by WRPS. This simulant was simply a solution of acetonitrile in water to which various concentrations of either persulfate or peroxide oxidants were added.

Tests with the steam stripping simulant were performed in both the micro- and the large-scale reactors (labeled "MR-S" and "LR-S," respectively).

3.4 Test Matrix

The test matrix for this work included a combination of tests with the ETF simulants and the steam stripping simulant on the micro-reactor and on the large reactor. The test conditions used and purpose of the tests are presented in Tables 3.5 – 3.8. Results from the tests are presented in Section 4.

SECTION 4.0
RESULTS AND DISCUSSION

4.1 Micro-Reactor Tests

4.1.1 Tests with ETF Simple Simulant and Persulfate

Micro-reactor tests were performed with the simple simulant, to which various other components (nothing (baseline), ammonium, chloride, nitrate, or bicarbonate), were added to investigate any interference effects of these anions on the destruction of acetonitrile by UV + persulfate. The concentration of each added anion is the same as that in the complex simulant except for chloride in Test MR-15, which is very much higher, as explained below. The results from these tests are provided in Table 4.1 and Figure 4.1.

The effects of nitrate and bicarbonate appear to be small, though bicarbonate shows some inhibition at early times. At the nominal concentrations, ammonium shows the largest effect at all except the longest time, where the effect of chloride is slightly larger. Even at the high chloride concentration, the effect of ammonium is highest up to about 5 minutes, beyond which the effect of chloride is higher. The effect of ammonium is consistent with previous work conducted at VSL [25] in which processes for destruction of ammonium in secondary liquid waste routed to ETF were developed. The most effective process evaluated was reaction of ammonium with persulfate (without UV but at elevated temperatures (75 and 90ºC)) [25]. Consequently, it is reasonable that ammonium would inhibit the destruction of acetonitrile by persulfate via consumption of persulfate.

As noted previously [9], data in the literature suggests that chloride has a powerful effect on quenching sulfate radicals [9, 13, 26, 27]. A previous micro-reactor test in which chloride was added to the simple simulant at 1000 mg/L showed significant inhibition of the acetonitrile destruction rate. However, there is also evidence in the literature that this effect is highly non-linear and at sufficiently high chloride concentrations, the destruction rate for some organics has been shown to increase [27]. Accordingly, a test at much higher chloride concentration was included in the present work (Test MR-15). However, the results show continued inhibition at this higher chloride concentration.

4.1.2 Tests with Steam Stripping Simulant and Persulfate

Micro-reactor tests were performed with the steam stripping simulant with various concentrations of acetonitrile between 60 g/L and 0.06 g/L with persulfate added to achieve a mole ratio of persulfate to acetonitrile of 1.5. The results are shown in Table 4.2 and Figure 4.2. The results show a clear systematic increase in the extent of acetonitrile destruction with decreasing concentration. Figure 4.3 plots the acetonitrile destruction after 60 minutes versus the

persulfate concentration, which shows a linear dependence on the log of the persulfate concentration.

The decreasing extent of acetonitrile destruction with increasing persulfate concentration, even though the mole ratio of persulfate to acetonitrile is fixed, is suggestive of the effects of increasing absorption of the UV radiation as the persulfate concentration increase (a so-called "inner filter" effect), which causes a steady decrease in the penetration depth. From the known concentrations and extinction coefficient of persulfate, the UV penetration depth is estimated to vary from about 9 cm at a persulfate concentration of 0.06 g/L, decreasing by a factor of ten for each tenfold increase in persulfate concentration, reaching 0.009 cm at 60 g/L. This can be compared with the path length through the fluid of 0.5 cm. Thus, at the higher persulfate concentrations, only a small fraction of the fluid is exposed to the UV radiation. At high concentrations with no mixing there is the potential for generation of a boundary layer in which the reaction proceeds, but which causes reaction beyond that layer to be subject to diffusional mass transport limitations. This effect would be expected to be particularly strong in the micro-reactor since there is no mixing of the fluid. However, as discussed below, a similar effect was evident in the corresponding large reactor tests, which did include mixing.

4.1.3 Tests with Steam Stripping Simulant and Peroxide

Micro-reactor tests were performed with the steam stripping simulant with concentrations of acetonitrile of 60 g/L and 6 g/L with peroxide added to achieve a mole ratio of peroxide to acetonitrile of 1.5. The results are shown in Table 4.3. The extent of acetonitrile destruction is lower that for the corresponding tests with persulfate. As with the persulfate tests, the extent of destruction decreases with increasing oxidant concentration at fixed oxidant to acetonitrile mole ratio.

4.1.4 Steam Stripping Simulant: Acetate Formation

The hydrolysis of nitriles typically involves conversion first to the amide and then to the carboxylic acid. Thus, acetonitrile would convert to acetamide and then to acetate. It was therefore of interest to analyze the fluids from the micro-reactor tests with the steam stripping simulant for acetate. However, it should be noted that in the UV/OX system, it is likely that all organics would be subject to some level of destruction.

The results of the analysis for acetate are shown in Table 4.4. The results clearly show the presence of acetate as a decomposition product. For both the persulfate and peroxide tests, the acetate concentrations decrease systematically with decreasing acetonitrile concentration.

The measured concentrations of acetate are a consequence of both its generation via the destruction of acetonitrile and the destruction of acetate via oxidation. The acetate concentrations are generally a few percent of the initial acetonitrile concentrations, and the absolute concentrations are uniformly lower for the persulfate tests than for the corresponding peroxide

tests. Nevertheless, such intermediate organics contribute to the total organic carbon and may need to be considered in prospective waste disposition pathways.

4.2 Large Reactor Tests

4.2.1 Tests with Complex Simulant and Peroxide

Table 4.5 shows the results of large reactor tests with the complex simulant; Test LR-1 shows the effect of UV without any oxidant while tests LR-2 and LR-16 show the effects of peroxide with a lamp power of 450 W and 4800 W, respectively. The results are plotted in Figure 4.4.

4.2.2 Tests with Complex Simulant and Persulfate

Table 4.6 shows the results of large reactor tests with the complex simulant and three values of the mole ratio of persulfate to acetonitrile and lamp powers of 450 W and 4800 W. Figure 4.5 shows the effect of mole ratio at fixed power; Figure 4.6 shows the effect of power at a mole ratio of 1.5; and Figure 4.7 shows the effect of power at a mole ratio of 6.

4.2.3 Tests with Complex Simulant and Peroxide: Acetamide and Acetate

Table 4.7 shows the results of large reactor tests with the complex simulant spiked with either acetamide or acetate; no acetonitrile was added. Peroxide was added at a mole ratio of peroxide to acetate of 1 and peroxide to acetamide of 2. The tests were designed to have twice the amount of radicals needed to completely convert each parent compound and subsequent reaction products (1.5 moles H_2O_2 needed per mole of acetonitrile, 1 mole H_2O_2 needed per mole of acetamide, and 0.5 moles of H_2O_2 needed per mole of acetate). The reaction progress was monitored via the acetate concentration, which would be expected to increase as a result of the decomposition of acetamide and decrease as a result of the decomposition of acetate. These trends are clearly evident in the data. Complete conversion of the 115 mg/L of added acetamide would yield 117 mg/L of acetate. However, the value measured at 60 minutes in Test LR-3 is about twice this. We have checked all of the logbook records and they all support the addition of the intended amount of acetamide. However, the only explanation that we have is that the acetamide might have actually been added twice. In Test LR-4, the added acetate concentration decreases by about 50% after 60 minutes.

4.2.4 Tests with Complex Simulant and Peroxide: Other Organics

Table 4.8 shows the results of large reactor tests with the complex simulant spiked with the other organics listed in Table 3.3. Peroxide was added at a mole ratio of peroxide to acetonitrile of 3 and at that same concentration of peroxide in the two tests that did not include acetonitrile. The reaction progress was monitored via the concentrations of acetone, acrylonitrile,

and methyl ethyl ketone (MEK). For Tests LR-2 and LR-16, which also included acetonitrile, the acetonitrile results are discussed in Section 4.2.1 and listed in Table 4.5. The results from the tests at the lower lamp power show that the relative ease of destruction is in the order acrylonitrile > MEK > acetone. However, in the test at higher power, little difference is discernable. The extent of destruction of acetone and acrylonitrile increases with increasing bicarbonate (or total CO_2 species), especially at early times; any effect is less clear for MEK.

It is worth noting that Test LR-16 directly mimics the full-scale ETF operations, and the results indicate that a large fraction of the acetone, acrylonitrile, and MEK will be destroyed during normal operations with a residence time of approximately 3.6 minutes.

4.2.5 Tests with Steam Stripping Simulant and Persulfate

Table 4.9 shows the results of tests with the steam stripping simulant with concentrations of acetonitrile of 60 g/L and 6 g/L with persulfate added to achieve mole ratios of persulfate to acetonitrile of 1.5 or 3. One test was performed without persulfate as a control. Four of the tests were performed with the 450 W lamp and one was performed with the 4800 W lamp. There was minimal destruction without persulfate. As was found in the micro-reactor tests, the extent of destruction was lower at the higher persulfate concentration. This is further supported by comparison of the results for Test LR-S2 and LR-S3, where the only difference is the higher mole ratio for LR-S3, which results in a higher persulfate concentration and a slightly *lower* extent of destruction. Figure 4.8 compares the results from Tests LR-S3 and LR-S5, which differ only in the lamp power; the results show considerably higher destruction at the higher power.

4.2.6 pH and Temperature for Large Reactor Tests

The large reactor is equipped with pH, temperature, and pressure sensors for monitoring these parameters throughout testing. These data were recorded using a custom LabVIEW control and data acquisition system and are shown in Figures 4.9 and 4.10. All tests were conducted starting with the fluid at room temperature and there was typically a gradual temperature rise (~5 - 10°C) over the course of the test. For the tests with the 450 W lamp, the rate of temperature change was roughly constant during each test. For the tests with the 4800 W lamp, there was an initial rapid rise after which point the temperature stabilized at abut 31°C. The temperature control was somewhat better for the tests with the 4800-W lamp because those tests were conducted later and used a higher capacity cooling system.

In all tests except for LR-4, the pH decreased from its initial value. LR-4, which is the test with acetate as the only organic with peroxide, showed a slight increase, likely due to the destruction of acetate. The corresponding test with acetamide (LR-3), showed a significant decrease, which is likely a result of the production of acetate.

Interestingly, both tests with acetonitrile but without any oxidant also showed decreases in pH, small for Test LR-1 with 80 mg/L acetonitrile and larger for Test LR-S4 with 6 g/L

acetonitrile, which is consistent with the small but detectable measured decrease in the acetonitrile concentration.

The pH generally decreased more rapidly and reached lower final values for the tests with persulfate than those with peroxide. Test with persulfate generally reached a final pH around 2 but approached pH 1 for some of the tests with the steam stripping simulant (LR-S1 and LR-S5).

The three tests with the 4800 W lamp with persulfate (LR-17, LR-18, and LR-S5) show a double step decrease in pH at early times that is not evident in the tests with the 450 W lamp. We believe the first step is due to slight leakage of the UV light around the metal shutter during the lamp warm up period; the second step occurs when the shutter is opened.

SECTION 5.0
PROCESS MODELING

This section describes an analysis of the observed acetonitrile destruction data in terms of simple kinetic models to determine rate constants that together allow for extrapolation of the results to project the performance of the full-scale ultra-violet/oxidation (UV/OX) system at ETF. The approach follows closely that reported previously [9] with modifications as described below.

A variety of models for UV/OX processes in general, and persulfate processes in particular, have been reported, many of which employ reaction networks involving dozens of reactions [11, 13, 15, 16, 27, 28, 29]. The model developed previously [9], included kinetic equations for several chemical reactions as well as:

- Effect of UV intensity at wavelengths other than 254 nm;
- Effects of non-planar geometry;
- Effects of reflections from stainless steel reactor surfaces.

The key elements of the model are summarized below.

5.1 UV Power Absorbed

The model considers a UV/OX reactor composed of coaxial cylinders of length L. The inner cylinder of radius r_1 is the UV source and the outer cylinder of radius r_2 is the body of the reaction cell; the annulus between the cylinders contains the fluid that is being treated. If we define I_0 as the incident intensity (at r_1), then the energy absorbed per unit time (power) per unit volume of liquid is [9]:

$$P_v = \frac{2r_1}{r_2^2 - r_1^2} I_0 (1 - \mu e^{-2c\varepsilon'(r_2 - r_1)} - (1 - \mu) e^{-c\varepsilon'(r_2 - r_1)}), \qquad (5.1)$$

where c is the concentration of the absorbing species (persulfate or peroxide in the present work) in the solution, μ is the reflectance of the surface at r_2, and ε' is the Naperian extinction coefficient of the absorbing species. The reflectance of UV at about 254 nm from stainless steel is about 40% [28]. The relationship between Naperian and decadic extinction coefficients, ε, is:

$$\varepsilon' = \varepsilon \ln 10;$$

typically, decadic extinction coefficients are the values quoted in the literature.

5.2 Kinetic Model for Persulfate

The kinetic model for persulfate developed previously [9] is summarized in this section. We consider a simple model that employs just two reactions: the photolysis of persulfate to produce sulfate radical ions and the subsequent reaction of those radical ions with acetonitrile:

$$S_2O_8^{2-} + h\nu \rightarrow 2SO_4^{-\bullet} \tag{5.2}$$

$$SO_4^{-\bullet} + CH_3CN \rightarrow decomposition\ products\,. \tag{5.3}$$

The rate equation for the persulfate concentration as a result of its consumption via Eq. 5.2 is:

$$\frac{d[S_2O_8^{2-}]}{dt} = -(\Phi KP_v)_{254} - (\Phi KP_v)_{185}, \tag{5.4}$$

where Φ is the quantum yield for Eq. 5.2 and K is the number of moles of photons of frequency ν per joule; the first term on the right is for absorption at 254 nm and the second is for absorption at 185 nm. Note that P_v, which is given by Eq. 5.1, depends on the concentration of the absorbing species (persulfate) through $c = [S_2O_8^{2-}]$.

The rate equation for the acetonitrile concentration as a result of its consumption via Eq. 5.3 is:

$$\frac{d[CH_3CN]}{dt} = -k_1[SO_4^{-\bullet}][CH_3CN]\,, \tag{5.5}$$

where k_1 is the rate constant for Eq. 5.3.

Finally, the rate equation for the sulfate radical ion concentration as a result of its generation via Eq. 5.2 and consumption via Eq. 5.3 is:

$$\frac{d[SO_4^{-\bullet}]}{dt} = (2\Phi KP_v)_{254} + (2\Phi KP_v)_{185} - k_1[SO_4^{-\bullet}][CH_3CN]. \tag{5.6}$$

In the present work, based on the lamp characteristics listed in Table 2.1, only a single UV line (at 254 nm) was used and all of the UV power was allocated to that line. Thus, Eq. 5.4 becomes:

$$\frac{d[S_2O_8^{2-}]}{dt} = -(\Phi KP_v)_{254}\,, \tag{5.7}$$

and Eq. 5.6 becomes:

$$\frac{d[SO_4^{-\bullet}]}{dt} = (2\Phi KP_v)_{254} - k_1[SO_4^{-\bullet}][CH_3CN]. \tag{5.8}$$

With the initial concentrations of persulfate and acetonitrile together with the parameter values defined by the experimental conditions and values from the literature (see below), the only unknown is the rate constant k_1. Thus, this system of differential equations can be solved numerically and the value of k_1 determined by least squares regression to best fit the available data.

It is noted that the present model does not include acetamide or acetate, which are the expected degradation products of acetonitrile. The data for the hydrogen peroxide tests with acetamide and acetate (Section 4.2.3) show that these compounds are degraded at least as rapidly as acetonitrile. Corresponding tests with persulfate were not performed, however.

It is also noted that simplified models, such as those employed here, that do not include terminating reactions that quench each and every radical will predict that those radicals are still present at the end of the reaction, which is, of course, not realistic. Since it is well known that radical lifetimes are typically very short and that there are many diverse quenching mechanisms, even much more complex reaction networks often do not bother to address this issue. Furthermore, there are typically large number of radicals in play (for persulfate, for example, this includes $SO_4^{-\cdot}$, $HO^{\cdot}$, $S_2O_8^{-\cdot}$, $Cl^{\cdot}$, $Cl_2^{-\cdot}$, $ClO_2^{\cdot}$, $ClHO^{-\cdot}$, $CO_3^{-\cdot}$, etc.).

5.3 Kinetic Model for Peroxide

The kinetic model for peroxide developed previously [9] is summarized in this section. The model parallels closely the one for persulfate described above. We consider a simple model that employs just two reactions: the photolysis of peroxide to produce hydroxyl radicals and the subsequent reaction of those radicals with acetonitrile:

$$H_2O_2 + h\nu \rightarrow 2HO^{\bullet} \tag{5.9}$$

$$HO^{\bullet} + CH_3CN \rightarrow decomposition\ products. \tag{5.10}$$

The rate equation for the peroxide concentration as a result of its consumption via Eq. 5.9 is:

$$\frac{d[H_2O_2]}{dt} = -(\Phi KP_v)_{254} - (\Phi KP_v)_{185}, \tag{5.11}$$

where Φ is the quantum yield for Eq. 5.9 and K is the number of moles of photons of frequency ν per joule; the first term on the right is for absorption at 254 nm and the second is for absorption

at 185 nm. Note that P_v, which is given by Eq. 5.1, depends on the concentration of the absorbing species (peroxide) through $c = [H_2O_2]$.

The rate equation for the acetonitrile concentration as a result of its consumption via Eq. 5.10 is:

$$\frac{d[CH_3CN]}{dt} = -k_1[HO^\bullet][CH_3CN], \tag{5.12}$$

where k_1 is the rate constant for Eq. 5.10.

Finally, the rate equation for the hydroxyl radical concentration as a result of its generation via Eq. 5.9 and consumption via Eq. 5.10 is:

$$\frac{d[HO^\bullet]}{dt} = (2\Phi KP_v)_{254} + (2\Phi KP_v)_{185} - k_1[HO^\bullet][CH_3CN]. \tag{5.13}$$

In the present work, based on the lamp characteristics listed in Table 2.1, only a single UV line (at 254 nm) was used and all of the UV power was allocated to that line. Thus, Eq. 5.11 becomes:

$$\frac{d[H_2O_2]}{dt} = -(\Phi KP_v)_{254}, \tag{5.14}$$

and Eq. 5.13 becomes:

$$\frac{d[HO^\bullet]}{dt} = (2\Phi KP_v)_{254} - k_1[HO^\bullet][CH_3CN]. \tag{5.15}$$

As with the persulfate model, with the initial concentrations of peroxide and acetonitrile together with the parameter values defined by the experimental conditions and values from the literature (see below), the only unknown is the rate constant k_1. Thus, this system of differential equations can be solved numerically and the value of k_1 determined by least squares regression to best fit the available data.

5.4 Data Sets and Parameter Values

5.4.1 Overview

The data from the large reactor tests with the ETF complex simulant were used for modeling. When tests that did not include acetonitrile are excluded, this leaves five tests with persulfate (LR-7, LR-8, LR-9, LR-17, and LR-18) and two tests with peroxide (LR-2 and LR-16).

The values of the parameters in the model are listed in Tables 5.1 – 5.3. The intensities were calculated from the respective UV lamp specifications, as described in Section 5.4.2. Literature data were used for the quantum yield [11, 15, 26 - 31] and extinction coefficients of persulfate [11, 15, 26 - 31]; for the quantum yield and extinction coefficients of hydrogen peroxide [11, 29, 32]; and for the reflectance of stainless steel [33].

5.4.2 Calculation of Lamp Intensities

The lamp intensities were calculated in the same manner as described previously [9].

Large Reactor

The large reactor used two different lamps with specifications listed in Table 2.1. For each lamp, the UV power for all UV-B and UV-C lines was summed and assigned to the 254 nm line for the purpose of modeling. This information was used to calculate the intensities at r_1, which is I_0. It is noted, however, that, in principle, the two terms for the UV lines at 254 nm and 185 nm in Eqs. 5.4 and 5.11 (and, correspondingly, with the minus signs replaced by 2 in Eqs. 5.6 and 5.15) could be replaced by a sum over corresponding terms for each of the N UV lines listed in Table 2.1:

$$\sum_{i}^{N} -(\Phi K P_v)_i \, . \tag{5.16}$$

However, this requires knowledge of the quantum efficiency Φ and the extinction coefficient ε at every wavelength, which is not available; data for the quantum efficiency at wavelengths other than 254 nm are particularly sparse.

Many vendor specification sheets state that the intensity scales as the inverse square of the distance. However, while that is true for a point source, these lamps are essentially line sources. To address this, as in the previous work [9], a Gaussian-surface approach was employed whereby the total power emitted by the source (at a given wavelength) is equal to the integral of the intensity over a surface that completely encloses the source. This calculation is simplified if the enclosing surface is chosen to be at a constant distance from the source. Thus, if the source has a length L and radius r_1 and we enclose it with surface in the form of a coaxial cylinder of radius R with hemispherical end caps also of radius R (so that essentially all of the surface is the same distance from the source), and if the UV power emitted by the source is P, then the intensity at R is approximately:

$$I(R) = \frac{P}{(2\pi RL + \alpha 4\pi R^2)}, \tag{5.17}$$

where α is a "view factor" for the hemispherical end caps, which is expected to be less than one. Clearly, the intensity scales as $1/R^2$ only when $L/R << 1$. Conversely, if $L >> R$, then the intensity scales more like $1/R$. The view factor was estimated in the previous work [9] to be α = 0.72.

Finally, if we set $R = r_1$, with L = 140 mm (450 W lamp) or L = 164 mm (4800 W lamp), then this gives the incident intensity (I_0) that we need. The values obtained from this calculation are provided in Tables 5.1 and 5.2.

Micro-Reactor

The data from the micro-reactor were not modeled in the present work but the intensities are presented for reference. The micro-reactor used a Pen Ray UV Lamp 90-0012-10 lamp. For the micro-reactor, r_1 = 0.65 cm and r_2 = 1.15 cm. The vendor specifications for that lamp indicate a UV power of 4750 uW/cm^2 at 254 nm at a distance of 0.75 inches from the surface (22.3 mm from the axis) and the power at 185 nm being about 5% of that at 254 nm. Equation 5.17 was used to calculate the intensity by setting $R = r_1$ and L = 53.8 mm and, in the absence of other information, α was set equal to one. This gives values of I_0 of 0.0240 and 0.0012 W/cm^2 at 254 nm and 185 nm, respectively.

Full-Scale Reactor

For the full-scale reactor, the same approach used in the previous work [9] was used. The vendor specification for various high-power, medium-pressure lamps were used to estimate a UV power at 254 nm of about 15% of the electrical power and the power at 185 nm being about 5% of that at 254 nm. The electrical power for each lamp is stated as 27.5 kW.

Equation 5.17 was used to calculate the intensity by setting $R = r_1$ and L = 112.2 cm; as for the large reactor, α was set equal to 0.72. The values obtained from this calculation are provided in Table 5.3.

5.5 Modeling Results and Discussion

The models for persulfate and peroxide described above were implemented in Mathematica (Wolfram), which was used to solve the system of differential equations and find the optimum value of the rate constant k_1 by minimizing the χ^2 statistic. The calculation of χ^2 employed an experimental uncertainty in the measurement of the acetonitrile concentration of 10% plus 5.76 x 10^{-6} mol/L.

5.5.1 Persulfate Tests

Table 5.4 lists the fitted values of the rate constant k_1 for each of the five persulfate data sets. Each data set was fitted individually ('individual fit") and then all five data sets were fitted

simultaneously with a single k_1 ("global fit"). As shown in Table 5.4, the global fit value is close to the mean of the individual fit values. Figure 5.1 shows the variation of the χ^2 statistic with k_1 for each of the fits; χ^2 is considerably larger for the global fit than for the individual fits.

Figures 5.2 – 5.6 show the percentage acetonitrile destruction for each of the five data sets in comparison to the model results for the individual fits. Figures 5.7 – 5.11 show the corresponding predicted concentrations of all species for each of the five data sets.

The results in Table 5.4 show that the fitted values of k_1 increase systematically with $[S_2O_8^{2-}]$ and with lamp power. This is more clearly evident in Figure 5.12. In fact, the values of k_1 are well represented by:

$$k_1 = a_0 + a_1 I_0 + a_2 [S_2O_8^{2-}], \tag{5.18}$$

with a_0 = -0.09656, a_1 = 0.1937, and a_2 = 51.12, with R^2= 0.979, for k_1, $[S_2O_8^{2-}]$, and I_0 in units of L/(mol s), mol/L, and W/cm^2, respectively. This fit is shown as the lines in Figure 5.12. Clearly, the fact that k_1 is not constant and shows these systematic variations is indicative of deficiencies in the model. From a practical perspective, this is particularly important for modeling the full-scale ETF system since use of the mean value of k_1 or the global fit value will significantly underestimate the value that is relevant for the full-scale system because it employs a higher value of I_0 than most of the tests in the data set. Consequently, the values from the two tests at 4800 W, which correspond to an intensity that is very close to the value for the full-scale system, are the most relevant.

The systematic variation in k_1 and the deviation from the model, particularly for LR-17 shown in Figure 5.5, led us to explore an extended model, as described in Section 5.5.2.

5.5.2 Persulfate Tests – Extended Model

In an effort to address some of the observed deficiencies in the model described in Section 5.2, that model was extended to include an additional process that consumes sulfate radical ions. One of the most significant such reactions is the reaction with water according to [11, 15]:

$$SO_4^{-\bullet} + H_2O \rightarrow HO^{\bullet} + HSO_4^- \tag{5.19}$$

$$HO^{\bullet} + S_2O_8^{2-} \rightarrow HSO_4^- + SO_4^{-\bullet} + \tfrac{1}{2} O_2 . \tag{5.20}$$

These reactions consume and regenerate a sulfate radical ion but the net result is the destruction of one persulfate ion. The rate equation for the hydroxyl radical concentration is then:

$$\frac{d[HO^{\bullet}]}{dt} = k_3 [H_2O][SO_4^{-\bullet}] - k_4 [HO^{\bullet}][S_2O_8^{2-}] . \tag{5.21}$$

If we assume a steady state for $[HO^{\bullet}]$, then $d[HO^{\bullet}]/dt = 0$ and therefore:

$$k_3[H_2O][SO_4^{-\bullet}] = k_4[HO^{\bullet}][S_2O_8^{2-}]. \quad (5.22)$$

We next add this new consumption mechanism into the rate equation for $[S_2O_8^{2-}]$ (Eq. 5.7) to give:

$$\frac{d[S_2O_8^{2-}]}{dt} = -(\Phi K P_v)_{254} - k_4[HO^{\bullet}][S_2O_8^{2-}]; \quad (5.23)$$

Substituting Eq. 5.22, we obtain:

$$\frac{d[S_2O_8^{2-}]}{dt} = -(\Phi K P_v)_{254} - k_3[H_2O][SO_4^{-\bullet}]. \quad (5.24)$$

The net result is that in the extended model, Eq. 5.7 is replaced by Eq. 5.24 and one additional parameter (k_3) is added; however, it is convenient to take that parameter to be $k_3[H_2O]$ since $[H_2O]$ is essentially constant at about 55.6 mol/L. The five data sets for tests with persulfate were then reanalyzed with this model, as described below. The analysis included provisions to prevent the concentrations from going negative, which is otherwise possible via Eq. 5.24.

Table 5.5 lists the fitted values of the rate constants k_1 and $k_3[H_2O]$ for each of the five persulfate data sets. Each data set was fitted individually ('individual fit") and then all five data sets were fitted simultaneously with a single pair of k_1 and $k_3[H_2O]$ values ("global fit"). Figures 5.13 – 5.17 show the percentage acetonitrile destruction for each of the five data sets in comparison to the model results for the individual fits. Figures 5.18 – 5.22 show the corresponding predicted concentrations of all species for each of the five data sets. The fits with the extended model are greatly improved compared to those with the original model.

Also shown in Table 5.5 are the results for the global fit. For the global fit, Figure 5.23 shows the variation of the χ^2 statistic with k_1 for values of $k_3[H_2O]$ at and around the best-fit value.

As is evident in Table 5.5, for Test LR-18, both the k_1 and $k_3[H_2O]$ values are vastly greater than the corresponding values for the other four tests. This is due to the very large influence of the second data point and a relatively flat χ^2 surface. This is illustrated in Figure 5.24, which shows the model results for Test LR-18 for various combinations of k_1 and $k_3[H_2O]$. These values are therefore not reliable and are excluded from the means shown in Table 5.5.

Despite the significant improvements in the fits, the results in Table 5.5 show that the fitted values of k_1 and $k_3[H_2O]$ increase systematically with $[S_2O_8^{2-}]$ and with lamp power, as was observed for k_1 with the original model. This is more clearly evident in Figures 5.25 and 5.26. In fact, the values of k_1 (excluding Test LR-18) are well represented by:

$$k_1 = b_0 + b_1 I_0 + b_2 [S_2O_8^{2-}], \quad (5.25)$$

with b_0 = -0.05675, b_1 = 3.657, and b_2 = 52.39, with R^2= 0.9997, for k_1, $[S_2O_8^{2-}]$, and I_0 in units of L/(mol s), mol/L, and W/cm^2, respectively. This fit is shown as the lines in Figure 5.25. Similarly, the values of $k_3[H_2O]$ (excluding Test LR-18) are well represented by:

$$k_3[H_2O] = d_0 + d_1 I_0 + d_2 [S_2O_8^{2-}], \quad (5.26)$$

with d_0 = -0.00335, d_1 = 0.1041, and d_2 = 0.8517, with R^2= 0.999997, for $k_3[H_2O]$, $[S_2O_8^{2-}]$, and I_0 in units of 1/s, mol/L, and W/cm^2, respectively. This fit is shown as the lines in Figure 5.26.

As noted above, the fact that k_1 and $k_3[H_2O]$ are not constant and show these systematic variations indicates that deficiencies still remain in the model. From a practical perspective, this is particularly important for modeling the full-scale ETF system since use of the mean value of k_1 or the global fit value will significantly underestimate the value that is relevant for that system because it employs a higher value of I_0 than most of the tests in the data set. Consequently, the values from the two tests at 4800 W, which correspond to an intensity that is very close to the value for the full-scale system, are the most relevant. However, as discussed above, the fit parameters for Test LR-18 are relatively poorly determined by simple fitting without additional constraints. One approach to this issue is to use the correlations in Eqs. 5.25 and 5.26 to obtain extrapolated values for k_1 and $k_3[H_2O]$ for Test LR-18, as shown in Table 5.5. In this way, the results from the other four tests are used to constrain the fit to Test LR-18. As shown in Table 5.5, if $k_3[H_2O]$ is fixed at the extrapolated value, the fit to the Test LR-18 data yields a value of k_1 very close to the extrapolated value. It is noteworthy also that these values are very close to the corresponding values obtained from the fit to the data for Test LR-17, which was also performed with the 4800 W lamp; both tests (LR-17 and LR-18) employed an intensity (I_0) that is essentially identical to that for the full-scale system. These fit parameter values are therefore the ones that are recommended for projecting the performance of the full-scale ETF system.

5.5.3 Peroxide Tests

Table 5.6 lists the fitted values of the rate constant k_1 for each of the two peroxide data sets. Each data set was fitted individually ('individual fit") and then both data sets were fitted simultaneously with a single k_1 ("global fit"). As shown in Table 5.6, the global fit value is close to the mean of the individual fit values. Figures 5.27 and 5.28 show the percentage acetonitrile destruction for each of the data sets in comparison to the model results. Figures 5.29 and 5.30 show the predicted concentrations of all species for each of the two data sets. The fit for Test LR-2 is considerably better than that for LR-16, which shows similar deviations to those seen for LR-17 in Figure 5.5. Although there are only two data sets, the value of k_1 is again higher for the test with the higher lamp intensity.

5.6 Full-Scale ETF System

The full-scale ETF UV/OX system is a Calgon Rayox system that employs three parallel units, each with eight reaction chambers fitted with 27.5 kW lamps [34]. The residence time is 3.62 minutes for the eight chambers or 0.45 minutes for each chamber. As in the previous work [9], the modeling was performed for a single chamber since the additional chambers simply increase the residence time. The parameter values for the full-scale ETF UV/OX system are summarized in Table 5.3; parameters not listed have the same values as were used in the modeling of the test system data. These values were used in the extended persulfate model and the peroxide model together with various sets of fitted values of k_1 and $k_3[H_2O]$ and persulfate and peroxide concentrations to calculate the acetonitrile destruction as a function of time. The results are shown in Figures 5.31 and 5.32. Since the ETF system is a flow-through system, here, the time can be interpreted as the residence time of the fluid in the reactor. The selected persulfate concentration of 0.00420 mol/L corresponds to 1000 mg/L of $Na_2S_2O_8$ for comparison to the previous work [9]; the value of 0.0170, which is about four times higher, corresponds to ten times the stoichiometric ratio. The selected peroxide concentration of 0.00339 mol/L corresponds to the stoichiometric ratio; the value of 0.0294, which is about ten times higher, corresponds to 1000 mg/L of H_2O_2 for comparison to the previous work [9];

The projected acetonitrile concentration in the feed from WTP to ETF is 46.4 mg/L and the ETF discharge limit is 1.2 mg/L (2.93×10^{-5} mol/L) [20], which is indicated on Figure 5.32. Therefore, the minimum required decontamination factor (DF) is 38.7 in the total system residence time of 3.62 minutes (217 seconds).

As shown in Figures 5.31 and 5.32, in all cases, the rate of destruction increases with increased oxidant concentration. For persulfate, the global fit results do not meet the ETF requirement at either concentration. However, as discussed in Section 5.5.2, the global fit underestimates the rate at higher intensities and concentrations and the extrapolated parameters are therefore preferred. The results with the extrapolated parameters show that the requirement can be achieved with persulfate: at 3.62 minutes, the predicted concentration of acetonitrile is 0.494 mg/L. As observed previously [9], persulfate clearly shows superior performance for acetonitrile destruction than hydrogen peroxide.

Figure 5.33 shows the time required to meet the 1.2 mg/L acetonitrile limit as a function of the initial persulfate concentration as calculated from the extrapolated persulfate model. An initial persulfate concentration of 0.0123 mol/L is required to meet this limit in 3.62 minutes.

Figure 5.34 shows the combinations of k_1 and $[S_2O_8^{2-}]$ that are needed to meet the required ETF DF in 3.62 minutes based on the extended model when $k_3[H_2O]$ is fixed at its global fit value; combinations above and to the right of the line meet the requirement whereas those below and to the left do not.

SECTION 6.0
SUMMARY AND RECCOMENDATIONS

The primary objective of this work was to perform an evaluation of the efficacy of potential methods for the destruction of acetonitrile in solutions representative of WTP secondary liquid effluents that would be fed to ETF for treatment under the DFLAW flow-sheet, building on the results from a previous study [9]. The testing evaluated irradiation with UV light alone and UV light in combination with sodium persulfate or hydrogen peroxide, based on the previous results [9]. In addition, WRPS is pursuing a steam stripping approach to remove acetonitrile from the feed to the ETF. In that approach, the stripped acetonitrile would be concentrated in a stream that is essentially pure water with high concentrations of acetonitrile. The present work therefore also evaluated the potential for a persulfate UV/OX process to destroy acetonitrile in that stream. In summary, therefore, this work addressed: (i) The destruction of acetonitrile at relatively low concentrations (tens of ppm) in representative ETF feed simulants and (ii) The destruction of acetonitrile at much higher concentrations (up to tens of grams per liter) in pure water, representative of the steam stripping stream. A further objective of this work was to perform testing at a larger-scale and with higher UV power in a configuration that is more closely representative of the UV/OX system at the ETF.

The testing with the ETF feed simulants addressed the impacts of persulfate concentration, acetonitrile concentration, the presence of other organics expected to be present in the ETF feed, and the presence of potential radical scavengers on the rate and extent of acetonitrile destruction using UV/OX with persulfate. Radical scavengers that were considered include ammonium, chloride, nitrate, and bicarbonate. Testing was also performed with the existing ETF treatment method of UV/OX with hydrogen peroxide as a baseline to compare with the persulfate results.

The testing was conducted at two scales. One set of tests was conducted in the same micro-scale (16 mL) reactor system used in the previous work [9]. A second set of tests was conducted on a new larger (~14 L) reactor system that was designed and constructed for this testing. The new reactor system represents a full-scale transverse section through one of the ETF full-scale reactor tubes. This test system was designed such that the UV lamp power could be varied and could achieve the same UV intensity as the full-scale system.

The results from this work were analyzed in terms of simple kinetic models to extract rate constants. The results were then used to project the extent of acetonitrile destruction expected for the full-scale ETF UV/OX system with either persulfate or peroxide.

The principal findings from this work include:

- Persulfate with UV was consistently more effective than peroxide with UV for destruction of acetonitrile.

- The kinetic models that were developed provide reasonable representations of the data on acetonitrile destruction. However, there are clearly still aspects of the mechanism that are not captured. In particular, adjustments to the models were required to describe the observed dependence on UV intensity, and the peroxide model (albeit with a much more limited data set) did not perform as well as the persulfate model.
- Ammonium and chloride showed the largest effects in reducing the extent of destruction of acetonitrile by persulfate.
- Results for the micro-reactor tests with the steam stripping simulant showed a clear systematic increase in the extent of acetonitrile destruction with decreasing persulfate concentration, possibly due to the absorption of UV by persulfate. Similar effects were seen in the large-scale tests.
- Acetate is formed as a decomposition product of acetonitrile. Acetamide, which is a likely intermediate, is converted to acetate in the UV/OX process.
- For peroxide, the results from the tests with the 450-W lamp in the large reactor show that the relative ease of destruction is in the order acrylonitrile > MEK > acetone. However, the test with the 4800-W lamp in the large reactor, showed complete degradation of all three compounds at the first sampling event (5 minutes).
- For peroxide, the extent of destruction of acetone and acrylonitrile *increases* with increasing bicarbonate (or total CO_2 species), especially at early times; any effect is less clear for MEK.
- The model projections for the full-scale ETF UV/OX system indicate that that system, with its assumed fluid residence time of 3.62 minutes, could meet the required acetonitrile destruction efficiency in that time with persulfate.
- The modeling results highlight the importance of testing at large scale and with near-prototypic UV intensities. Considerable care must be exercised in translating the results from tests conducted at lower UV intensities to full-scale systems that use much higher intensities.

Overall, the results from this work indicate that the UV-persulfate process is far superior to the UV-peroxide process for destruction of acetonitrile and can achieve the required destruction efficiencies for acetonitrile and the other organics expected to be present in the feed to ETF. However, there are many details that would still need to be addressed to support selection and implementation of this process and to define the system modifications that might be necessary. Accordingly, additional testing is recommended to further develop and characterize this process. The new large reactor test system with variable UV power capability provides a valuable platform for further development. Additional testing should include:

- Testing to further assess the effects of UV power through systematic variations in the UV power while keeping other test parameters fixed. The effects of UV intensity need to be better defined in order to address some of the deficiencies in the kinetic model.

- Further testing of the effects of persulfate concentration to support refinement of the kinetic model.
- Further refinement of the kinetic model to better capture the effects of UV intensity and persulfate concentration. Assess possible further expansion of the reaction network.
- Additional testing at high UV power (full-scale intensity) at shorter times (less than about 5 minutes) to better define the early reaction kinetics and improve the model.
- The results from the previous tests showed a greatly reduced extent of destruction for the complex simulant as compared to the simple simulant. This effect appears to exceed what would be expected on the basis of the results of the one-at-a-time variations performed in the present work. Additional testing is required to better understand this difference. A subtractive, as compared to an additive approach is recommended whereby selected anions are removed one-at-a-time from the complex simulant. Such information could provide the basis for potential mitigation of this interference.
- Testing to further define the residual concentrations of organic reaction products, such as acetate and acetamide, since these contribute to total organic carbon, which may be subject to discharge limits.
- Testing would be useful to investigate the potential benefits of sensitizers and radical enhancers that could increase the effectiveness of persulfate and increase the rate of destruction.
- The impact of UV/OX processes of the speciation and fate of radio-iodine is of potential concern and should be evaluated in future tests.

SECTION 7.0
REFERENCES

[1] "Compilation of Off-Gas Vapor and Liquid Phase Organic Information from Scale Melter Testing of LAW Simulants," K.S. Matlack and I.L. Pegg, VSL-17S4450-1, Rev. 0, Vitreous State Laboratory, The Catholic University of America, Washington, DC, 12/13/17.

[2] "Estimates of Acetonitrile Generation from Scale Melter Testing of LAW Simulants," K.S. Matlack and I.L. Pegg, Summary Report, VSL-19S4573-1, Rev. A, Vitreous State Laboratory, The Catholic University of America, Washington, DC, 10/10/19.

[3] "DFLAW Glass and Feed Qualifications with AP-107 to Support WTP Start-Up and Flow-Sheet Development," K.S. Matlack, H. Abramowitz, I.S. Muller, I. Joseph, and I.L. Pegg, Final Report, VSL-18R4500-1, Rev. 0, Vitreous State Laboratory, The Catholic University of America, Washington, DC, 9/27/18.

[4] "EMF Evaporation Testing to Support WTP Start-Up and Flowsheet Development," K.S. Matlack, H. Abramowitz, M. Brandys, and I.L. Pegg, Final Report, VSL-19R4640-1, Rev. 0, Vitreous State Laboratory, The Catholic University of America, Washington, DC, 9/30/19.

[5] "Testing to Address Flowsheet Gaps for DFLAW Startup and Operations," Statement of Work, Requisition # 328892, Washington River Protection *Solutions*, Richland, WA, July 1, 2019.

[6] "Treatment for Acetonitrile," M. Brandys and I.L. Pegg, Summary Report, VSL-19S4730-1, Rev. 0, Vitreous State Laboratory, The Catholic University of America, Washington, DC, 10/20/19.

[7] "Acetonitrile Destruction in ETF Feed Solutions by UV/OX and Persulfate," Statement of Work, Requisition # 334406, Rev. 0, Washington River Protection *Solutions*, Richland, WA, January 7, 2020.

[8] "Acetonitrile Destruction in ETF Feed Solutions by UV/OX and Persulfate," M. Brandys, H. Abramowitz, and I.L. Pegg, Test Plan, VSL-20T4850-1, Rev. 0, Vitreous State Laboratory, The Catholic University of America, Washington, DC, 4/29/20.

[9] "Testing of UV Oxidation Process for Acetonitrile Destruction," M. Brandys, N.A. Mecholsky, H. Abramowitz, R. Cecil, and I. L. Pegg, Final Report, VSL-20R4730-1, Rev. 0, Vitreous State Laboratory, The Catholic University of America, Washington, DC, 7/31/20.

[10] "A Review on the Degradation of Organic Pollutants in Waters by UV Photoelectro-Fenton and Solar Photoelectro-Fenton," E. Brillas, J. Braz. Chem. Soc., 25, 393 (2014).

[11] "Degradation of Acetonitrile Residues Using Oxidation Processes," R.C. da C. M. Micaroni, M. Izabel, M.S. Bueno, and W. de F. Jardim, J. Braz. Chem. Soc., 15, 509 (2004).

[12] "Photocatalytic Oxidation of Acetonitrile in Gas–Solid and Liquid–Solid Regimes," M. Addamo, V. Augugliaro, S. Coluccia, M. Giulia Faga, E. Garcia-Lopez, V. Loddo, G. Marci, G. Martra, and L. Palmisano, Journal of Catalysis 235, 209 (2005).

[13] "Photocatalytic Oxidation of Acetonitrile in Aqueous Suspension of Titanium Dioxide Irradiated by Sunlight," V. Augugliaro, A. Bianco Prevot, J. Caceres Vazquez, E. Garcıa-Lopez, A. Irico, V. Loddo, S. Malato Rodrıguez, G. Marcı, L. Palmisano, and E. Pramauro, Advances in Environmental Research, 8, 329 (2004).

[14] "Sulfate Radical-Based Water Treatment in Presence of Chloride: Formation of Chlorate, Inter-Conversion of Sulfate Radicals into Hydroxyl Radicals and Influence of Bicarbonate, H. V. Lutze, N. Kerlin, T. C. Schmidt, Water Research, 72, 349 (2015).

[15] Ferrioxalate-Mediated Solar Degradation of Organic Contaminants in Water," A. Safarzadeh-Amiri, J. R. Bolton, and S. R. Cater, Solar Energy, 56, 439, (1996).

[16] Synergistic Effect Between UV and Chlorine (UV/Chlorine) on the Degradation of Carbamazepine: Influence Factors and Radical Species," W. Wang, Q. Wu, N. Huang, T. Wang, and H. Hu, Water Research, 98, 190 (2016).

[17] "Review of Photochemical Reaction Constants of Organic Micropollutants Required for UV Advanced Oxidation Processes in Water," B.A. Wols and C.H.M. Hofman-Caris, Water Research, 46, 2815 (2012).

[18] "Impact of Chloride Ions on UV/H2O2 and UV/Persulfate Advanced Oxidation Processes," W. Zhang, S. Zhou, J. Sun, X. Meng, J. Luo, D. Zhou, J. Crittenden, Environ. Sci. Technol., 52, 7380 (2018).

[19] "Oxidation Mechanisms of the UV/Free Chlorine Process: Kinetic Modeling and Quantitative Structure Activity Relationships," S. Zhou, W. Zhang, J. Sun, S. Zhu, K. Li, X. Meng, J. Luo, Z. Shi, D. Zhou, and J. C. Crittenden, Environ. Sci. Technol., 53, 4335, (2019).

[20] "Quality Assurance Project Plan for WRPS Support Activities Conducted by VSL," VSL-QAPP-WRPS, Rev. 5, Vitreous State Laboratory, The Catholic University of America, Washington, DC, 9/30/19.

[21] "Master List of Controlled VSL Manuals and Standard Operating Procedures in Use," QA-MLCP, Rev. 174, Vitreous State Laboratory, The Catholic University of America, Washington, DC, 9/28/20.

[22] "Simulant for Acetonitrile Tests," R. Skeen, email to I. Joseph and I.L. Pegg, Washington River Protection *Solutions*, Richland, WA, 8/8/19; HNF-3172_ETF_Profile_RevC_2018, "Waste Profile Sheet for Liquid Effluent Retention Facility and Effluent Treatment Facility," Bechtel National. Inc., Richland WA.

[23] "Assessment of Effluent Treatment Facility's Ultraviolet Oxidation System Capability to Treat Direct Feed Low Activity Waste Effluents from the Waste Treatment and Immobilization Plant," A. B. Carlson, A.G. Miskho, and W. L. Willis, Washington River Protection *Solutions*, Richland, WA, August 2019.

[24] "Target Organics," M. Landon email to I. Joseph, Washington River Protection *Solutions*, Richland, WA, 9/11/19.

[25] "Ammonia Remediation in Hanford WTP Liquid Secondary Waste," H. Abramowitz, M. Brandys, C. Viragh, and I. L. Pegg, Final Report, VSL-18R4550-1, Rev. 0, Vitreous State Laboratory, The Catholic University of America, Washington, DC, 9/18/18.

[26] "Probing the Radical Chemistry in UV/Persulfate-Based Saline Wastewater Treatment: Kinetics Modeling and Byproducts Identification," R. Yuan, Z. Wang, Y. Hub, B. Wanga, S. Gao, Chemosphere, 109, 106 (2014).

[27] "UVA-UVB Activation of Hydrogen Peroxide and Persulfate for Advanced Oxidation Processes: Efficiency, Mechanism and Effect of Various Water Constituents," W. Huang, A. Biancoa, M. Brigantea, and G. Mailhot, J. Hazardous Materials, 347, 279 (2018).

[28] "The Photolysis of Potassium Peroxodisulphate in Aqueous Solution in the Presence of tert-Butanol: a Simple Actinometer for 254 nm Radiation," G. Mark, M.N. Schuchmann, H.-P. Schuchmann, C. von Sonntag, J. Photochem. Photobiol. A: Chemistry, 55, 157 (1990).

[29] "A Mechanistic Understanding of the Degradation of Trace Organic Contaminants by UV/Hydrogen Peroxide, UV/Persulfate and UV/Free Chlorine for Water Reuse, W. Li, T. Jain, K. Ishida and H. Liu, Environ. Sci.: Water Res. Technol., 3, 128 (2017).

[30] "Degradation of Acetic Acid with Sulfate Radical Generated by Persulfate Ions Photolysis," J. Criquet, N. Karpel, V. Leitner, Chemosphere, 77 194 (2009).

[31] "On the Photolysis of Simple Anions and Neutral Molecules as Sources of O^-/OH, SO_x^- and Cl in Aqueous Solution," H. Herrmann, Phys. Chem. Chem. Phys., 9, 3935 (2007).

[32] "A Spectrophotometric Method for Measuring the Breakdown of Hydrogen Peroxide by Catalase," J. Biol. Chem., 195, 133 (1952).

[33] "Procedures and Standards for Accurate Spectrophotometric Measurements of Specular Reflectance, J.C. Zwinkels, M. Noel, and C.X. Dodd, Applied Optics, 33, 7933 (1994).

[34] "Comments to Organic Destruction Test Plan," R.S. Skeen, email to I.L. Pegg, Washington River Protection *Solutions*, Richland, WA, 4/6/20.

Table 2.1. Vendor Specifications for the Two Hanovia Medium Pressure Mercury UV Lamps Used in the Large Reactor.

Lamp Model		**PC451.050**	**6906A453**
Lamp Power (nom.), [W]		450	4800
Lamp Voltage, $[V]_{rms}$		135±10	390±20
Lamp Current, $[A]_{rms}$		3.5	12.5
Mercury Line, [nm]	Band	Radiated Energy, [W]	
1367.3	IR	2.6	36.9
1128.7		3.3	25.2
1014.0		10.5	115
578.0 (Y)	VIS	20.0	252
546.1 (G)		24.5	147
435.8 (B)		20.2	193
404.5 (V)		11.0	88.1
366.0	UVA	25.6	353
334.1		2.4	25.2
313.0	UVB	13.2	184
302.5		7.2	120
296.7		4.3	55.3
289.4		1.6	16.1
280.4		2.4	50.6
275.3	UVC	0.7	15.3
270.0		1.0	17.7
265.2		4.0	101
257.1		1.5	22.9
253.7		5.8	87.7
248.2		2.3	36.9
240.0		1.9	26.6
238.0		2.3	30.6
236.0		2.3	22.6
232.0		1.5	27.8
222.4		3.7	33.5
Total, [W]		176	2086

Table 3.1. Simulant Composition for Parametric Tests (Right-Most Column).

Charged Species	**From Reference [19]**			**Simulant for the Present Work* (mg/L)**
	From HNF-3172_ETF_Profile _RevC_2018 (mg/L)	Charge Balanced Using HCO_3^- (mg/L)	After pH Adjustment with H_2SO_4 (mg/L)	
Na^+	1473.00	1473.00	1473.00	1473.00
K^+	0.03	0.03	0.03	-
Ca^{2+}	0.03	0.03	0.03	-
Mg^{2+}	0.00	0.00	0.00	-
Al^{3+}	0.02	0.02	0.02	-
NH_4^+	68.30	68.30	68.30	68.30
Cl^-	2.97	2.97	2.97	2.97
SO_4^{2-}	0.03	0.03	2102.00	-
HCO_3^-	1920.00	4119.00	4119.00	4119.00
$NO3^-$	16.20	16.20	16.20	16.20
NO_2^-	0.28	0.28	0.28	-
F^-	0.04	0.04	0.04	-
PO_4^{3-}	0.05	0.05	0.05	-

- Empty data field

* Simulant was charge balanced and adjusted to the pH specified for each test by addition of sulfuric acid or sodium hydroxide.

Table 3.2. Complex Simulant and Concentrate Recipes.

Source	Reagent Mass [g/L]	Reagent Mass [g/14L]	Concentrate (x28) [g/10L]
H_2SO_4	0.0368	0.5156	10.311
Na_2SO_4	4.518	63.25	1265
NH_4OH (58%)	0.2303	3.224	64.5
NaCl	0.0049	0.0686	1.372
$NaHCO_3$	0.0005	0.0067	0.1345
$NaNO_3$	0.0223	0.3125	6.249
H_2O	997	14962	9444

Table 3.3. Additional Organics: Target Concentrations and Recipes for Concentrate Solutions Used in Tests.

Constituent	CAS Number	Formula	Assay, %	Mw	d @ 20°C [g/ml]	Concentration [22]		Concentrate Solutions			
						[mg/L]	[µl/L]	µl/18ml ActN	mg/18ml ActN	µl/2ml Acetone	mg/2ml Acetone
2-Butoxyethanol	111-76-2	$C_6H_{14}O_2$	99.5	118.175	0.900	1.21	1.34	239	215	500	450
Acetone	67-64-1	C_3H_6O	99.5	58.080	0.785	4.24	5.40	961	754	2000	1569
bis(2-ethylhexyl) phthalate	117-81-7	$C_{24}H_{38}O_4$	98	390.562	0.985	0.400	0.41	73	72	153	151
Cresols (total as p-Cresol)	106-44-5	C_7H_8O	99.0	108.140	1.08	7.33	6.79	1212	1309	2537	2740
di-n-octyl pthalate	117-84-0	$C_{24}H_{38}O$	98	390.562	0.980	0.544	0.56	100	98	210	205
2-Butanone (MEK)	78-93-3	C_4H_8O	99.9	72.107	0.805	1.46	1.81	321	258	672	541
n-Nitrosodimethylamine	62-75-9	$C_2H_6N^2O$	98.3	74.082	1.01	0.0178	0.0176	3.2	3.2	6.6	6.7
Tri-n-butyl phosphate	126-73-8	$C_{12}H_{27}O_4P$	99	266.317	0.979	1.17	1.20	213	209	447	437
Acetonitrile (ActN)	75-05-8	C_2H_3N	99.8	41.052	0.786	80.0	101.8	18000	14148	0	0
Acrylonitrile (AcrN)	107-13-1	C_3H_3N	98	53.063	0.810	0.880	1.09	196	159	410	332
								[µl]	[mg]	[µl]	[mg]
							In 14.0 L Batch (equivalent of 1425 µl acetonitrile):	1688	1364	257	238

Table 3.4. Calculated Solution Speciations (Molal) for Large Reactor Tests with Carbon Dioxide Over-Pressure.

Species	Medium Bicarbonate Test LR-5 14.7 psi Air + 6 psi CO_2	High Bicarbonate Test LR-6 31.6 psi CO_2
CO_2 Fugacity (atm)	0.41	2.15
H_2CO_3 (aq)	0.0111	0.0583
HCO_3^-	0.00111	0.00462
$NaHCO_3$ (aq)	1.72E-05	7.20E-05
CO_3^{--}	1.99E-08	6.56E-08
$NaCO_3^-$	0.00E+00	2.24E-08
Total Carbon	0.0123	0.0630
Total Carbon as CO_3^{--} in mg/kg (ppm)	738	3780
CO_3^{--} in mg/kg (ppm)	1.19E-03	3.94E-03

Table 3.5. Test Matrix for Micro-Reactor Tests with ETF Simple Simulant.

Test	Simulant	Simulant Additive Concentration	Acetonitrile Concentration		Other Organics	$S_2O_8^{2-}$ to Acetonitrile Mole Ratio	$S_2O_8^{2-}$ Concentration		Test Purpose
			mg/L	M			M	mg/L	
10	Simple	--	80	1.95E-03	No	3	5.85E-03	1123	Test inhibition by simulant additives
11	Simple + NH_4^+	68.3 mg/L NH_4^+	80	1.95E-03	No	3	5.85E-03	1123	Test inhibition by individual simulant additive (NH_4^+)
12	Simple + Cl^-	2.97 mg/L Cl^-	80	1.95E-03	No	3	5.85E-03	1123	Test inhibition by individual simulant additive (Cl^-)
13	Simple + NO_3^-	16.2 mg/L NO_3^-	80	1.95E-03	No	3	5.85E-03	1123	Test inhibition by individual simulant additive (NO_3^-)
14	Simple + HCO_3^-	50 mg/L HCO_3^-	80	1.95E-03	No	3	5.85E-03	1123	Test inhibition by individual simulant additive (HCO_3^-)
15	Simple + Cl^-	7 g/L Cl^-	80	1.95E-03	No	3	5.85E-03	1123	Test mitigation of inhibition by Cl^- at high concentration

-- Empty data field

Table 3.6. Test Matrix for Large Reactor Tests with ETF Complex Simulant.

Test	Simulant	Simulant Additive Concentration	Acetonitrile Concentration		Other Organics	Oxidant to Organic Mole Ratio	$S_2O_8^{2-}$ Concentration		H_2O_2 Concentration		Test Purpose
			mg/L	M			M	mg/L	M	mg/L	
LR-1	Complex	--	80	1.95E-03	No	3	--	--	--	--	Control – UV light only
LR-2	Complex	--	80	1.95E-03	Yes	3	--	--	5.85E-03	199	H_2O_2 baseline test with acetonitrile and other organics
LR-3	Complex	115 mg/L Acetamide	0	0.00E+00	No	2	--	--	3.89E-03	132	Kinetics of decomposition product
LR-4	Complex	111 mg/L Acetate	0	0.00E+00	No	1	--	--	1.95E-03	66	Kinetics of decomposition product
LR-5	Complex + HCO_3^-	Medium HCO_3^-	0	0.00E+00	Yes	-	--	--	5.85E-03	199	H_2O_2 other organics only, medium HCO_3^-
LR-6	Complex + HCO_3^-	High HCO_3^-	0	0.00E+00	Yes	-	--	--	5.85E-03	199	H_2O_2 other organics only, high HCO_3^-
LR-7	Complex	--	80	1.95E-03	No	1.5	2.92E-03	562	--	--	Test $S_2O_8^{2-}$ concentration dependence
LR-8	Complex	--	80	1.95E-03	No	3	5.85E-03	1123	--	--	Test $S_2O_8^{2-}$ concentration dependence
LR-9	Complex	--	80	1.95E-03	No	6	1.17E-02	2246	--	--	Test $S_2O_8^{2-}$ concentration dependence
LR-16	Complex	--	80	1.95E-03	Yes	3	--	--	5.85E-03	199	Same as Test 2 but at higher UV power
LR-17	Complex	--	80	1.95E-03	No	1.5	2.92E-03	562	--	--	Same as Test 7 but at higher UV power
LR-18	Complex	--	80	1.95E-03	No	6	1.17E-02	2246	--	--	Same as Test 9 but higher UV power

-- Empty data field
Blue shaded tests used 4800-W lamp, all others used 450-W lamp

Table 3.7. Test Matrix for Micro-Reactor Tests with Steam Stripping Simulant.

Test	Acetonitrile Concentration		Other Organics	Oxidant to Acetonitrile Mole Ratio	$S_2O_8^{2-}$ Concentration		H_2O_2 Concentration		Test Purpose
	g/L	M			M	g/L	M	g/L	
MR-S1	60	1.46E+00	No	1.5	2.19E+00	4.21E+02	-	-	$S_2O_8^{2-}$ baseline test
MR-S3	60	1.46E+00	No	0	0.00E+00	0.00	-	-	Control: UV light only, no oxidant
MR-S4	6	1.46E-01	No	1.5	2.19E-01	42.12	-	-	$S_2O_8^{2-}$: Concentration dependence
MR-S5	0.6	1.46E-02	No	1.5	2.19E-02	4.21	-	-	$S_2O_8^{2-}$: Concentration dependence
MR-S6	0.06	1.46E-03	No	1.5	2.19E-03	0.42	-	-	$S_2O_8^{2-}$: Concentration dependence
MR-S7	60	1.46E+00	No	1.5	-	-	2.19E+00	74.58	H_2O_2 : Concentration dependence
MR-S9	6	1.46E-01	No	1.5	-	-	2.19E-01	7.46	H_2O_2 : Concentration dependence

- Empty data field

Table 3.8. Test Matrix for Large Reactor Tests with Steam Stripping Simulant.

Test	Lamp Power, W	Acetonitrile Concentration		$S_2O_8^{2-}$ to Acetonitrile Mole Ratio	$S_2O_8^{2-}$ Concentration		Test Purpose
		g/L	mol/L		mol/L	g/L	
LR-S1	450	60	1.46E+00	1.5	2.19E+00	421	Effect of acetonitrile concentration
LR-S2	450	6	1.46E-01	1.5	2.19E-01	42.1	Base case
LR-S3	450	6	1.46E-01	3	4.38E-01	84.2	Effect of oxidant to acetonitrile mole ratio
LR-S4	450	6	1.46E-01	-	0	0	Control – No oxidant
LR-S5	4800	6	1.46E-01	3	4.38E-01	84.2	Effect of lamp power

- Empty data field

Table 4.1. Results from Micro-Reactor Tests. Effect of Individual Anions. Simple Simulant, 80 mg/L Acetonitrile (1.95E-3 mol/L), 1123 mg/L $S_2O_8^{2-}$ (5.83E-3 mol/L), $S_2O_8^{2-}$ to Acetonitrile Mole Ratio = 3.

Test	Additive	Acetonitrile Destruction vs. Time (minutes)							
		0	1	2	5	10	15	30	60
MR-10	None	0.0%	24.1%	47.1%	58.4%	75.9%	84.4%	91.8%	98.9%
MR-11	68.3 mg/L NH_4^+	0.0%	3.8%	8.4%	16.5%	38.6%	55.0%	72.6%	95.1%
MR-12	2.97 mg/L Cl^-	0.0%	15.6%	33.5%	62.1%	67.4%	67.9%	72.1%	83.9%
MR-13	16.2 mg/L NO_3^-	0.0%	16.0%	28.5%	50.0%	59.1%	81.1%	90.5%	99.1%
MR-14	50 mg/L HCO_3^-	0.0%	3.6%	14.4%	43.8%	72.3%	82.6%	91.6%	98.0%
MR-15	7 g/L Cl^-	0.0%	13.7%	16.4%	18.0%	14.2%	32.2%	20.6%	35.5%

Table 4.2. Results from Micro-Reactor Tests. Steam Stripping Simulant, $S_2O_8^{2-}$ to Acetonitrile Mole Ratio = 1.5.

Test	Acetonitrile Concentration		$S_2O_8^{2-}$ Concentration		Acetonitrile Destruction vs. Time (minutes)							
	mol/L	g/L	mol/L	g/L	0	1	2	5	10	15	30	60
MR-S1	1.46E+00	60	2.19E+00	421	0.0%	9.8%	5.3%	8.8%	3.7%	5.9%	5.4%	11.2%
MR-S3	1.46E+00	60	0.00E+00	0	0.0%	-1.9%	2.9%	1.6%	8.2%	-1.0%	10.6%	7.0%
MR-S4	1.46E-01	6	2.19E-01	42.12	0.0%	6.0%	7.7%	10.4%	18.5%	23.5%	30.7%	48.2%
MR-S5	1.46E-02	0.6	2.19E-02	4.21	0.0%	7.7%	12.7%	23.2%	40.4%	47.4%	62.6%	67.4%
MR-S6	1.46E-03	0.06	2.19E-03	0.42	0.0%	7.1%	17.9%	42.6%	61.7%	69.6%	81.4%	99.3%

Table 4.3. Results from Micro-Reactor Tests. Steam Stripping Simulant, H_2O_2 to Acetonitrile Mole Ratio = 1.5.

Test	Acetonitrile Concentration		H_2O_2 Concentration		Acetonitrile Destruction vs. Time (minutes)							
	mol/L	g/L	mol/L	g/L	0	1	2	5	10	15	30	60
MR-S7	1.46E+00	60	2.19E+00	74.58	0.0%	5.3%	3.9%	3.8%	6.5%	7.0%	5.5%	9.8%
MR-S9	1.46E-01	6	2.19E-01	7.46	0.0%	1.9%	2.5%	5.2%	6.7%	9.5%	13.1%	29.8%

Table 4.4. Results from Micro-Reactor Tests. Steam Stripping Simulant. Acetate Concentrations at 60 Minutes.

Test	Acetonitrile Concentration		$S_2O_8^{2-}$ Concentration		Acetate Concentration, mg/L
	mol/L	g/L	mol/L	g/L	
MR-S1	1.46E+00	60	2.19E+00	421	867
MR-S3	1.46E+00	60	0.00E+00	0	31.2
MR-S4	1.46E-01	6	2.19E-01	42.12	302
MR-S5	1.46E-02	0.6	2.19E-02	4.21	118
MR-S6	1.46E-03	0.06	2.19E-03	0.42	0.08

Test	Acetonitrile Concentration		H_2O_2 Concentration		Acetate Concentration, mg/L
	mol/L	g/L	mol/L	g/L	
MR-S7	1.46E+00	60	2.19E+00	74.58	2367
MR-S9	1.46E-01	6	2.19E-01	7.46	697

Table 4.5. Results from Large Reactor Tests. Complex Simulant, 80 mg/L Acetonitrile (1.95E-3 mol/L).

Test	Lamp Power, W	H_2O_2 Concentration		Acetonitrile Destruction vs. Time (minutes)					
		mol/L	mg/L	0	5	10	15	30	60
LR-1	450	0.00E+00	0	0.0%	0.0%	0.0%	2.0%	0.7%	4.4%
LR-2	450	5.85E-03	199	0.0%	1.9%	6.1%	7.0%	16.0%	37.2%
LR-16	4800	5.85E-03	199	0	36.7%	39.2%	40.4%	44.3%	46.8%

Table 4.6. Results from Large Reactor Tests. Complex Simulant, 80 mg/L Acetonitrile (1.95E-3 mol/L).

Test	Lamp Power, W	$S_2O_8^{2-}$/Acetonitrile Mole Ratio	$S_2O_8^{2-}$ Concentration		Acetonitrile Destruction vs. Time (minutes)					
			mol/L	mg/L	0	5	10	15	30	60
LR-7	450	1.5	2.92E-03	562	0.0%	22.5%	30.5%	39.7%	55.0%	66.9%
LR-8	450	3	5.85E-03	1123	0.0%	27.2%	43.8%	53.6%	73.8%	90.9%
LR-9	450	6	1.17E-02	2246	0	39.7%	62.2%	77.2%	98.8%	99.8%
LR-17	4800	1.5	2.92E-03	562	0.0%	66.6%	68.0%	70.6%	74.3%	78.5%
LR-18	4800	6	1.17E-02	2246	0.0%	99.9%	99.9%	99.9%	99.9%	99.9%

Note: Value shown shaded was measured at 8 minutes instead of 5 minutes.

Table 4.7. Results from Large Reactor Tests. Complex Simulant, 450 W Lamp Power.

Test	Additive	H_2O_2 Concentration		Acetate Concentration (mg/L) vs. Time (minutes)					
		mol/L	mg/L	0	5	10	15	30	60
LR-3	115 mg/L Acetamide	3.89E-03	132	0	10.98	40.77	74.29	157.94	245.29
LR-4	111 mg/L Acetate	1.95E-03	66	105.91	88.52	83.32	70.85	59.17	52.13

Table 4.8. Results from Large Reactor Tests with Other Organics. Complex Simulant.

Test	Lamp Power, W	Additive	H_2O_2 Concentration		Organic Destruction vs. Time (minutes)						
			mol/L	mg/L	Organic	0	5	10	15	30	60
LR-2	450	80 mg/L acetronitile	5.85E-03	199	Acetone	0.0%	6.1%	20.7%	38.8%	81.6%	98.8%
					Acrylonitrile	0.0%	90.6%	100.0%	100.0%	100.0%	100.0%
					MEK	0.0%	39.6%	81.3%	97.8%	100.0%	100.0%
LR-5	450	Medium bicarbonate*	5.85E-03	199	Acetone	0.0%	7.9%	25.6%	49.6%	83.6%	95.5%
					Acrylonitrile	0.0%	99.7%	100.0%	100.0%	100.0%	100.0%
					MEK	0.0%	67.9%	96.4%	99.6%	100.0%	100.0%
LR-6	450	High bicarbonate*	5.85E-03	199	Acetone	0.0%	18.1%	36.4%	54.5%	83.9%	95.3%
					Acrylonitrile	0.0%	99.6%	100.0%	100.0%	100.0%	100.0%
					MEK	0.0%	30.4%	96.6%	99.6%	99.7%	99.7%
LR-16	4800	80 mg/L acetronitile	5.85E-03	199	Acetone	0.0%	99.1%	99.6%	99.5%	99.7%	99.8%
					Acrylonitrile	0.0%	99.8%	99.9%	99.9%	100.0%	100.0%
					MEK	0.0%	99.6%	99.9%	99.8%	100.0%	100.0%

* Medium bicarbonate corresponds to 14.7 psi air + 6 psi CO_2; high bicarbonate corresponds to 31.6 psi CO_2.

Table 4.9. Results from Large Reactor Tests. Steam Stripping Simulant.

Test	Lamp Power, W	Acetonitrile Concentration		$S_2O_8^{2-}$ to Acetonitrile Mole Ratio	$S_2O_8^{2-}$ Concentration		Acetonitrile Destruction vs. Time (minutes)					
		g/L	mol/L		mol/L	g/L	0	5	10	15	30	60
LR-S1	450	60	1.46E+00	1.5	2.19E+00	421	0.0%	1.3%	1.1%	1.8%	4.1%	7.1%
LR-S2	450	6	1.46E-01	1.5	2.19E-01	42.1	0.0%	-1.5%	4.8%	8.0%	9.9%	15.9%
LR-S3	450	6	1.46E-01	3	4.38E-01	84.2	0.0%	4.1%	4.2%	5.2%	8.9%	10.7%
LR-S4	450	6	1.46E-01	-	0	0	0.0%	0.0%	1.1%	5.4%	6.7%	5.2%
LR-S5	4800	6	1.46E-01	3	4.38E-01	84.2	0.0%	7.8%	14.1%	21.1%	35.5%	56.6%

Table 5.1. Parameters Used for Modeling; Large Reactor with Persulfate.

Parameter	Value	Units
φ	0.7	mol $S_2O_8^{2-}$/mol photon
ε @ 254 nm	22	liter/(mol cm)
I_0 @254 nm – 450 W	0.122	W/cm^2
I_0 @254 nm – 4800 W	1.65	W/cm^2
K @254 nm	2.124E-06	mol photon/Joule
R_1	3.75	cm
R_2	16.95	cm
Reflectivity Ratio, μ	0.4	None

Table 5.2. Parameters Used for Modeling; Large Reactor with Peroxide.

Parameter	Value	Units
φ	0.7	mol H_2O_2/mol photon
ε @ 254 nm	21.2	liter/(mol cm)
I_0 @254 nm – 450 W	0.122	W/cm^2
I_0 @254 nm – 4800 W	1.65	W/cm^2
K @254 nm	2.124E-06	mol photon/Joule
R_1	3.75	cm
R_2	16.95	cm
Reflectivity Ratio, μ	0.4	None

Table 5.3. Parameters Used for Modeling ETF Full-Scale Reactor.

Parameter	Value	Units
I_0 @254 nm	1.662	W/cm^2
I_0 @185 nm	0.0831	W/cm^2
R_1	3.375	cm
R_2	17.305	cm
Reflectivity Ratio, μ	0.4	None

Table 5.4. Fitting Results for Large Reactor Tests with Persulfate. Complex Simulant, 80 mg/L Acetonitrile (1.95E-3 mol/L).

Test	Lamp Power, W	$S_2O_8^{2-}$ /Acetonitrile Mole Ratio	$S_2O_8^{2-}$ Concentration		Fitted k_1, L/(mol s)
			mol/L	g/L	
LR-7	450	1.5	2.92E-03	562	0.1007
LR-8	450	3	5.85E-03	1123	0.1616
LR-9	450	6	1.17E-02	2246	0.5662
LR-17	4800	1.5	2.92E-03	562	0.3918
LR-18	4800	6	1.17E-02	2246	0.8024
				Mean	0.4045
				Global Fit	0.3519

Table 5.5. Extended Model Fitting Results for Large Reactor Tests with Persulfate. Complex Simulant, 80 mg/L Acetonitrile (1.95E-3 mol/L).

Test	Lamp Power, W	$S_2O_8^{2-}$ /Acetonitrile Mole Ratio	$S_2O_8^{2-}$ Concentration		Fitted k_1, L/(mol s)	Fitted $k_3[H_2O]$, 1/s
			mol/L	g/L		
LR-7	450	1.5	2.92E-03	562	0.5854	0.0120
LR-8	450	3	5.85E-03	1123	0.6322	0.0141
LR-9	450	6	1.17E-02	2246	1.024	0.0194
LR-17	4800	1.5	2.92E-03	562	6.131	0.1709
LR-18	4800	6	1.17E-02	2246	1546	7.138
Mean (excluding Test LR-18)					2.093	0.0541
Global Fit (all five tests)					0.9235	0.0195
Extrapolated Values for Test LR-18					6.591	0.1784
Fitted k_1 for Test LR-18 with $k_3[H_2O]$ fixed at the extrapolated value					6.881	0.1784 (fixed)

Table 5.6. Fitting Results for Large Reactor Tests with Peroxide. Complex Simulant, 80 mg/L Acetonitrile (1.95E-3 mol/L).

Test	Lamp Power, W	H_2O_2/Acetonitrile Mole Ratio	H_2O_2 Concentration		Fitted k_1, L/(mol s)
			mol/L	g/L	
LR-2	450	3	5.85E-03	199	0.0141
LR-16	4800	3	5.85E-03	199	0.0297
Mean					0.0219
Global Fit					0.0220

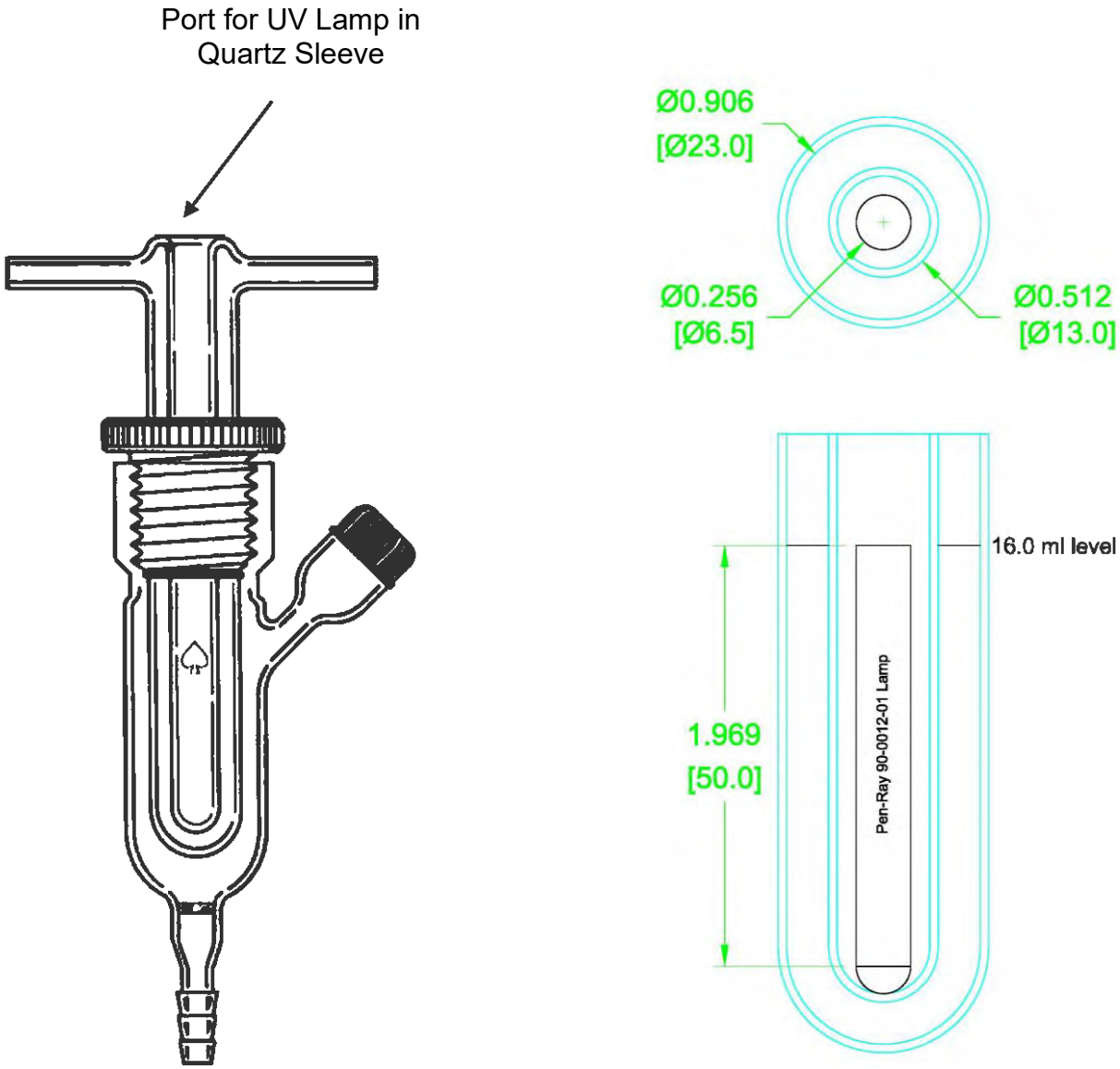

Figure 2.1. Acetonitrile destruction Micro-Reactor (left) and diagram showing dimensions (right) in inches and [millimeters].

Figure 2.2. Micro-reactor assembly showing cooling jacket and syringe sampling line.

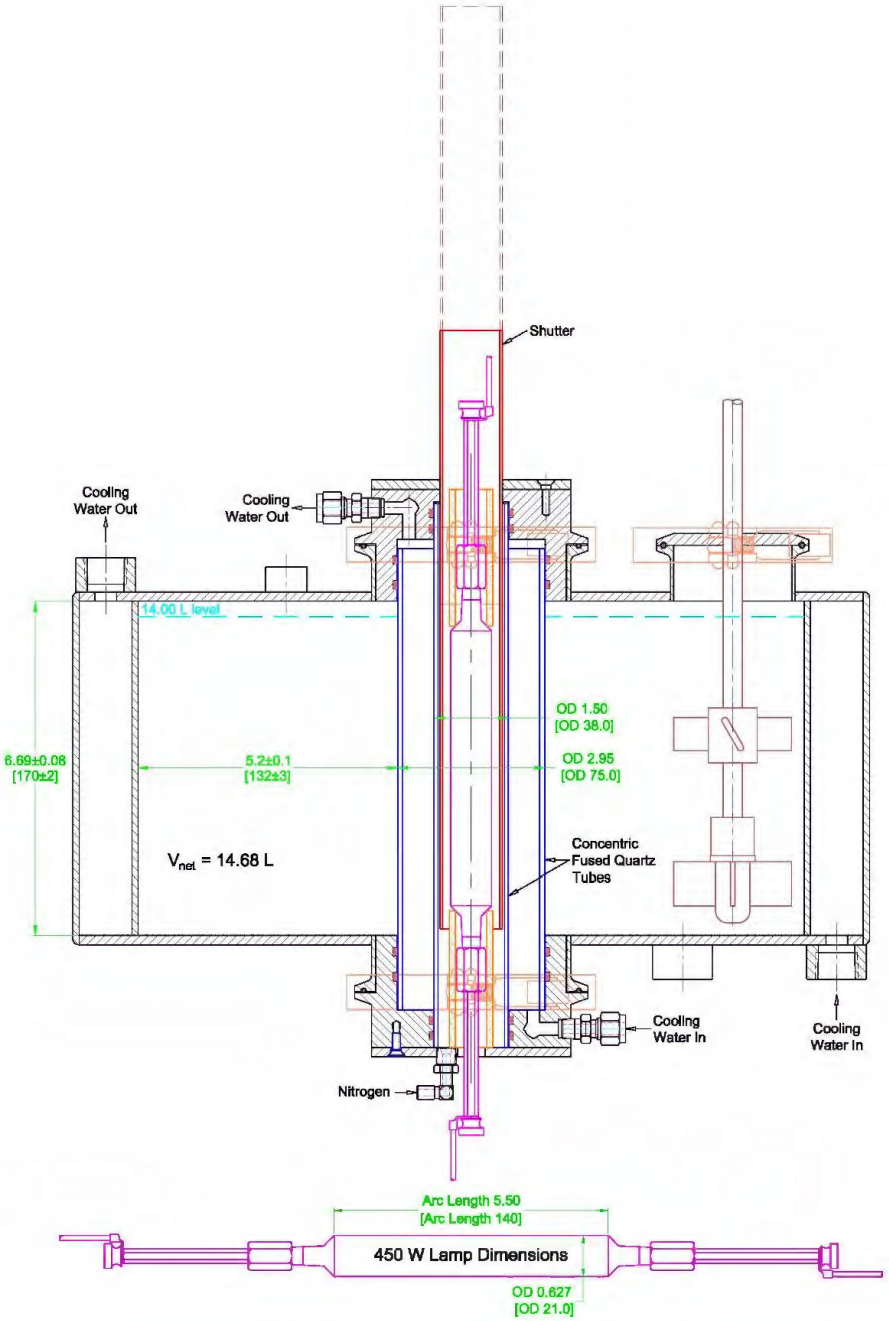

Figure 2.3. Cross-sectional diagram of the large reactor with the 450 W UV lamp. Dimensions shown in inches and [millimeters].

Figure 2.4. Large reactor setup with the 450 W UV lamp.

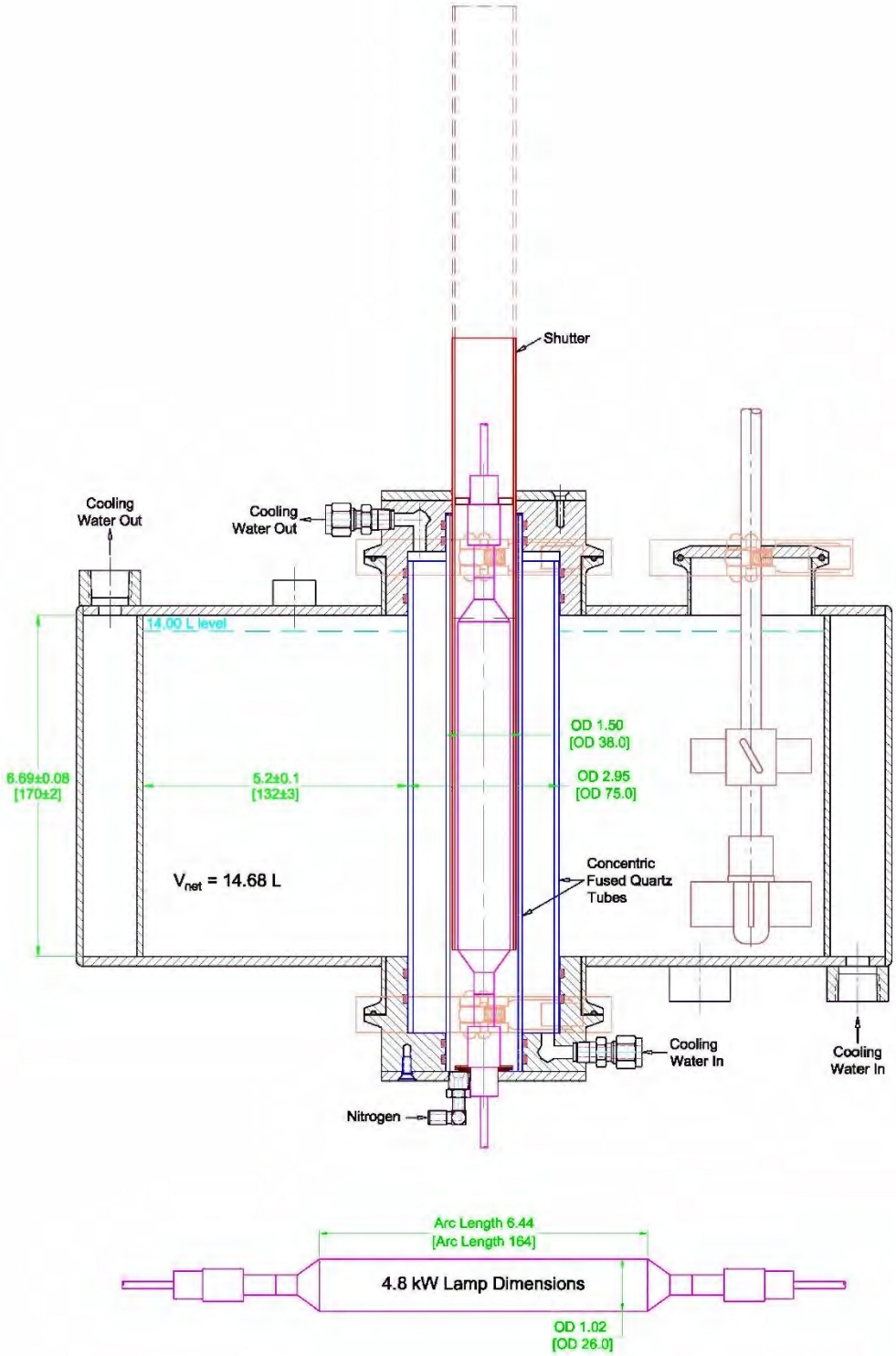

Figure 2.5. Cross-sectional diagram of the large reactor with the 4800 W UV lamp. Dimensions shown in inches and [millimeters].

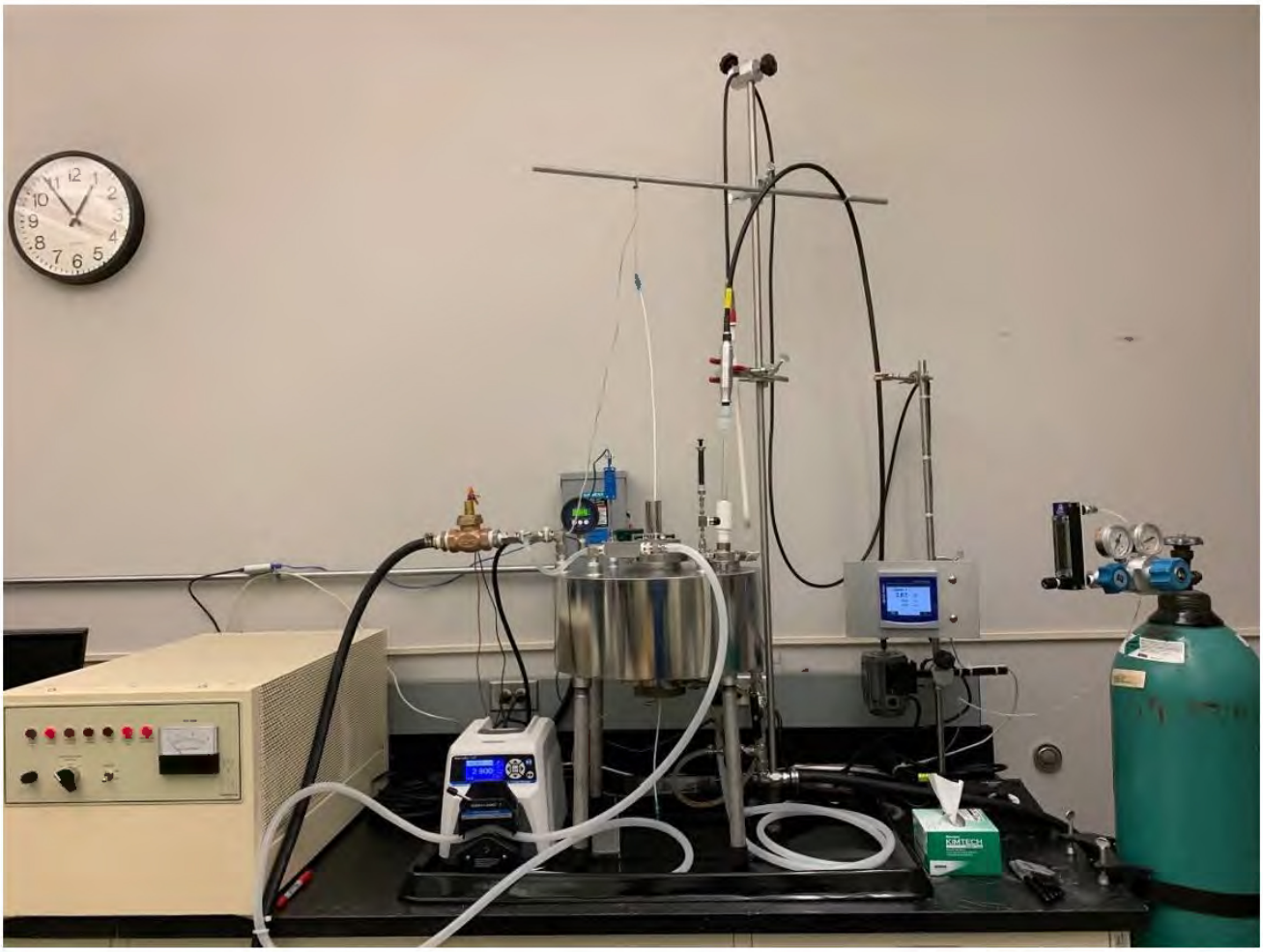

Figure 2.6. Large reactor setup with the 4800 W UV lamp. Lamp power supply is on the left.

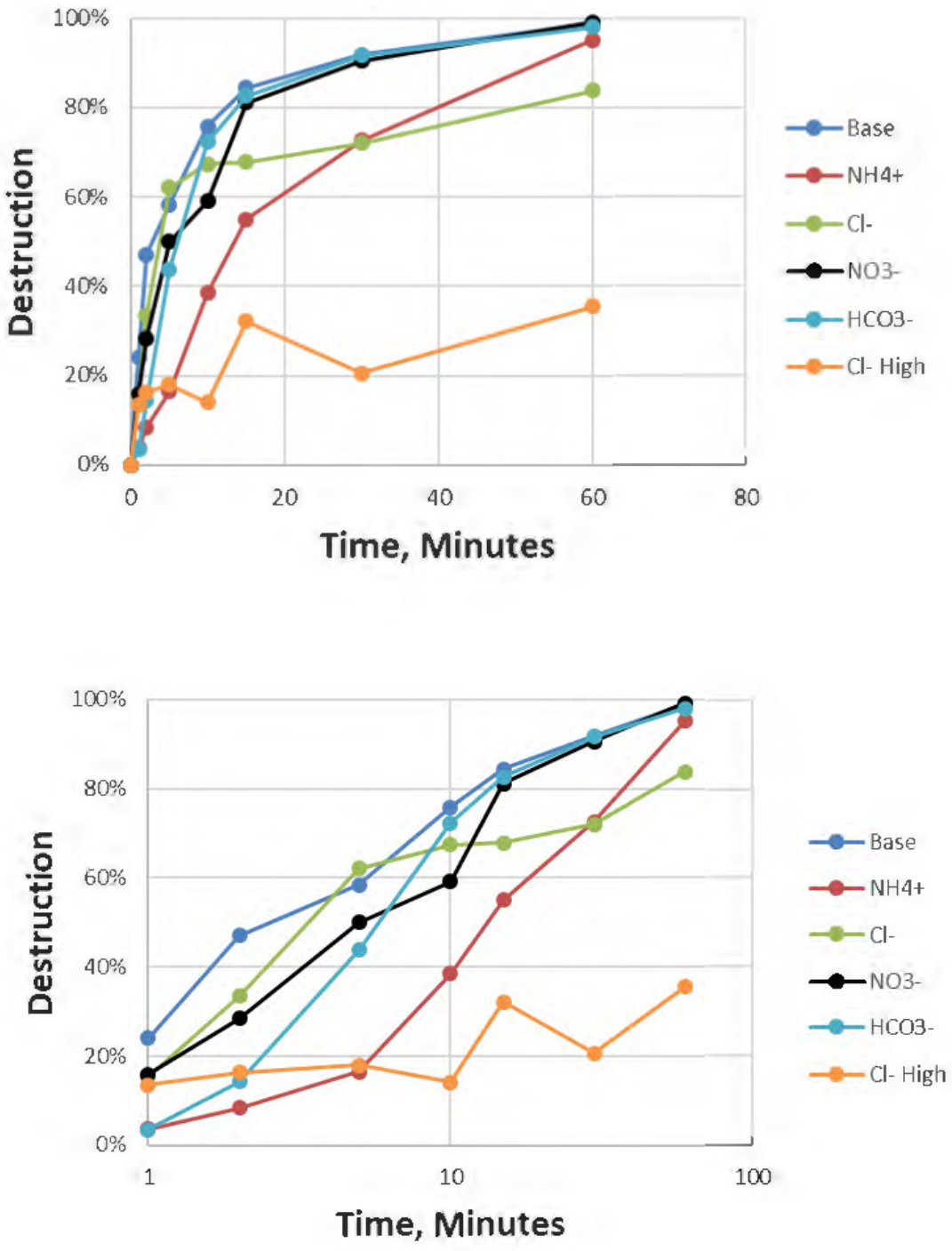

Figure 4.1. Effect of added anions on acetonitrile destruction. Bottom plot shows the same data on a log scale. Micro-reactor, persulfate, simple simulant.

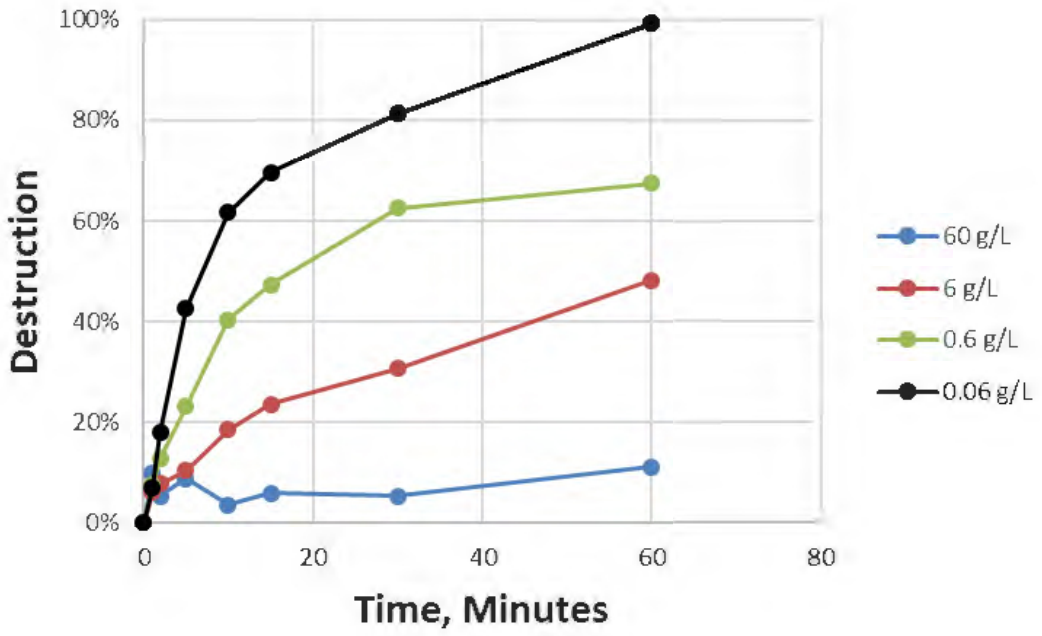

Figure 4.2. Micro-reactor tests with steam stripping simulant at various concentrations of acetonitrile. Mole ratio of persulfate to acetonitrile = 1.5.

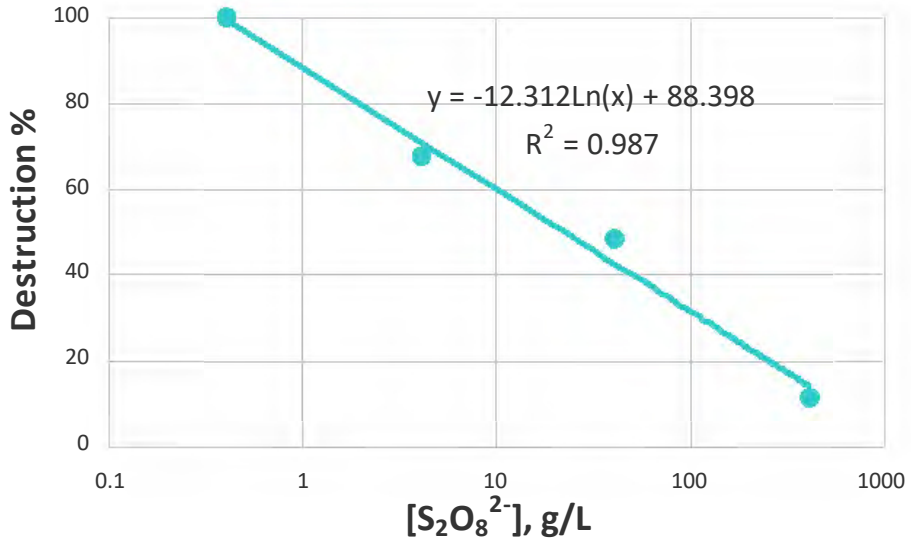

Figure 4.3. Data from Figure 4.2 at 60 minutes versus persulfate concentration.

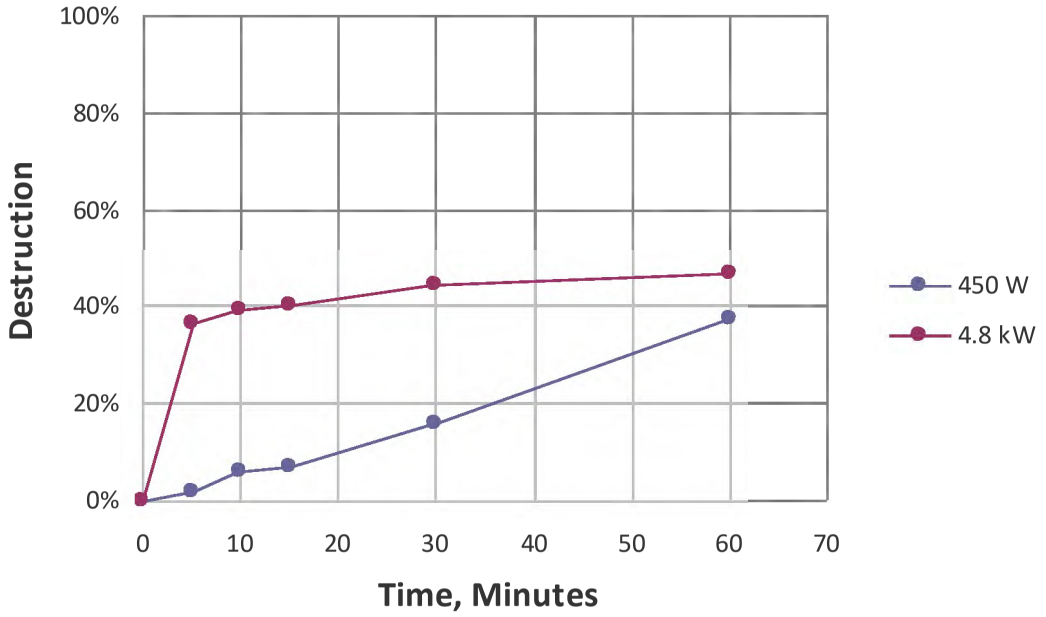

Figure 4.4. Results from large reactor tests with complex simulant and peroxide showing the effect of lamp power. Acetonitrile concentration = 1.95E-3 mol/L; acetonitrile to peroxide mole ratio = 3.

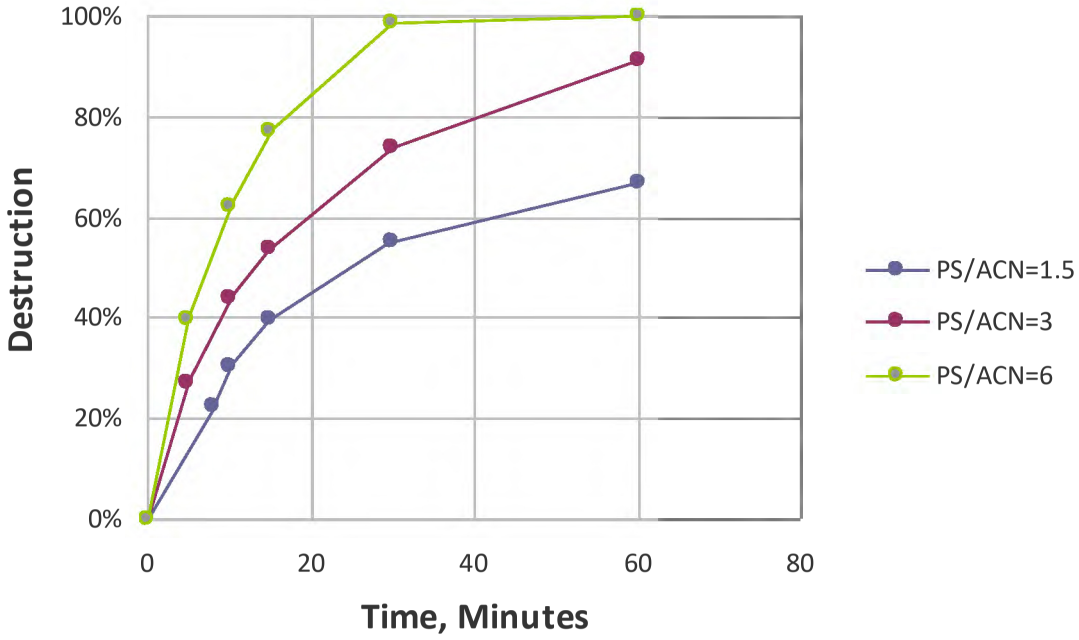

Figure 4.5. Results from large reactor tests with complex simulant and persulfate showing effect of the ratio of persulfate to acetonitrile. Acetonitrile concentration = 1.95E-3 mol/L; lamp power = 450 W.

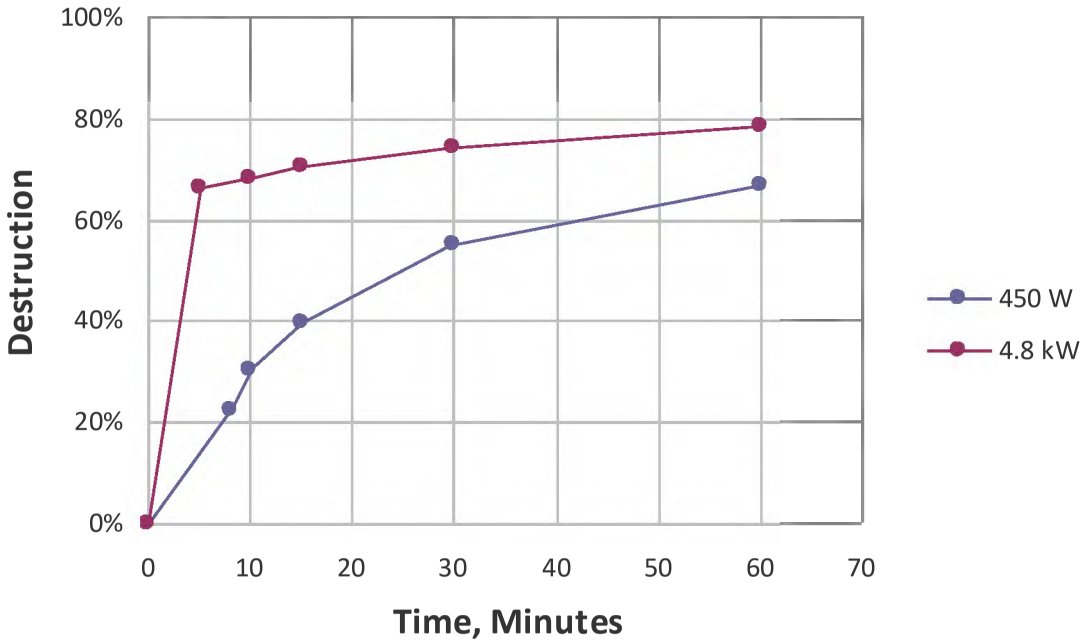

Figure 4.6. Results from large reactor tests with complex simulant and persulfate showing effect of lamp power at a ratio of persulfate to acetonitrile of 1.5; acetonitrile concentration = 1.95E-3 mol/L.

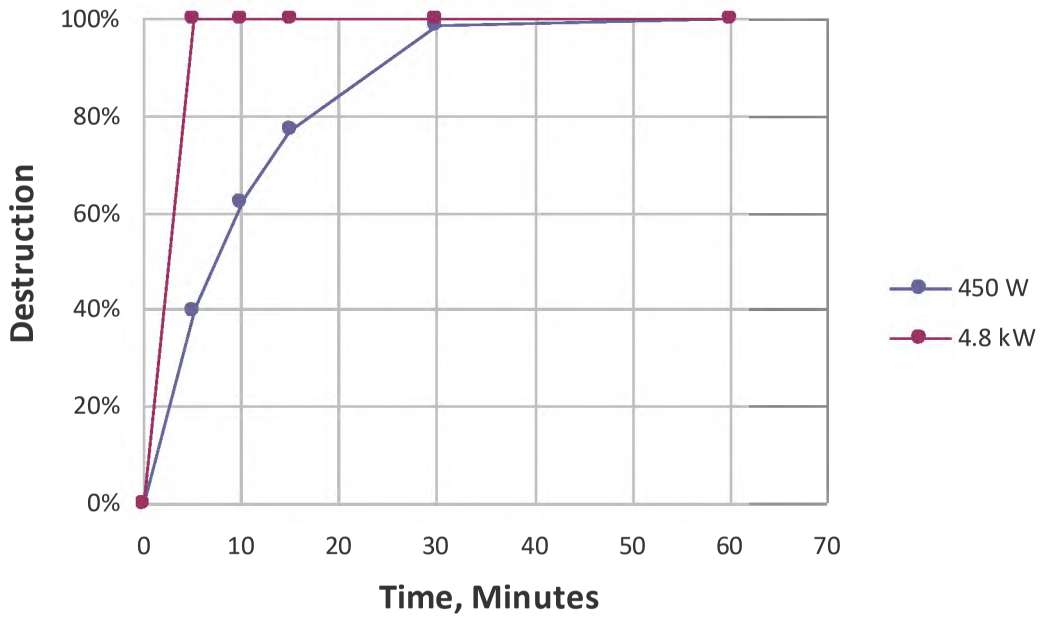

Figure 4.7. Results from large reactor tests with complex simulant and persulfate showing effect of lamp power at a ratio of persulfate to acetonitrile of 6; acetonitrile concentration = 1.95E-3 mol/L.

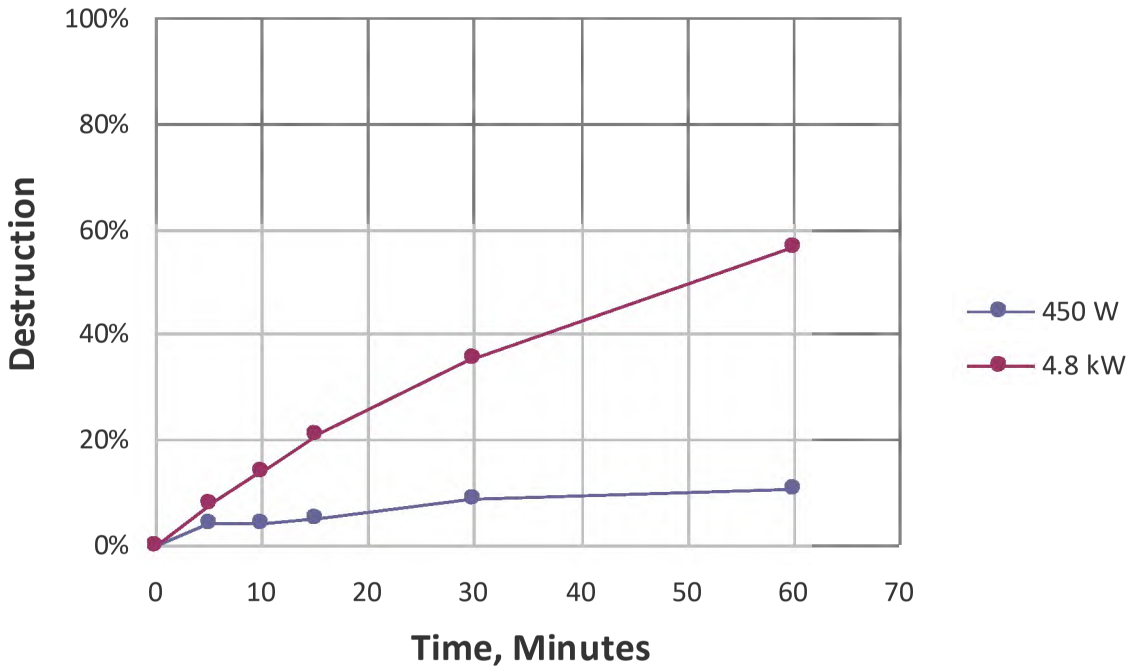

Figure 4.8. Results from large reactor tests with steam stripping simulant and persulfate showing effect of lamp power at a ratio of persulfate to acetonitrile of 3; acetonitrile concentration = 1.46E-01 mol/L.

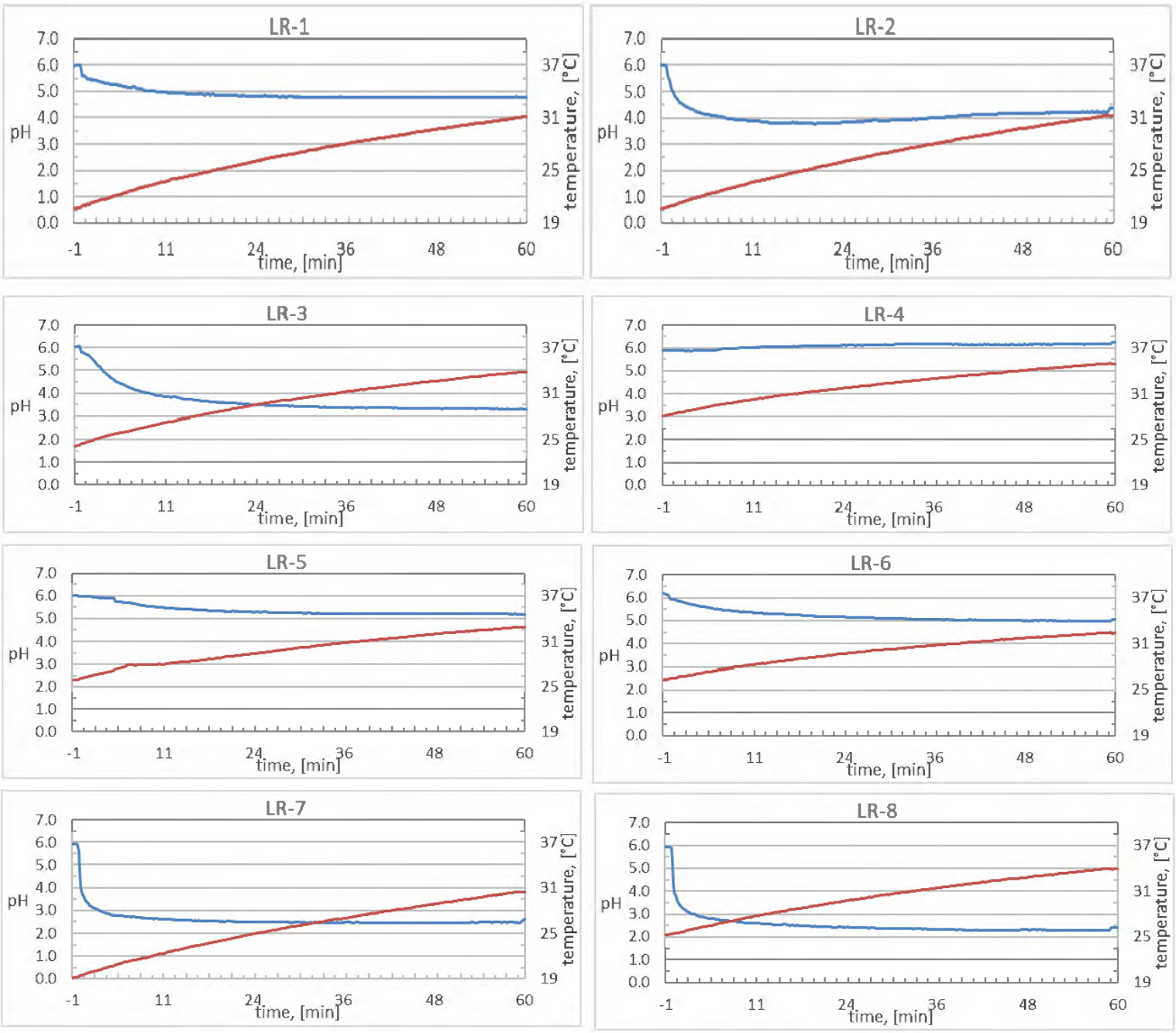

Figure 4.9. Temperature (red line) and pH (blue line) during large reactor tests.

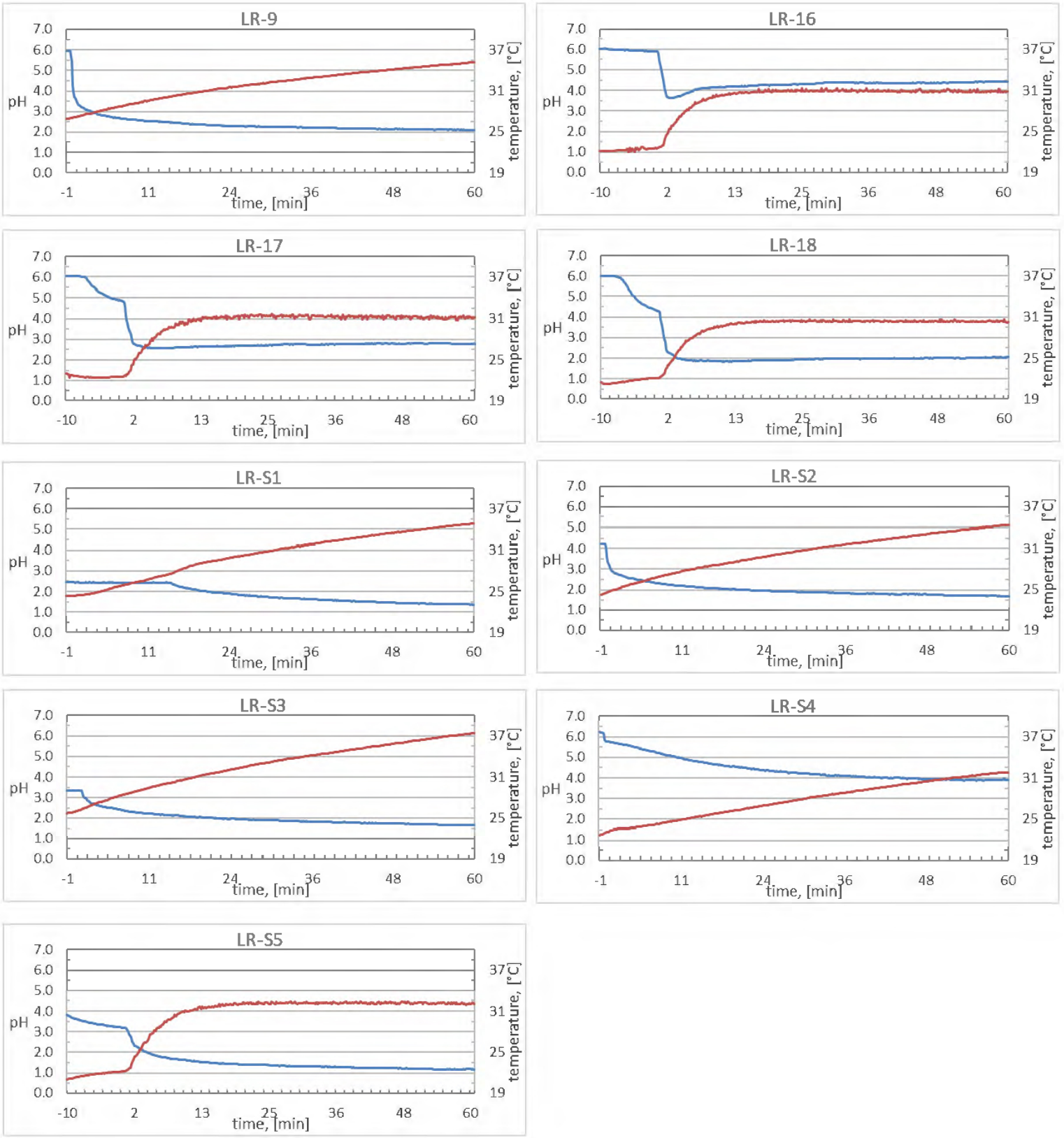

Figure 4.10. Temperature (red line) and pH (blue li

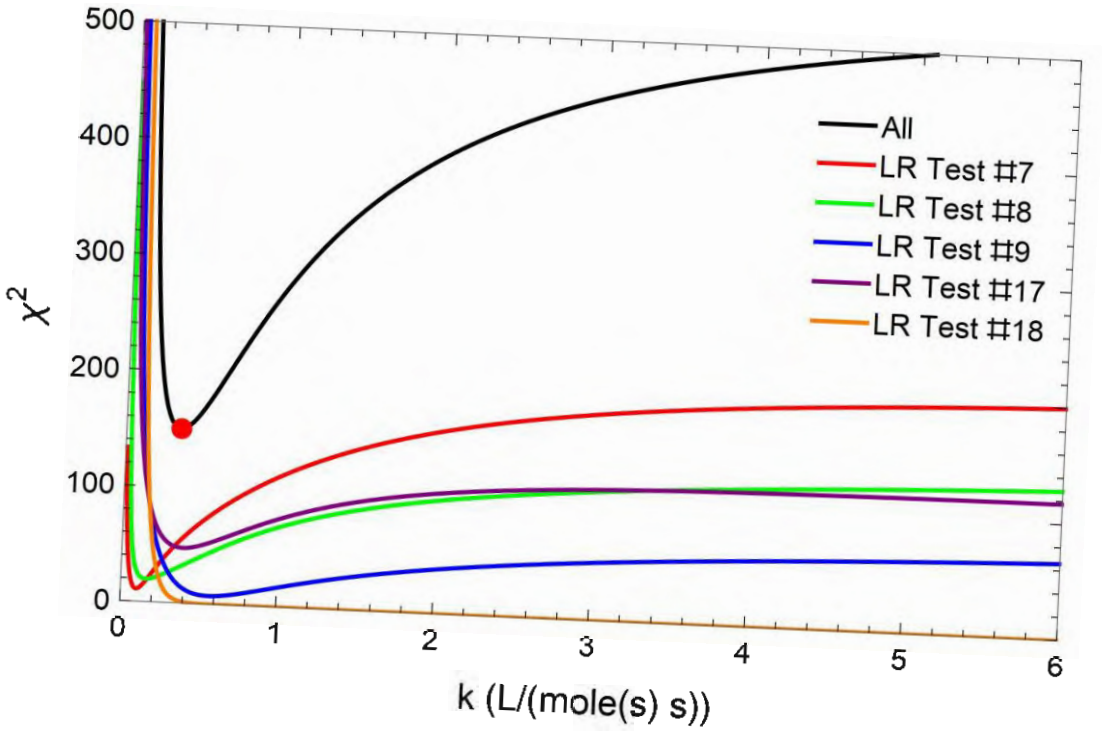

Figure 5.1. Goodness of fit plot. Individual fits to tests with large reactor and persulfate and global fit (black). k_1-only model.

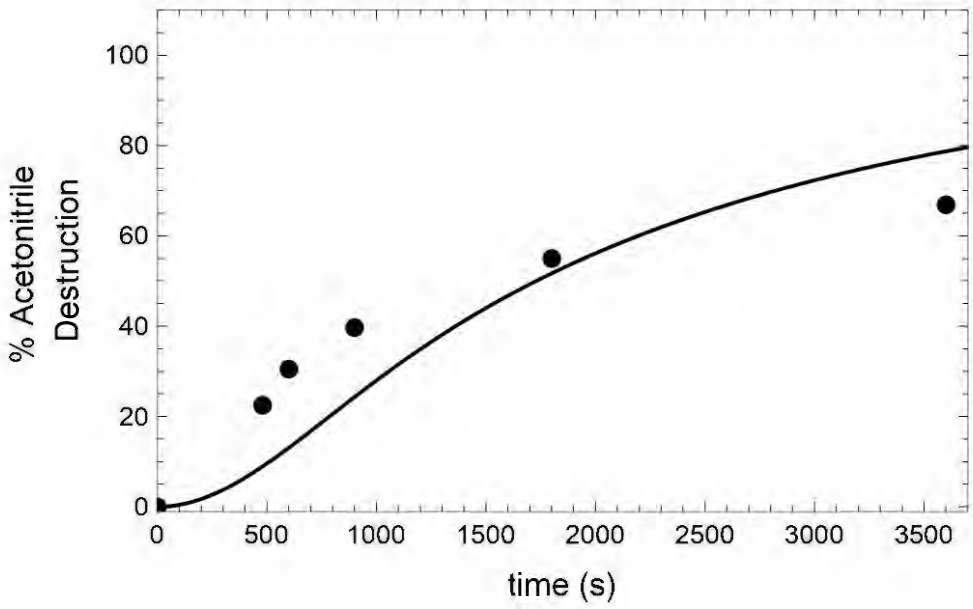

Figure 5.2. k_1-only model fit to Test LR-7.

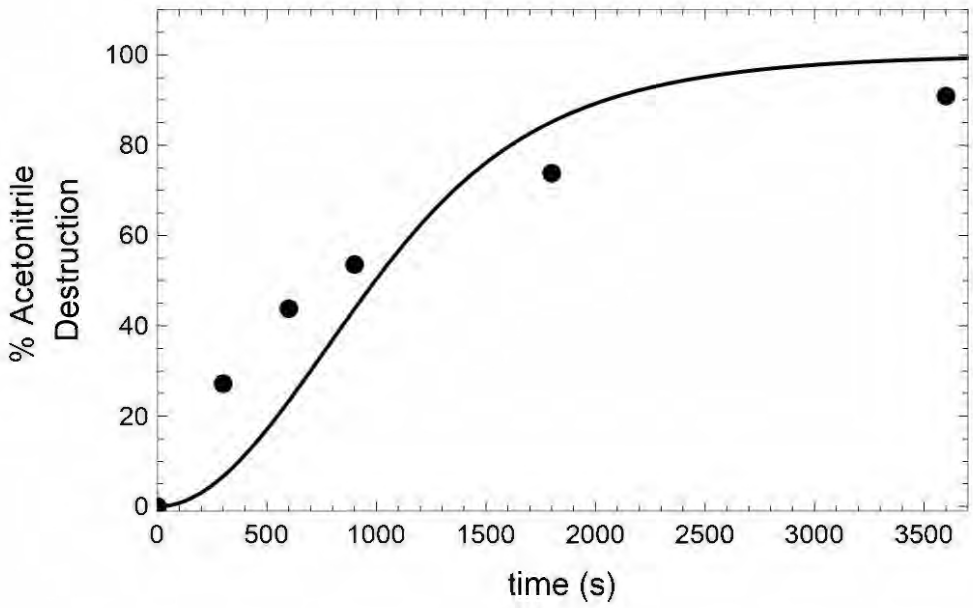

Figure 5.3. k_1-only model fit to Test LR-8.

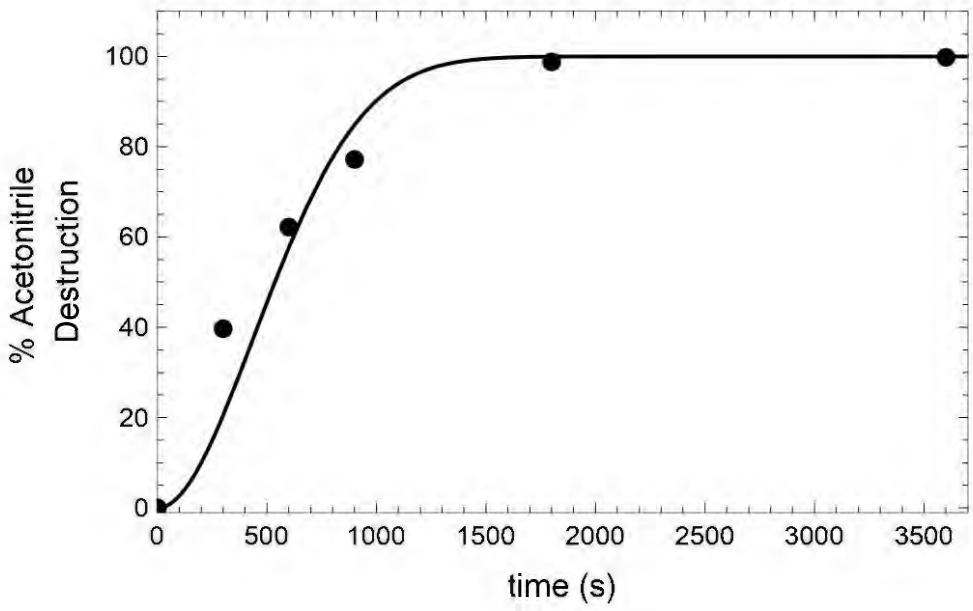

Figure 5.4. k_1-only model fit to Test LR-9.

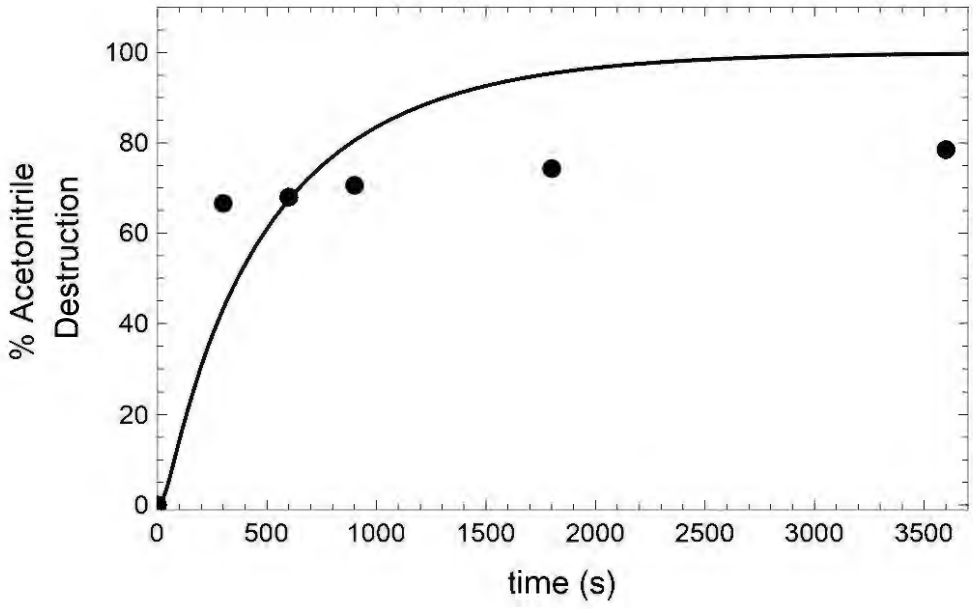

Figure 5.5. k_1-only model fit to Test LR-17.

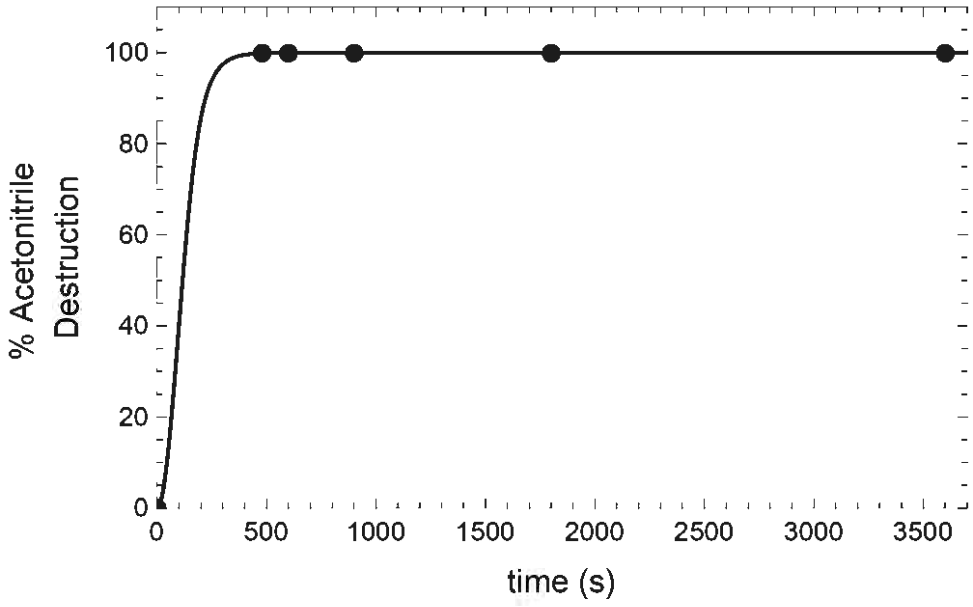

Figure 5.6. k_1-only model fit to Test LR-18.

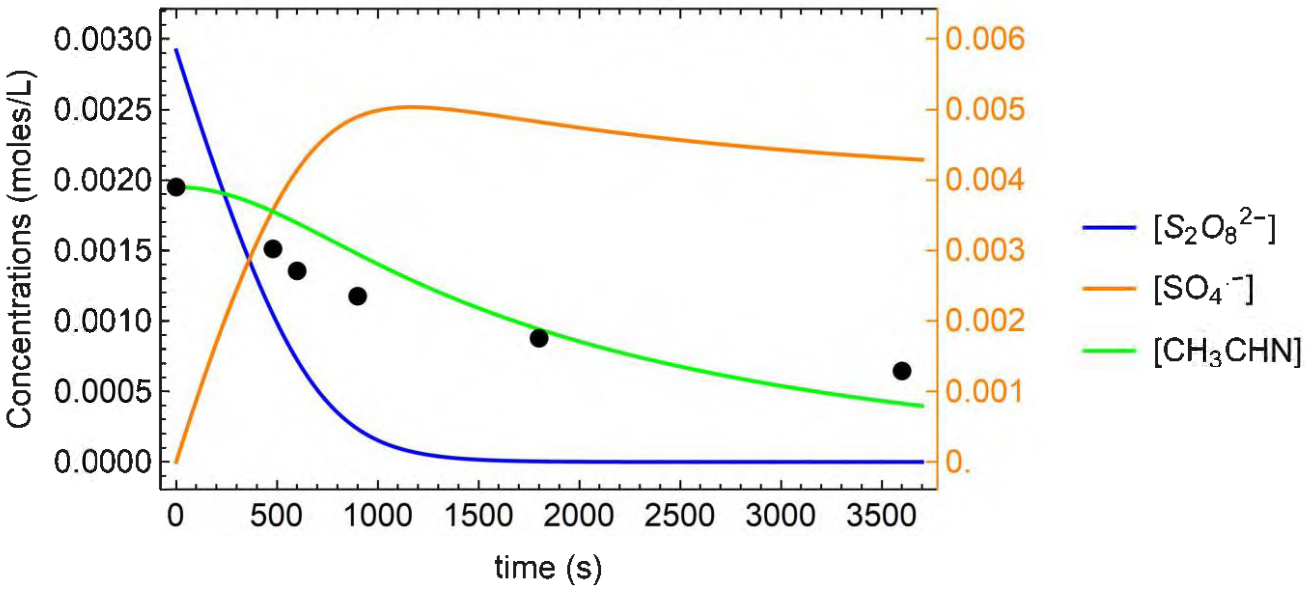

Figure 5.7. k_1-only model fit to Test LR-7.

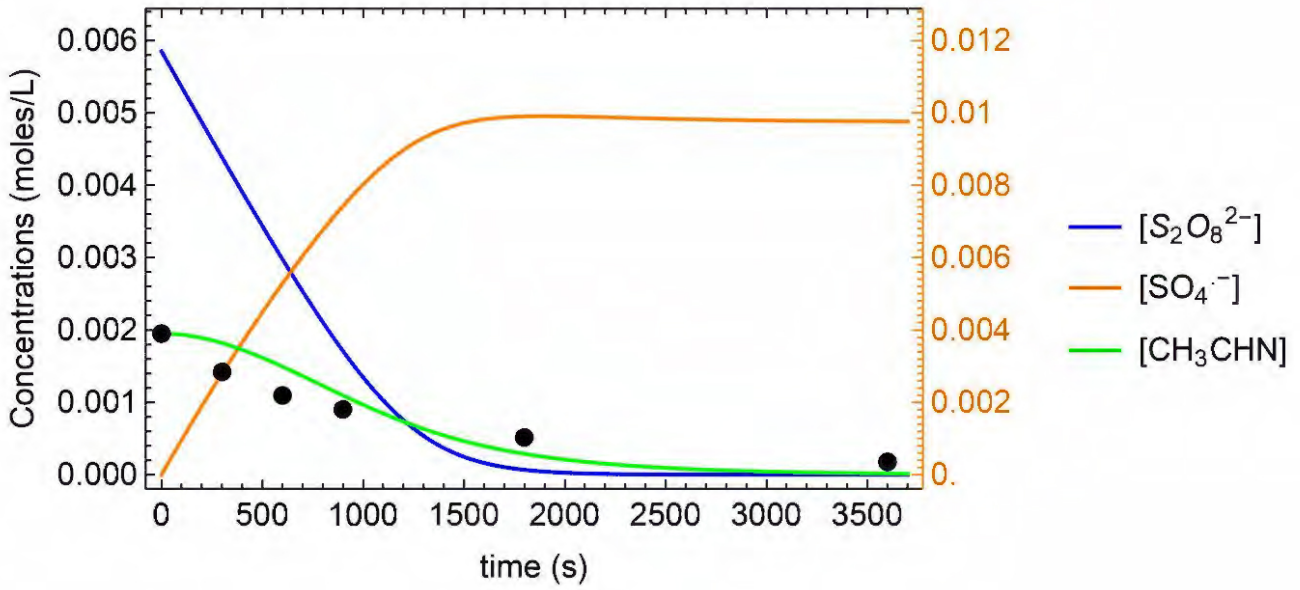

Figure 5.8. k_1-only model fit to Test LR-8.

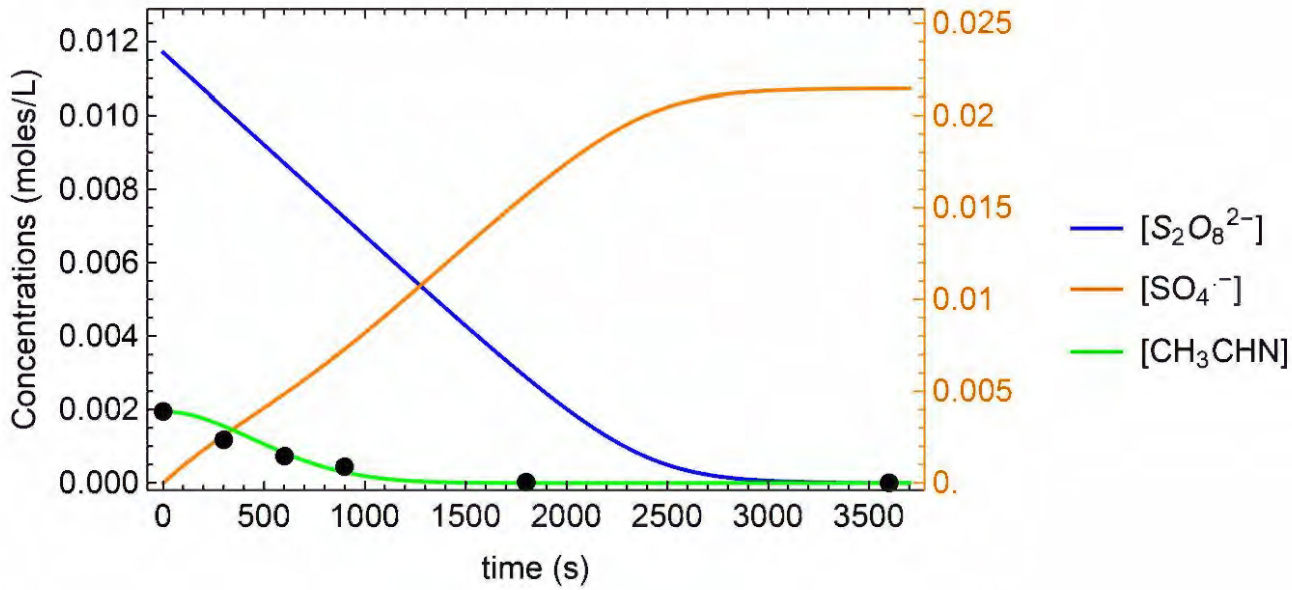

Figure 5.9. k_1-only model fit to Test LR-9.

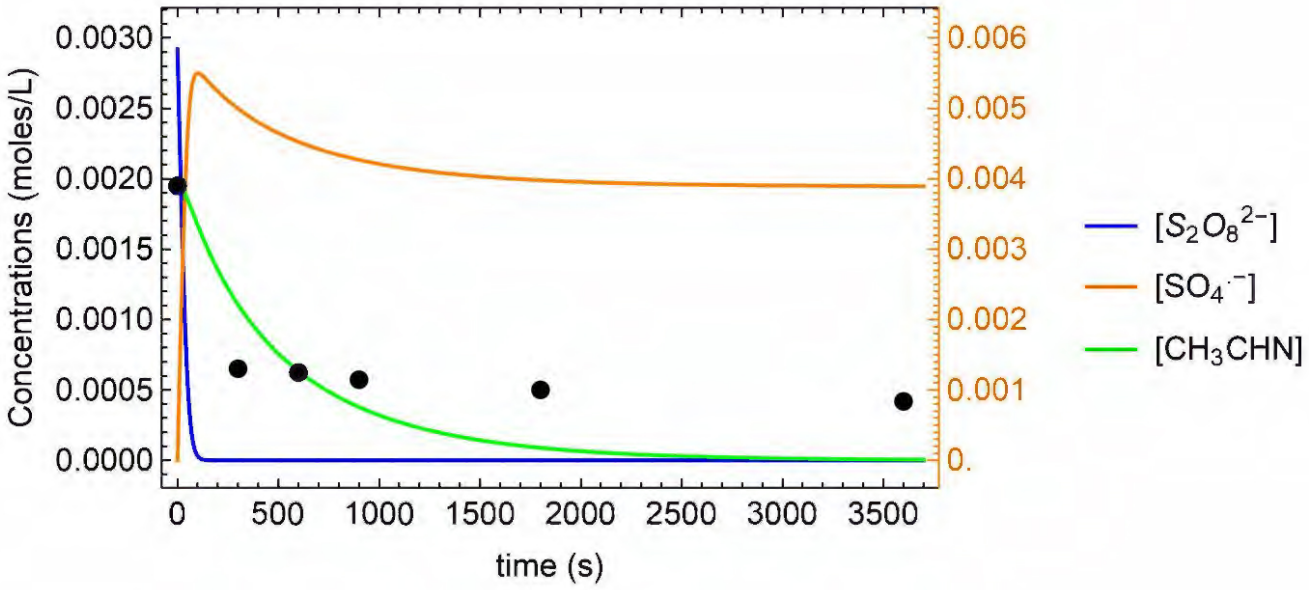

Figure 5.10. k_1-only model fit to Test LR-17.

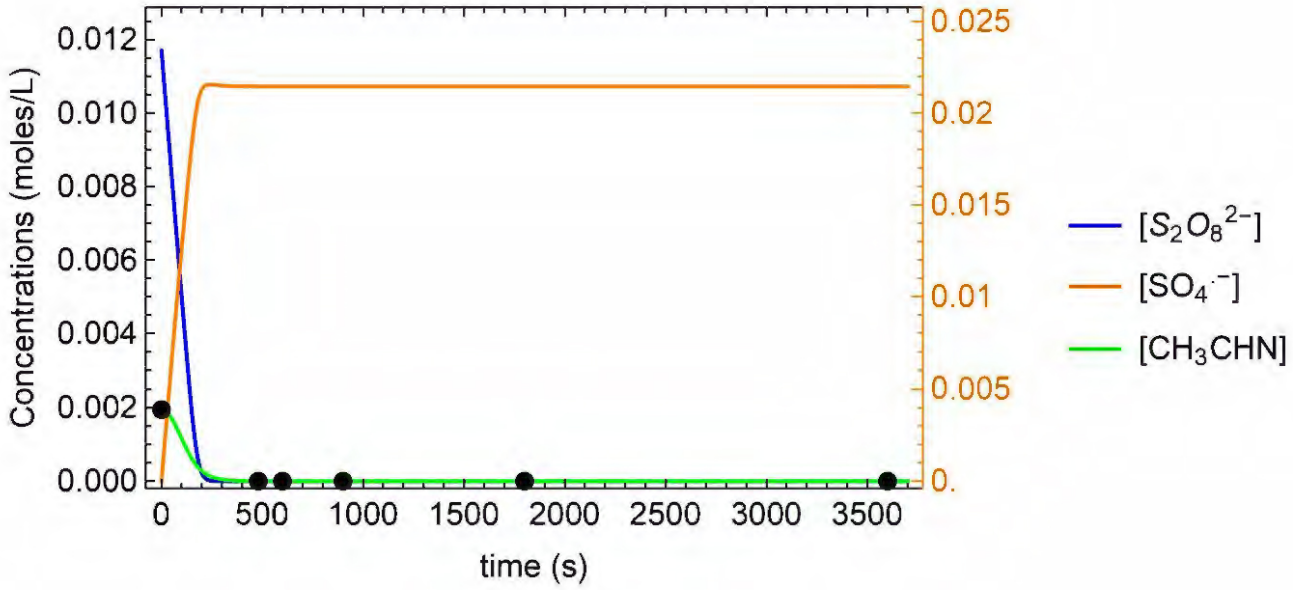

Figure 5.11. k_1-only model fit to Test LR-18.

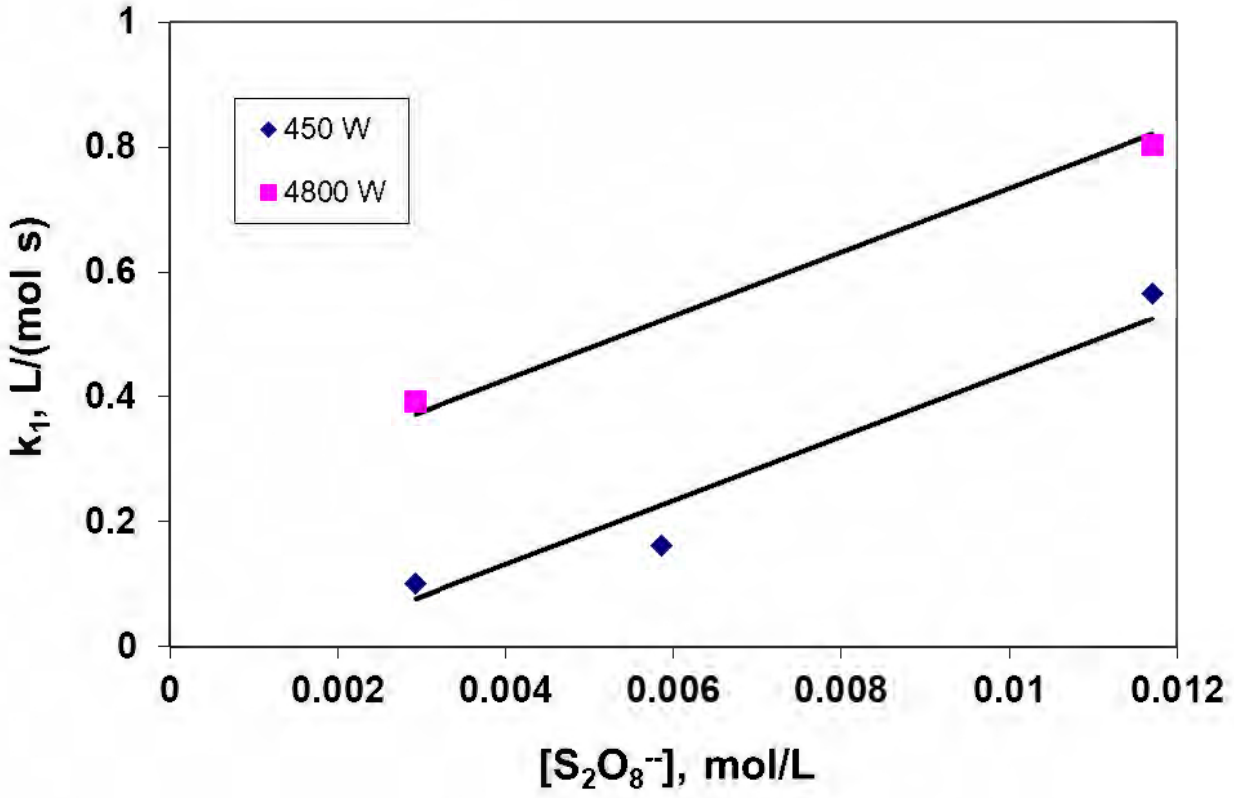

Figure 5.12. Dependence of k_1 on persulfate concentration and lamp intensity for the k_1-only model.

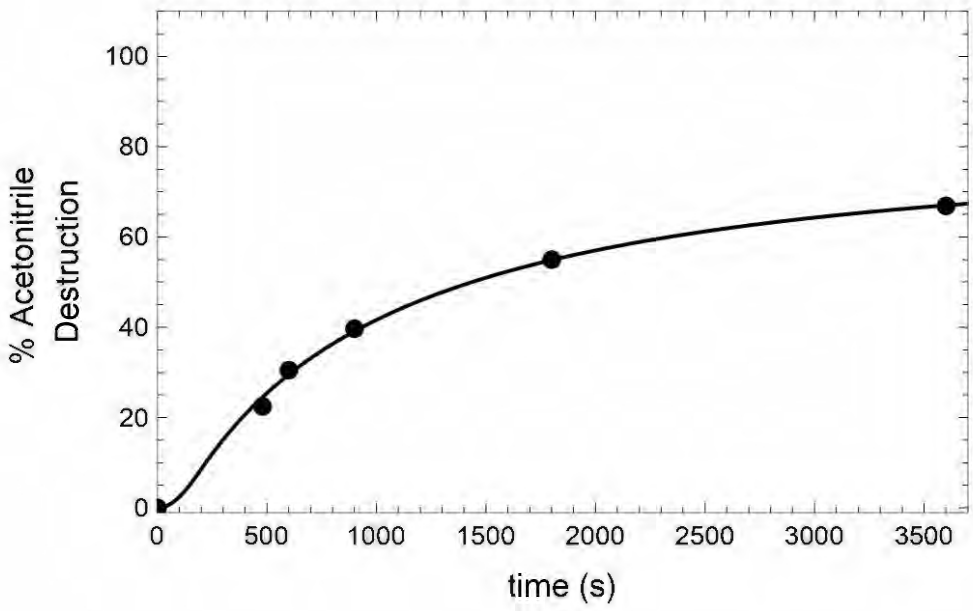

Figure 5.13. Extended model fit to Test LR-7.

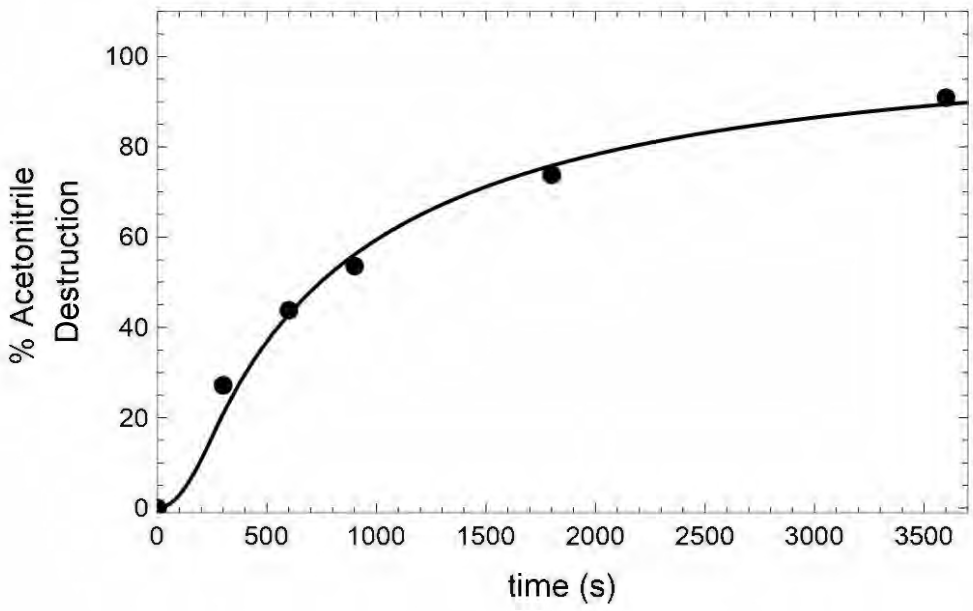

Figure 5.14. Extended model fit to Test LR-8.

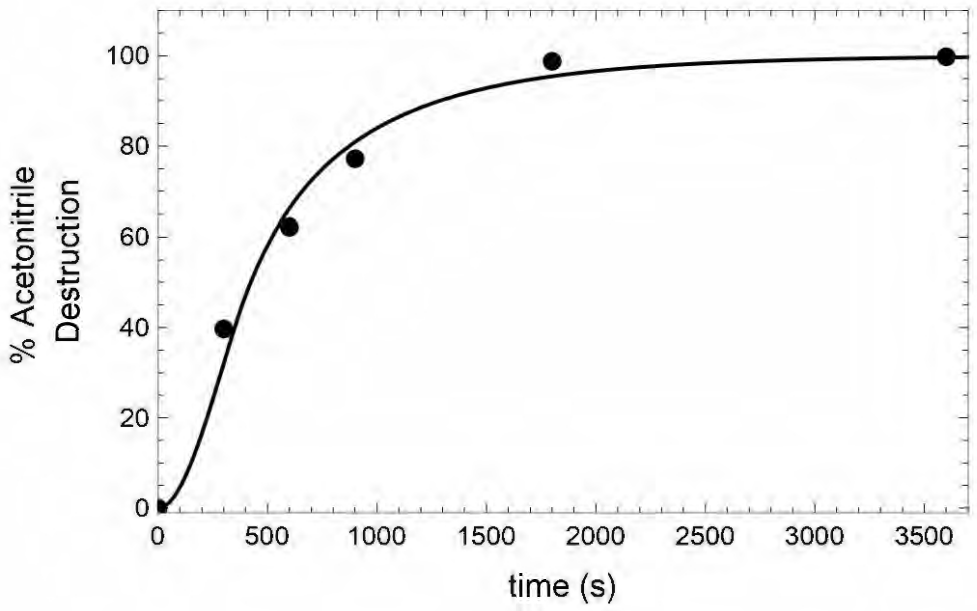

Figure 5.15. Extended model fit to Test LR-9.

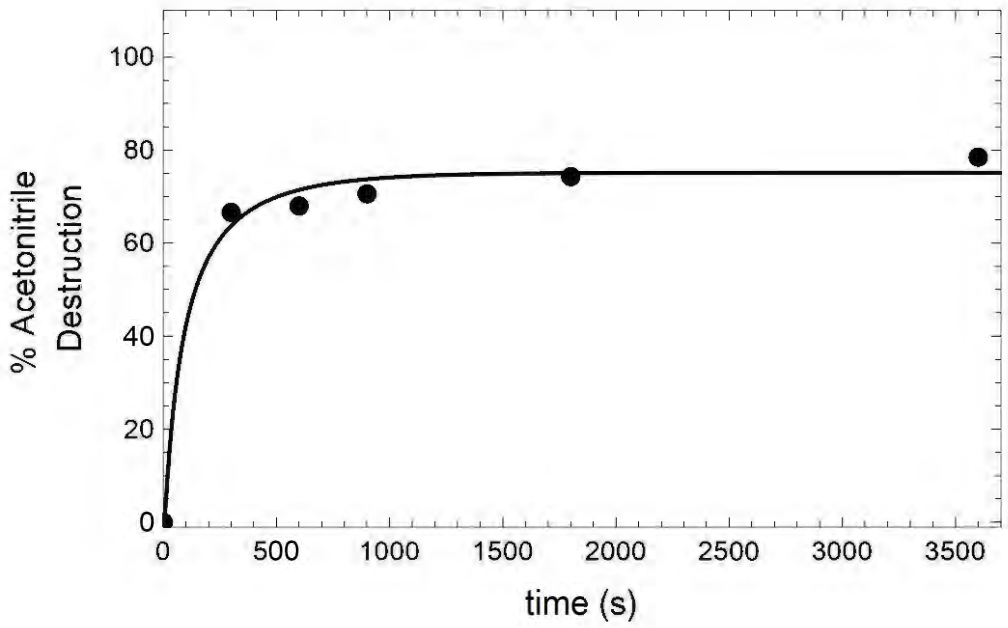

Figure 5.16. Extended model fit to Test LR-17.

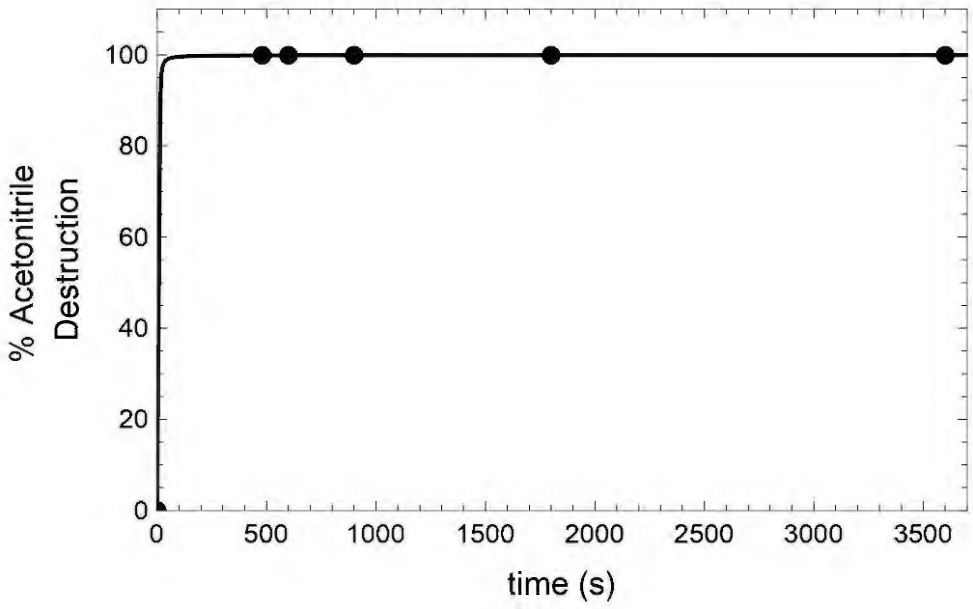

Figure 5.17. Extended model fit to Test LR-18.

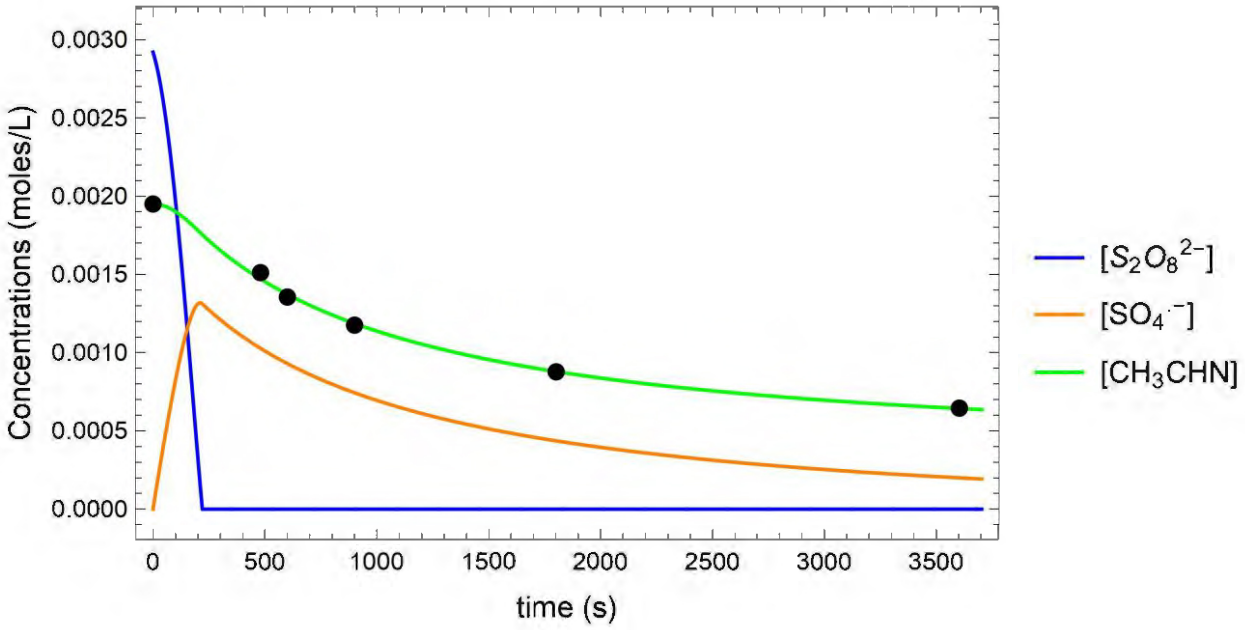

Figure 5.18. Extended model fit to Test LR-7.

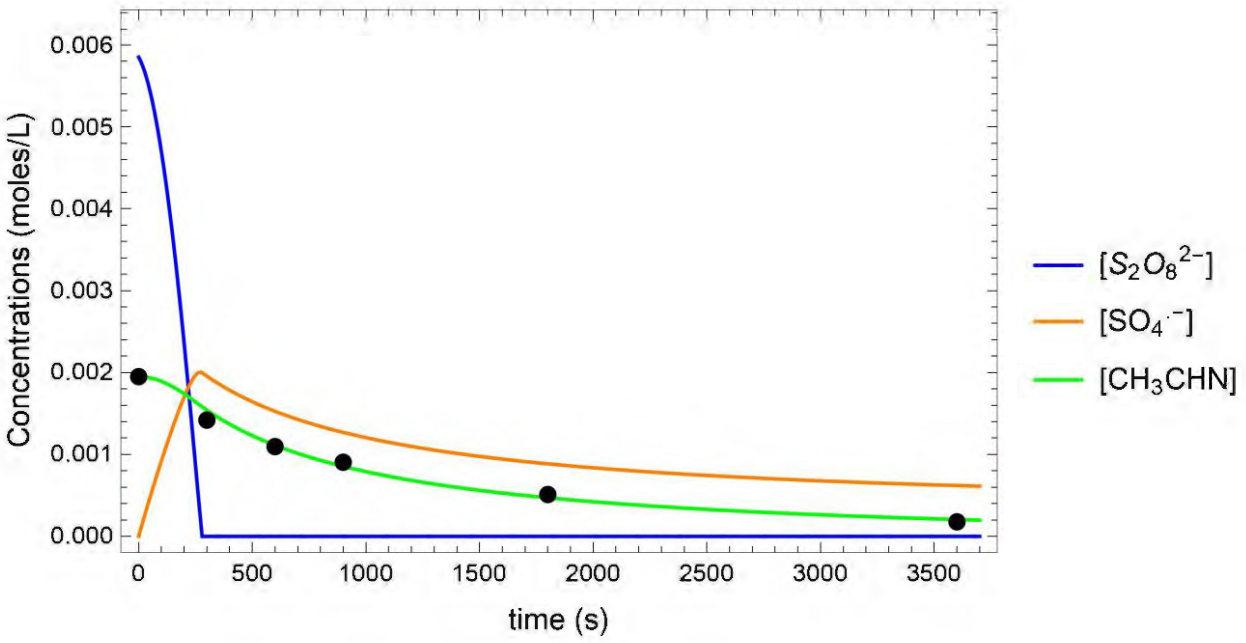

Figure 5.19. Extended model fit to Test LR-8.

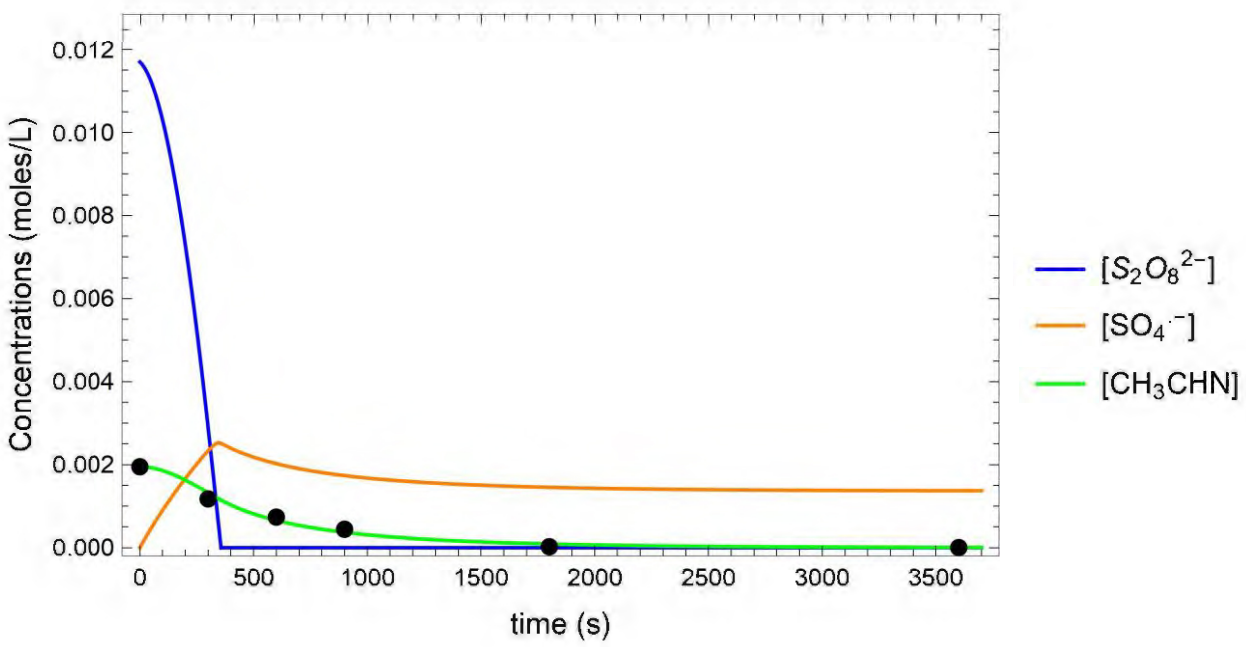

Figure 5.20. Extended model fit to Test LR-9.

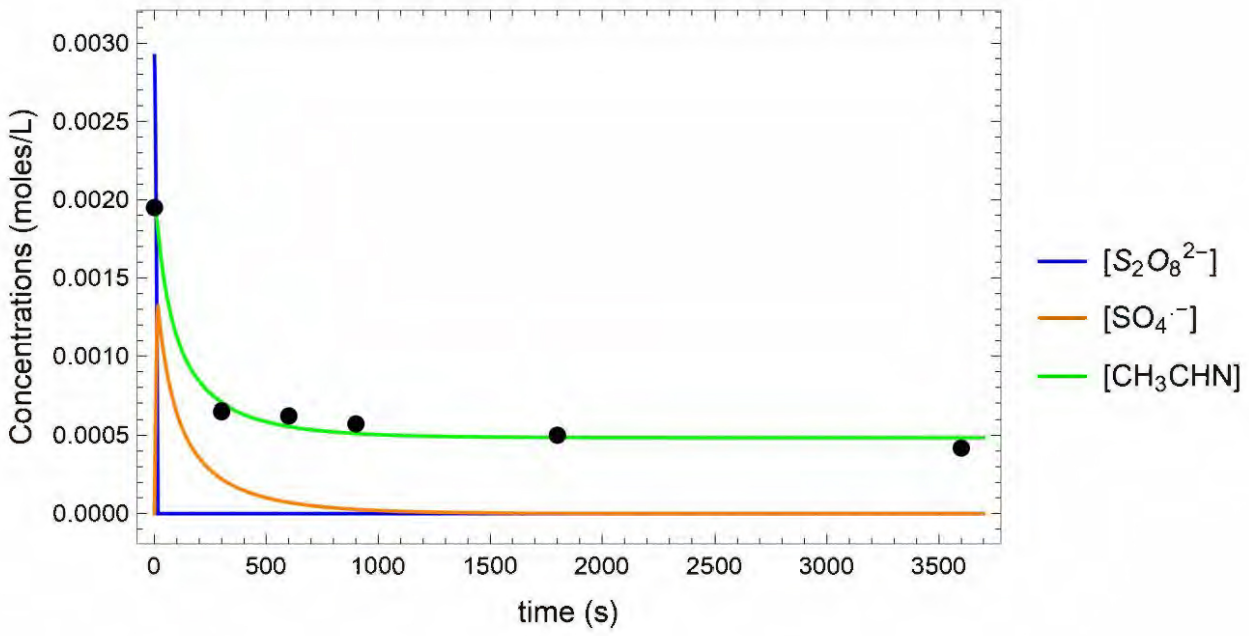

Figure 5.21. Extended model fit to Test LR-17.

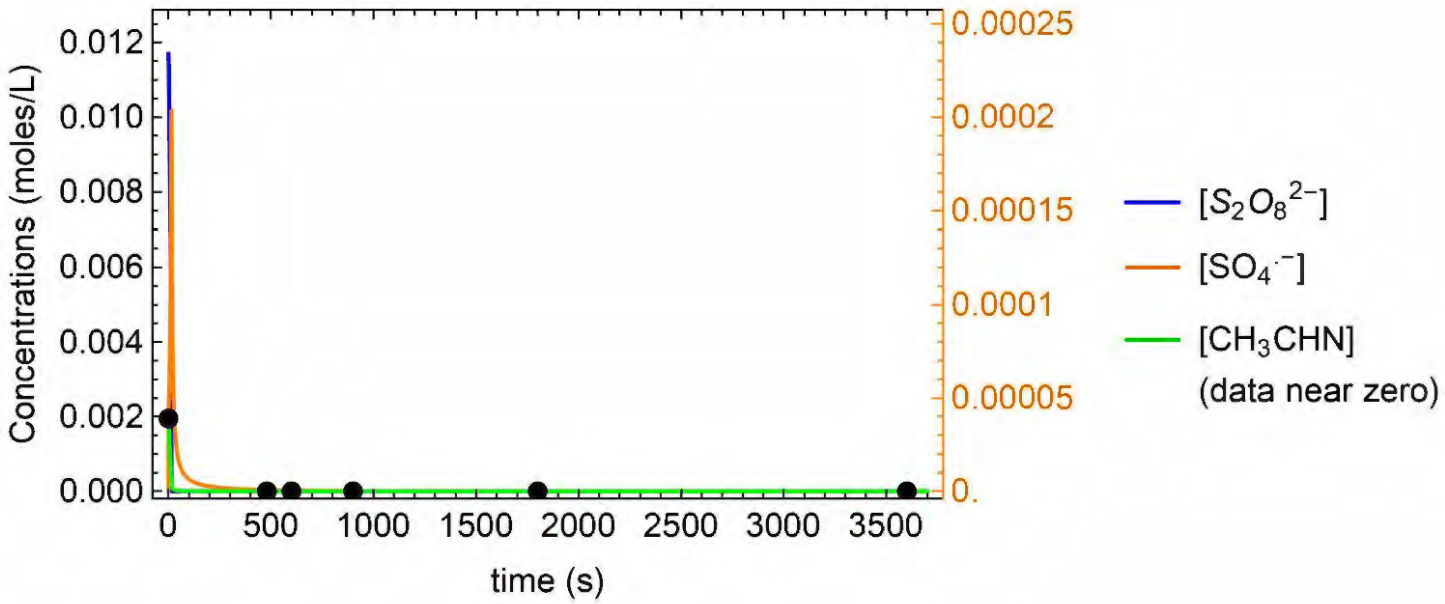

Figure 5.22. Extended model fit to Test LR-18.

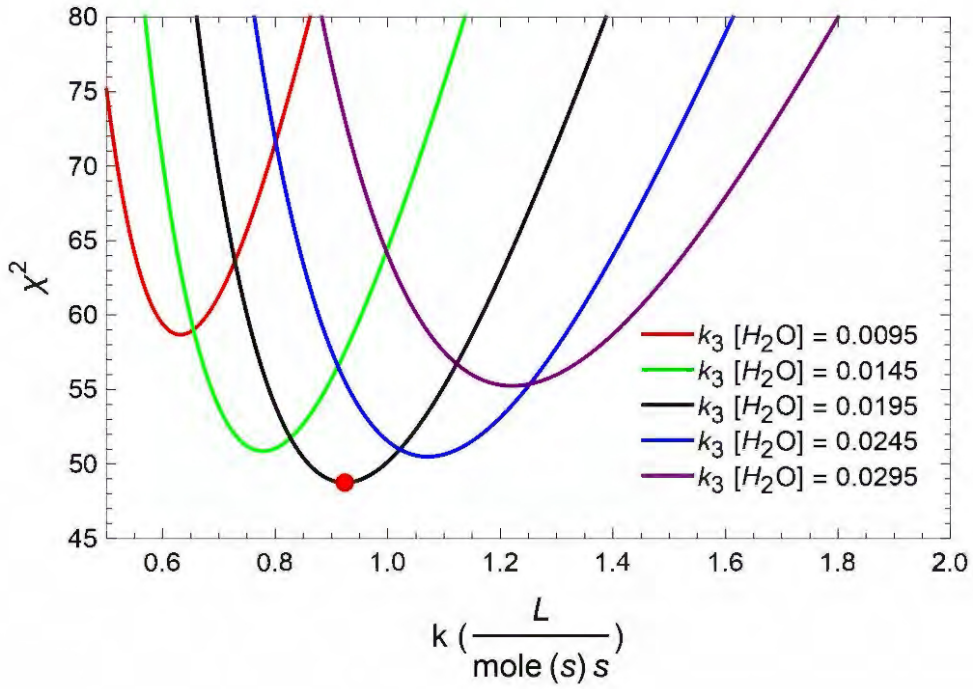

Figure 5.23. Global fit with extended model for best-fit value of k_3[H_2O] (black) and nearby values.

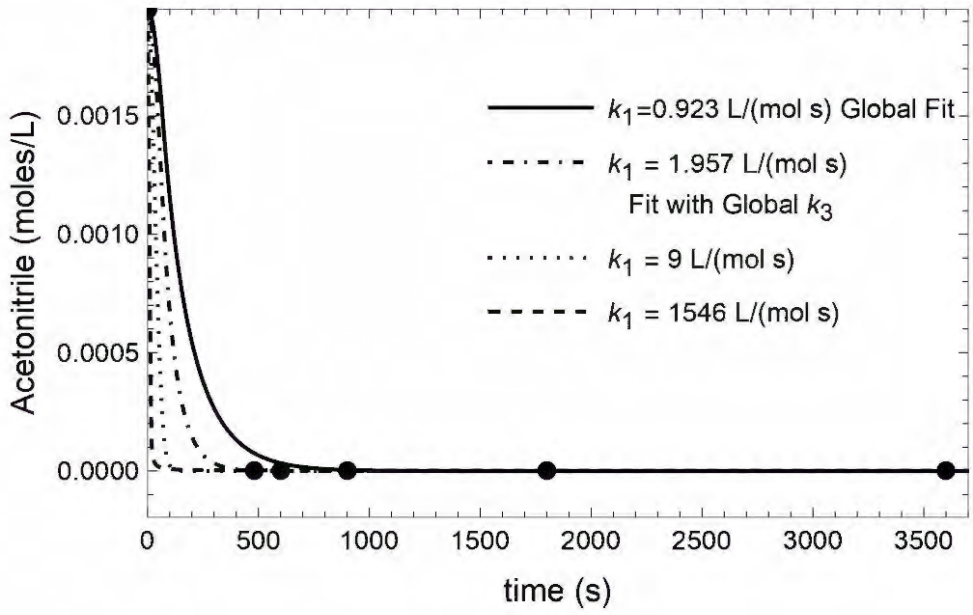

Figure 5.24. Fits to Test LR-18 with the extended model showing the effect of k_1.

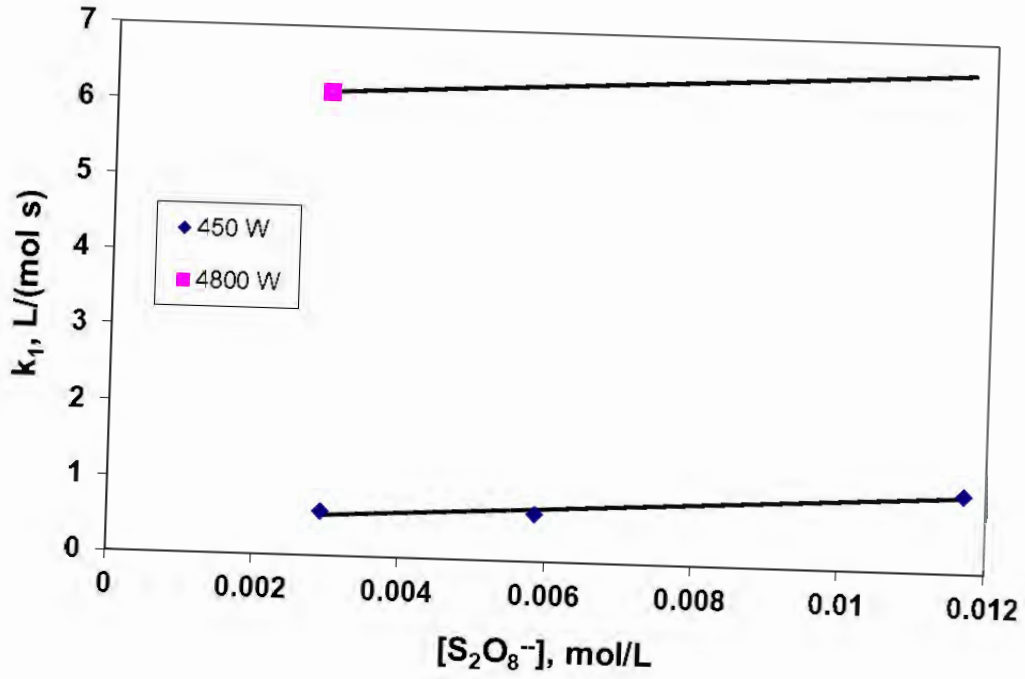

Figure 5.25. Dependence of k_1 on persulfate concentration and lamp intensity for the extended model.

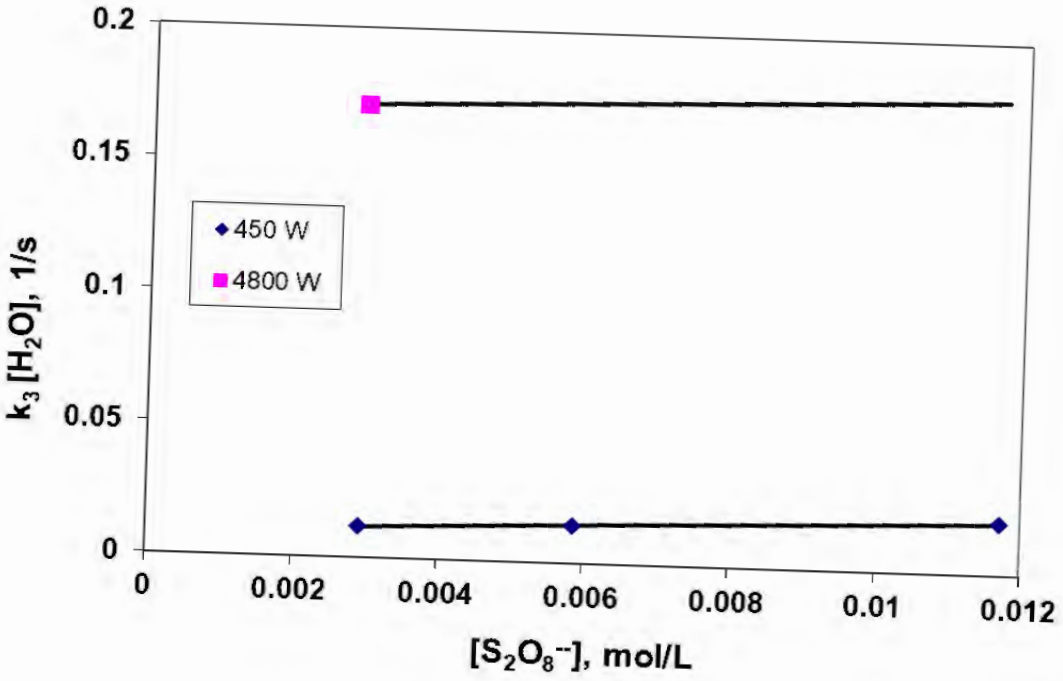

Figure 5.26. Dependence of $k_3[H_2O]$ on persulfate concentration and lamp intensity for the extended model.

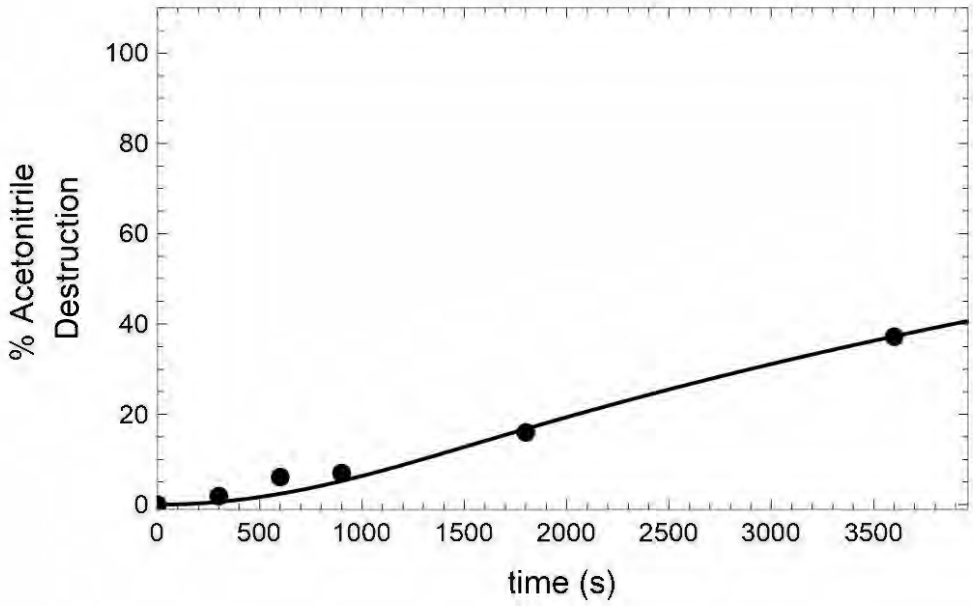

Figure 5.27. Model fit to peroxide Test LR-2.

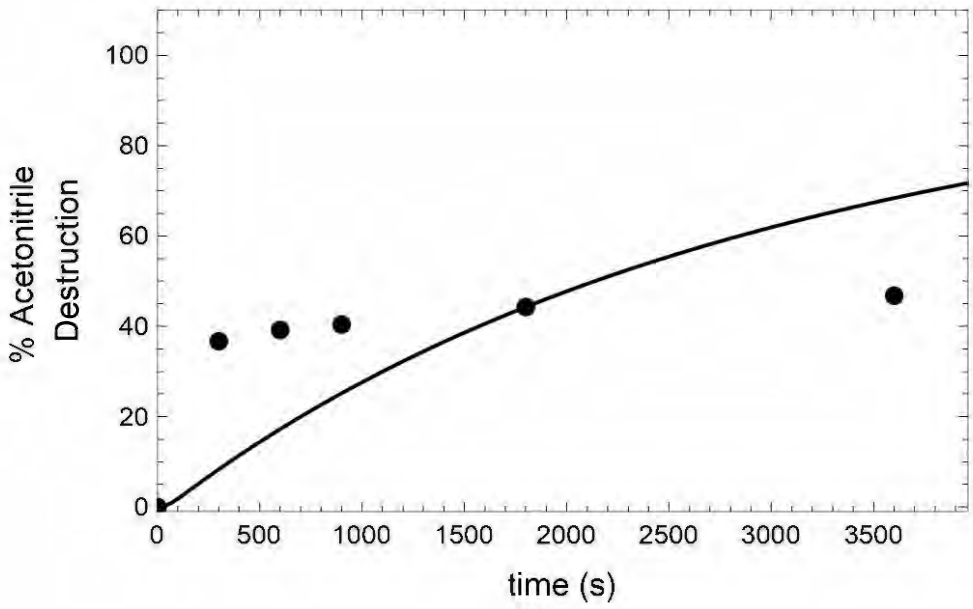

Figure 5.28. Model fit to peroxide Test LR-16.

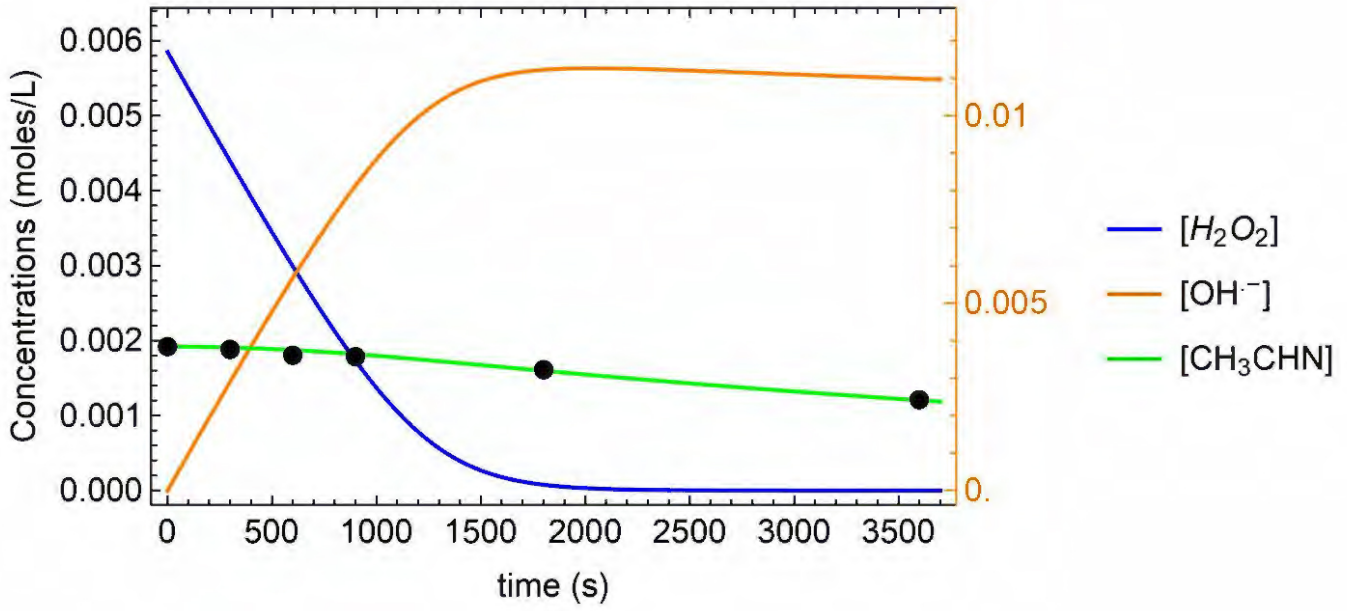

Figure 5.29. Model fit to peroxide Test LR-2.

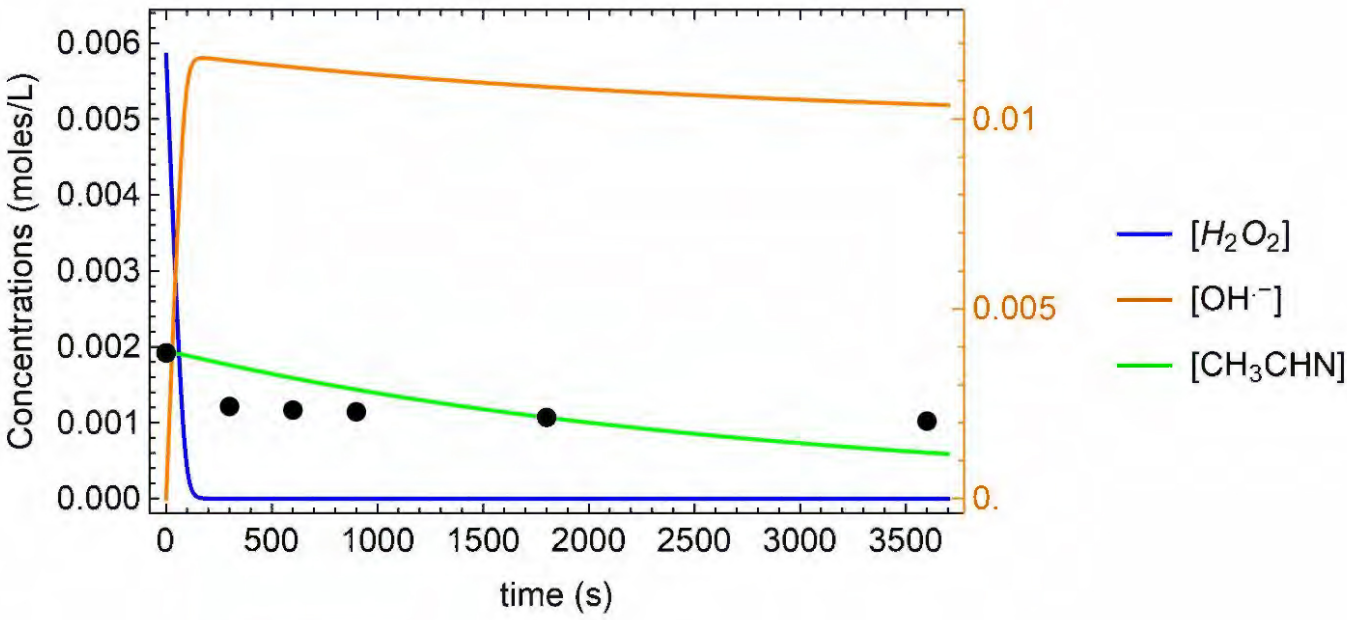

Figure 5.30. Model fit to peroxide Test LR-16.

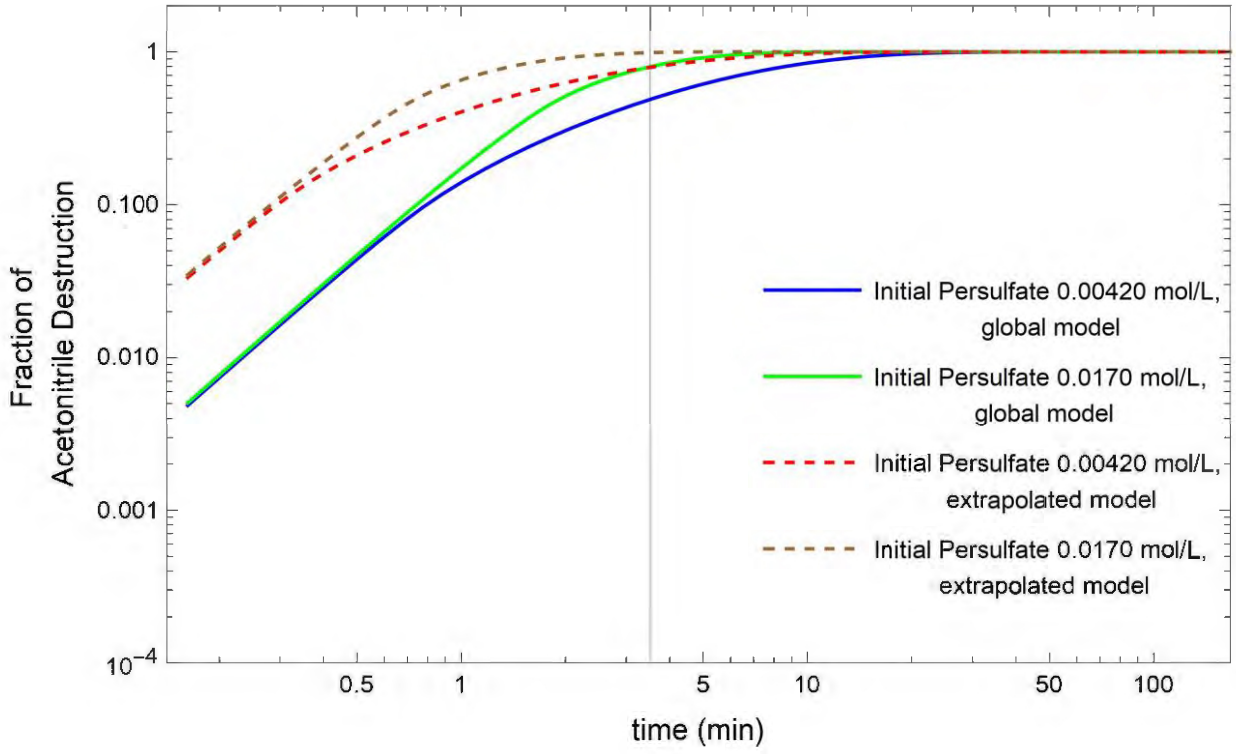

Figure 5.31. Model prediction for full-scale ETF UV/OX system.

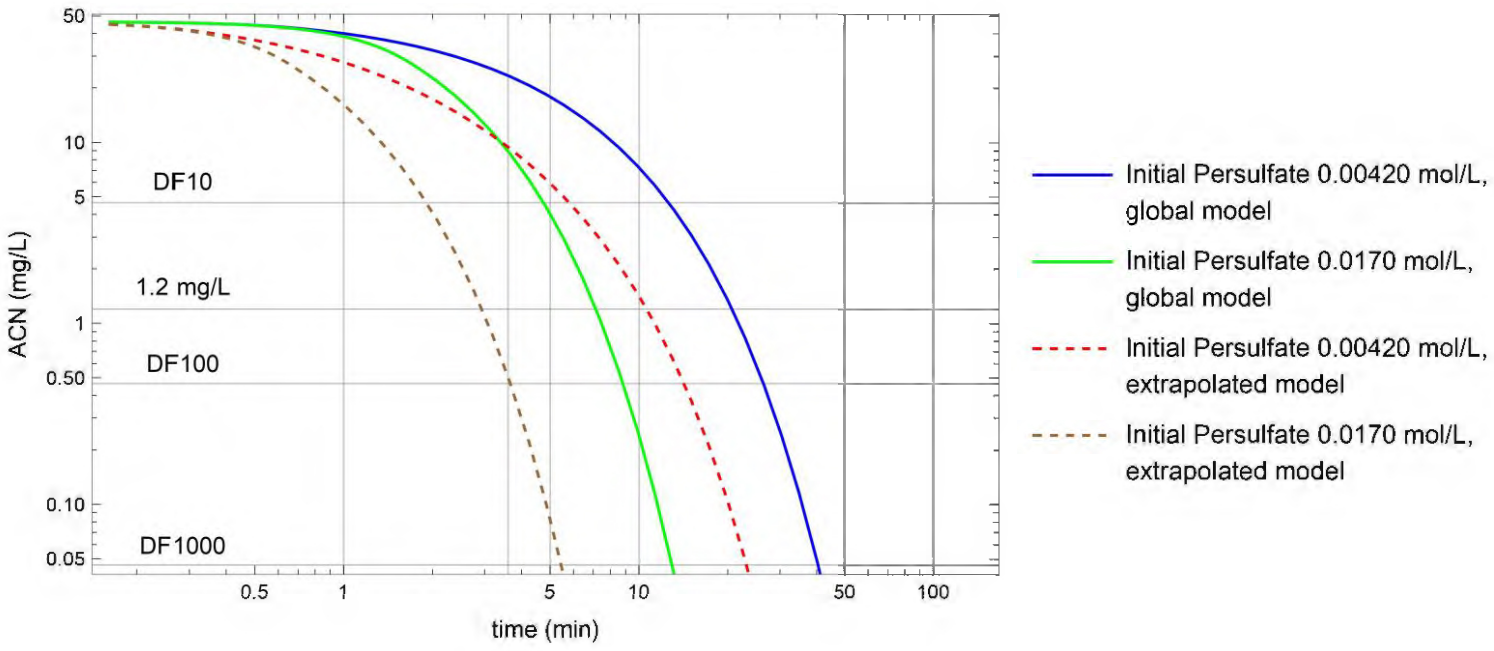

Figure 5.32. Model prediction for full-scale ETF UV/OX system. The acetonitrile concentration of 1.2 mg/L corresponds to a DF of 38.7.

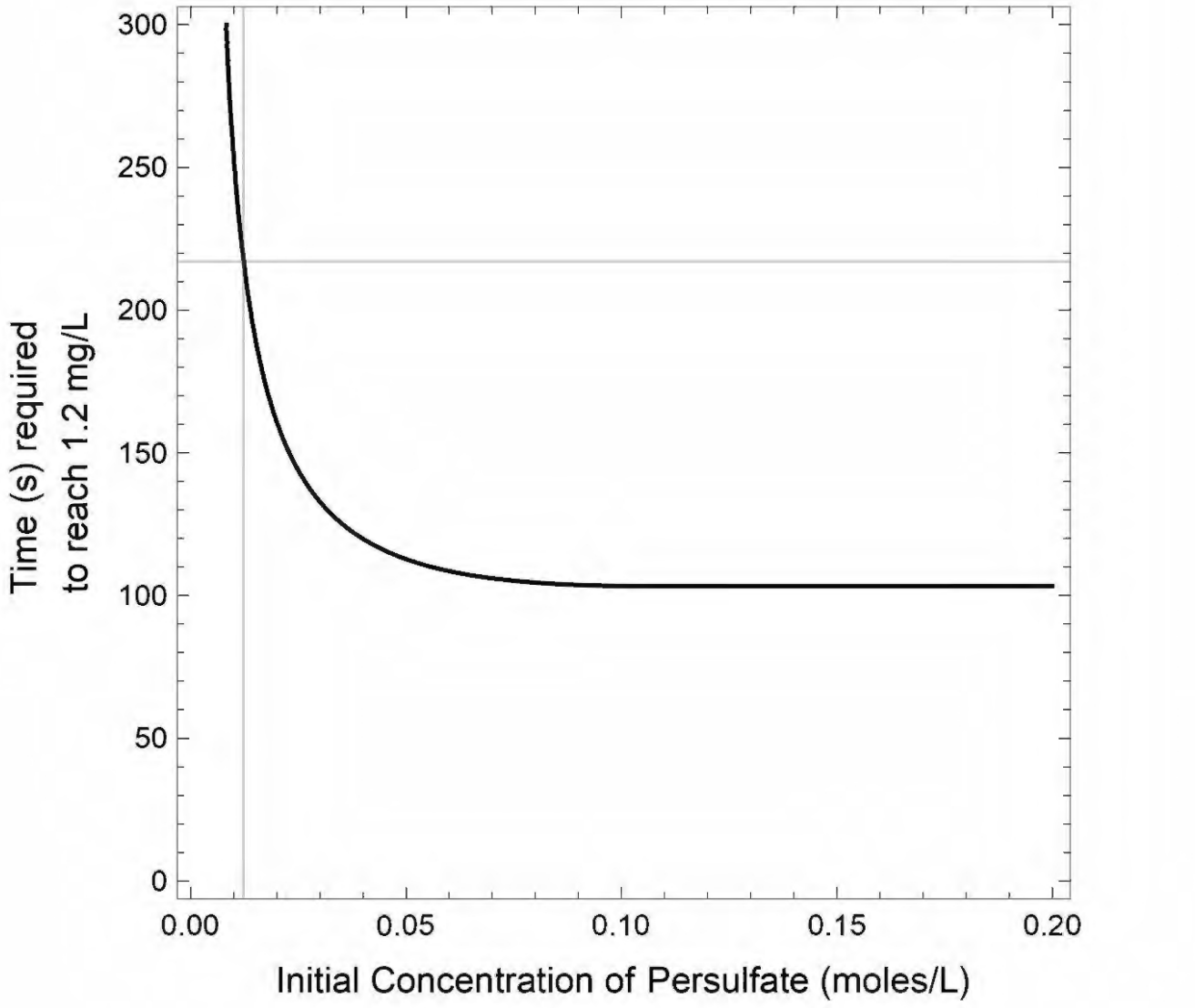

Figure 5.33. Time required to meet the 1.2 mg/L acetonitrile limit as a function of the initial persulfate concentration as calculated from the extrapolated persulfate model.

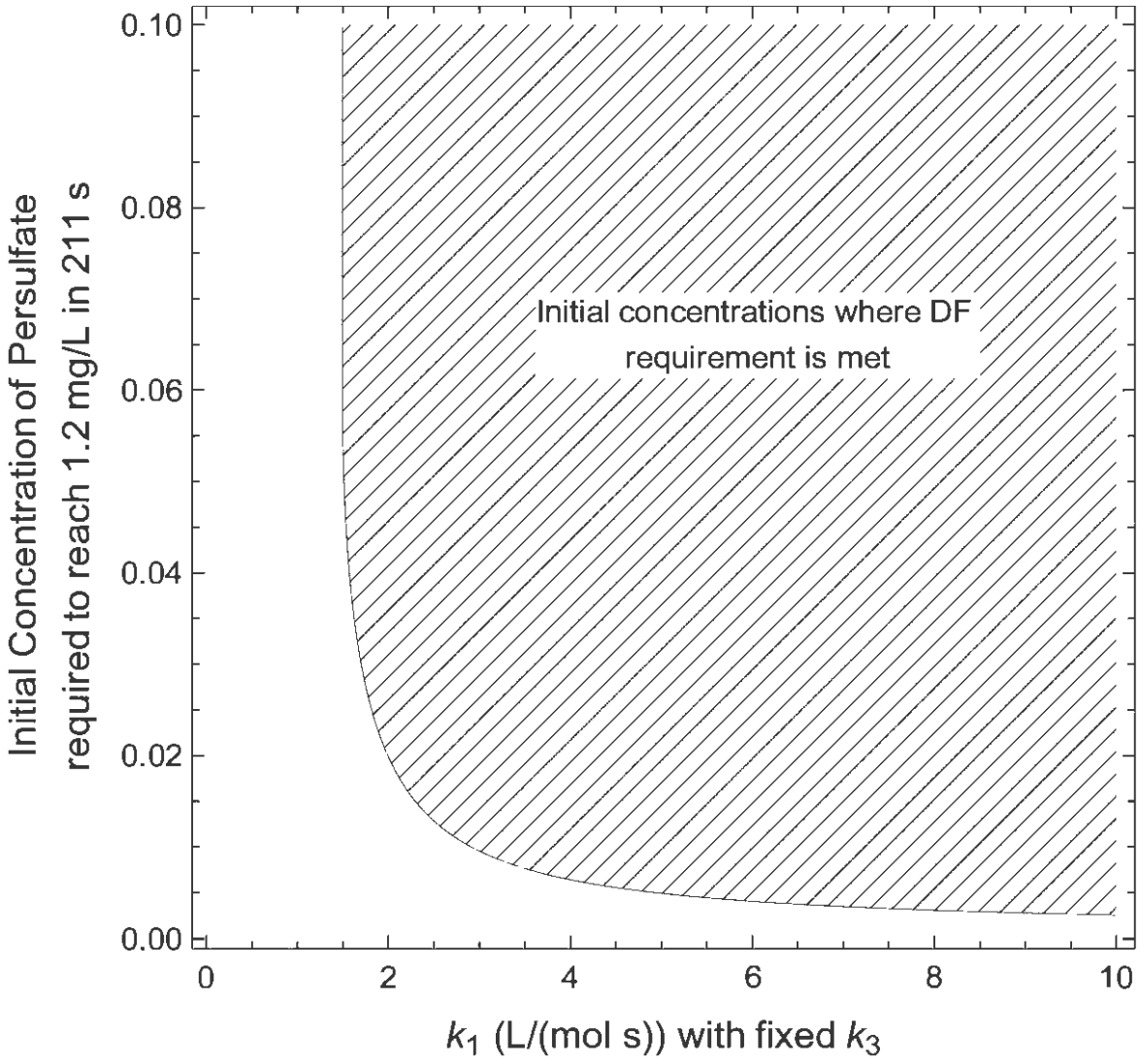

Figure 5.34. Combinations of k_1 and initial $[S_2O_8^{2-}]$ (mol/L) that are needed to meet the required ETF DF in 3.62 minutes based on the extended model. $k_3[H_2O]$ is fixed at the global value. Gray lines show the global fit value and persulfate concentration for Test LR-18.